Development of a Multiple Evaporator Nitrogen Pulsating Heat Pipe for Space Cryogenics Applications

Mason Mok

A Thesis submitted in partial fulfillment of

the requirements for the degree of

Master of Science

(Mechanical Engineering)

at the

UNIVERSITY OF WISCONSIN-MADISON

2017

Graduate Student: Mason Mok

Campus ID: 906-352-0317

Title: Development of a Multiple Evaporator Nitrogen Pulsating Heat Pipe for Space Cryogenics Applications

Approved by

Assistant Professor Franklin Miller

Department of Mechanical Engineering

Signature: _____ Date: _____

Abstract

Pulsating Heat Pipes (PHPs) are simple two-phase heat transfer devices, which have received increased attention in recent years due to their flexibility, low cost and reliability. Developed to improve upon the shortcomings of conventional heat pipes, PHPs have exhibited many qualities that are attractive to engineers across many disciplines. Their ability to operate over a wide range of temperatures and heat loads has motivated a significant amount of research into understanding their operating principles. Simply put, a PHP consists of a partially filled tube that meanders between an evaporator, where heat is absorbed, and a condenser, where heat is rejected. Effective conductivities of up 90,000 W/m-K have been observed for nitrogen. The motivation of this work is to investigate the concept of using a nitrogen PHP as a cryogenic distributed cooling device for space science applications.

Commonly, PHPs are comprised of one evaporator and one condenser. A novel idea of having one continuous length of tubing connect three isothermal evaporators to just one condenser is explored through this work. An apparatus was designed, fabricated and tested in a cryogenic facility in order to characterize performance under various operating conditions. The heat loads applied to each evaporator section were varied independently to study the PHPs ability to operate with various heat loading configurations. Results show that to a certain degree, the distribution of the total heat load doesn't have an effect on the performance of the PHP. The percent difference between the maximum and minimum heat loads applied can be up to 50%. Furthermore, for this particular PHP a minimum total heat load of 3.5 W must be applied to the evaporators in order to sustain operation. However, this heat load can be distributed among the evaporators unequally.

Acknowledgements

I have been very fortunate with the opportunities I have been granted through the University of Wisconsin. This work is the culmination of everything I have been exposed to at this amazing university. Many people have greatly helped me reach this point in my career, including family, friends, colleagues and advisors.

I would first like to thank my advisor Franklin Miller for his guidance and support throughout my time here at UW. He believed in me as an undergraduate and gave me the tools to become a great engineer. His insight into my project has helped evolve a pulsating heat pipe that seemed like it would never work into a device that proves a never-before-seen concept. Thank you to my other advisor John Pfotenhauer for his weekly intuition. I have learned a great deal from you and I have undoubtedly become a better engineer through your courses in Cryogenics and Vacuum Technology. In addition to my advisors, I would like to thank Jim Maddocks for his wisdom during the initial phases of my project.

To my family who has continuously supported me throughout both my degrees here at UW. My grandparents, mom and dad instilled in me the ideal of hard work. This has consistently helped me persevere through obstacles during this project. To all my lab mates for making my time here enjoyable and fulfilling. Especially to Diego for being a role model and inspiration throughout every aspect of my project. Even when I thought I knew what I was doing, Diego somehow found a way to help me do it better. I owe a great deal of the success of my PHP to you.

Table of Contents

List of Tables

List of Equations

List of Figures

1 Introduction

Over 50 years, the goal of NASA, and private aerospace companies alike, has transformed from putting humans in orbit around earth to putting humans on Mars, a destination that is 34 million miles away. Reaching such a distance requires a significant amount of fuel, in this case, liquid cryopropellant. NASA's best-suited rocket for launching satellites into earth's orbit and probes into deep space, Centaur, boasts a fuel boil-off rate of 0.1% per day. Even with this low boil-off rate, over the 200-day trip to Mars, this results in 18% loss in propellant mass [1]. Maintaining cryopropellants at temperatures below their boiling point during such a lengthy trip is an engineering challenge undertaken by NASA and the aerospace industry in order to ensure an efficient mission to Mars. Known as zero-boil-off systems (ZBO), NASA has deemed methods involving active cooling techniques necessary for a mission of such magnitude [2].

A collaborative effort between several NASA centers focused on testing a large-scale ZBO system on a 10 ft. ø and 10 ft. tall hydrogen tank. The system circulated the hydrogen across a GM-type cryocooler using a pump and then reinjected it into the tank using a spray bar. The group was successful at demonstrating that ZBO is possible for the life of the mechanical equipment [30]. In another collaboration between NASA Ames and NASA Glenn, researchers worked to prove a ZBO system can be achieved by circulating a chilled fluid in tubes attached to the outside of a cryopropellant tank. Using liquid nitrogen to imitate cryopropellant, the group built a ZBO system which uses a reverse turbo-Brayton cycle to circulate neon through 0.25 in diameter tubing attached to the outside of the tank [3]. These two systems have been successful at demonstrating that an active cooling method is necessary for ZBO, however, it is not ideal to have so many mechanical components present on a spacecraft. A system that can achieve ZBO

with a reduced mass and complexity is desired. A pulsating heat pipe that can pick up discrete heat loads from multiple locations while rejecting to one cryocooler would be an ideal solution.

First described in the early 1990's, pulsating heat pipes (PHPs) are being investigated by numerous research groups today. A PHP is a device that consists of a length of capillary tube that meanders in a serpentine manner between an evaporator and condenser section. The tubes are filled with a fluid, which exists in two-phases as shown in Figure 1. As heat is applied in the evaporator section, the increased pressure of the vapor plugs formed in the evaporator causes them to overcome capillary forces and move towards the condenser. As the vapor bubble reaches the condenser, it begins to condense into a liquid slug and pressure is reduced. The pressure imbalance causes flow oscillations of the order of 2 Hz and facilitates incredibly effective heat transfer [31]. PHPs can achieve conductivities of up to 90,000 W/m-K, as shown in this work. Figure 1 depicts the operation of a PHP.

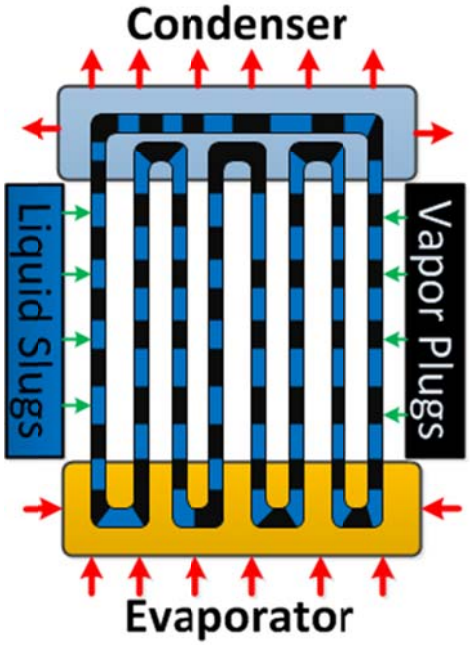

Figure 1: Schematic showing general layout of a PHP. Red arrows indicate heat flow.

Although the intricacies of PHP operation are still not well understood, researchers have been working on their application to thermal systems. Concepts such as using PHPs to cool superconducting magnets, server racks, electronics and vehicles have been investigated. A more complete understanding of the operation of PHPs is needed so that reliable PHP design tools can be developed.

PHPs are a viable candidate for a ZBO system due to their ability to operate without the use of a pump. By winding loops of capillary tubing around a tank, a pulsating heat pipe would inherently circulate a working fluid while distributing heat loads and rejecting them to a cryocooler. No data exist to prove that PHP's will work with multiple independently heated evaporators. This work describes the construction, and experimental evaluation of a nitrogen PHP with three separate evaporators and one condenser. This proof of concept device has been fabricated and tested to support the design of a zero boil-off system.

1.1 Thesis Outline

The following body of work is the culmination of work completed for partial fulfilment of a Master of Science Degree in Mechanical Engineering by Mason Mok at the University of Wisconsin-Madison. The scope of the project along with supporting data and analysis is described in detail.

2 PHP background

2.1 Conventional Heat Pipe

A conventional heat pipe is a two-phase heat transfer device that can transfer heat with high conductance across a wide temperature range. Generally comprised of an evacuated vessel, a two-phase working fluid and a wick structure, these devices have been implemented in many

applications including laptop computers and spaceflight thermal control systems. On one end of the heat pipe, the working fluid is evaporated due to an incident heat flux. On the other end, the fluid is condensed as heat is rejected to a cold sink. The wick structure acts to separate the liquid and vapor phase of the working fluid and to pump the liquid from the condenser to the evaporator by capillary action as shown in Figure 2. Loop heat pipes can be used to improve overall heat transfer between a hot and cold body [4]. While heat pipes have enjoyed widespread success, there are some limitations, which make them unsuitable for some applications.

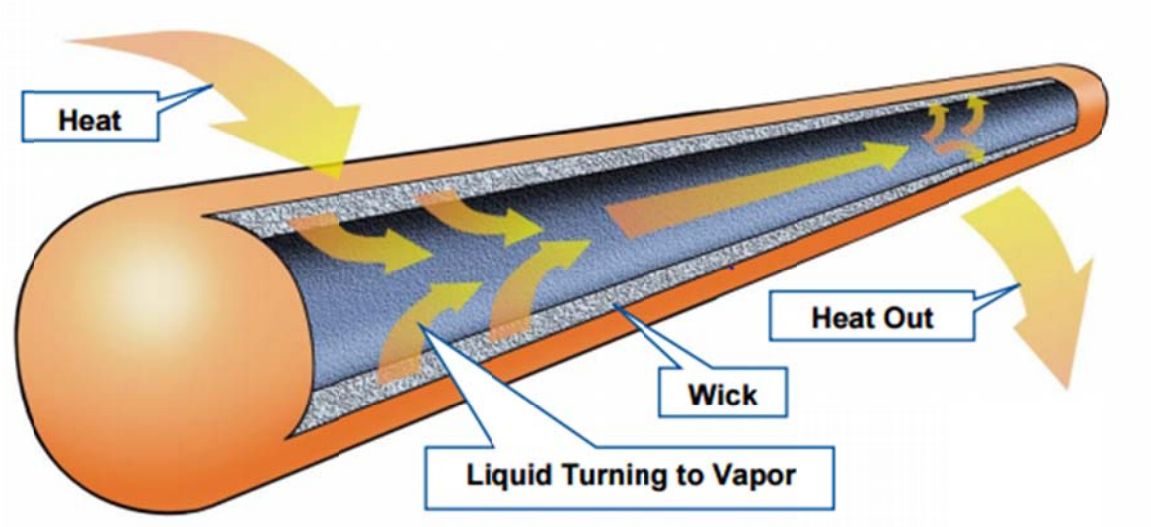

Figure 2: Schematic of conventional heat pipe [4].

First, the capillary action of the working fluid is limited by the geometry of a conventional heat pipe. The capillary action of the wick cannot overcome gravitational forces, vapor pressure drop and liquid pressure drop in some cases. Thus, the orientation of a heat pipe affects its operation. Second, the boiling limit is reached when the radial heat flux exceeds some maximum value and dry-out occurs; the heat flux is too high and an insufficient amount of liquid exists on the warm end of the heat pipe. Third, the entrainment limit is reached when the sheer force of the vapor flowing from the evaporator to the condenser causes some liquid to be

entrained from the wick structure and carried to the condenser section. These limits of a heat pipe caused Akachi to invent the pulsating heat pipe in 1990.

The PHP was proposed by Akachi in a patent filed in 1988 and was originally referred to as a wick-less heat pipe. In addition to the limits described above, in his patent Akachi also addresses the presence of length and diameter limits of a wick-type heat pipe and the difficulty in mounting a wick-type heat pipe. Akachi proposed the PHP as a device that can overcome many of the limits of a standard heat pipe.

Four main types of PHPs have been investigated: closed-end (a), closed-loop (b), closed-loop with check valve (c) and open-end (d). A depiction of each type can been seen in Figure 3 below [5].

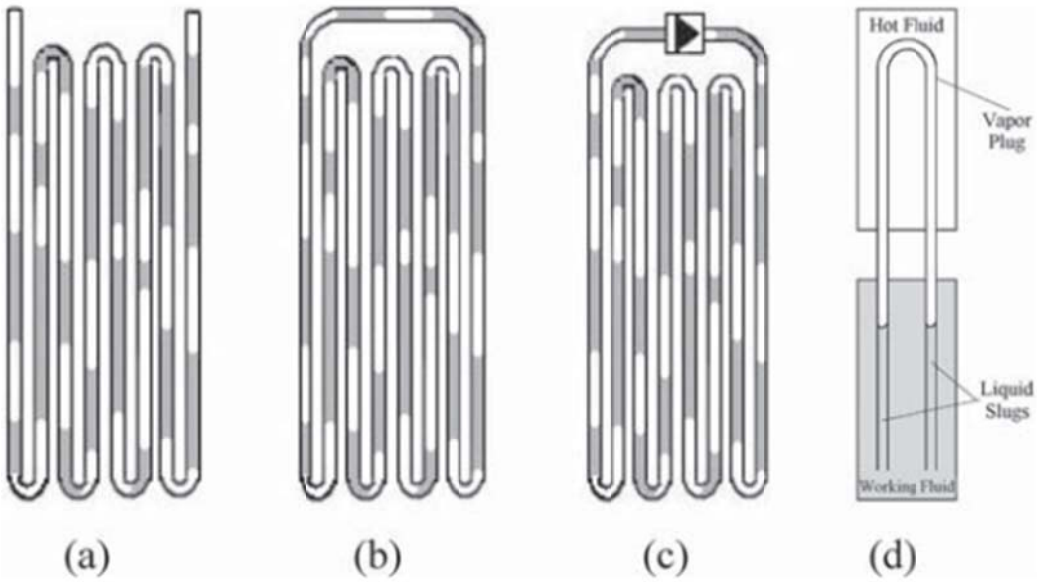

Figure 3: Four PHP configurations. (a) closed-end, (b) closed-loop, (c) closed-loop with check valve and (d) open-end [5].

Thus far, experimental data has shown that a closed-loop PHP has better heat transfer performance [5]. Some research groups have investigated the closed loop PHP with a check-valve; however, at cryogenic temperature this would be difficult to implement. The reduced weight and complexity of a PHP make them ideal for space applications.

2.2 Operating Principle of PHPs

For a given fluid, there are many parameters of a PHP that can be varied to study performance. These parameters generally fall into one of two categories: geometric parameters and operational parameters. Evaporator, condenser and adiabatic section length, size, shape and relative configuration are geometric parameters. Fill ratio, inclination angle, heat flux and temperature are examples of operational parameters that can be varied. Furthermore, in the world of PHP research there exists two distinct fields of study: theoretical/computational and experimental research. Theoretical research involves modeling PHP systems using programs like Fluent ® and Matlab ® to determine expected performance of a device geometry. This thesis will focus on experimental laboratory work where a PHP was manufactured and its performance characterized with respect to a range of operating parameters.

A PHP can be constructed in a way that allows geometric as well as operational parameters to be adjusted easily. For example, the PHP can be designed to have the ability to vary the length of the adiabatic section relatively easily. Then data can be compared to determine performance characteristics associated with adiabatic length. It is more common to vary operational parameters because these changes can be made without modifying the construction of the PHP. A few of geometric and operational considerations that researchers consider are discussed in detail below.

2.2.1 Fill Ratio

The amount of fluid present in the PHP is an experimental parameter that needs to be carefully controlled as performance of the PHP can vary greatly with fill ratio. Fill ratio is defined at the volume of liquid in the PHP to the total volume of the PHP:

$$V_{fill} = \frac{V_{liq}}{V_{PHP}}$$

Equation 1: Fill Ratio.

The method of setting the fill ratio for this experiment is outlined in section 4.6 of this thesis. Investigators such as Khandekar et al. have found that no matter the operating temperature, there exists an optimal fill ratio where the PHP performs best [6]. This optimal fill ratio also depends on the working fluid. According to Khandekar, their PHP operated as a true PHP between the limits of 20% and 70% with maximum performance for water of 15-30%, 25-55% for ethanol and 35-60% for R-123. Due to different PHP geometries and the properties of fluids under various conditions, the optimal fill ratio can lie anywhere in the range of 20-80% [7].

Furthermore, Yang et al. tested an ethanol flat-plat PHP and compared thermal resistance at various fill ratios and heat inputs. They showed that for horizontal heating mode there exists an optimal fill ratio around 60%. Shown in Figure 4, this group also found that this optimal fill ratio is independent of heat load [8].

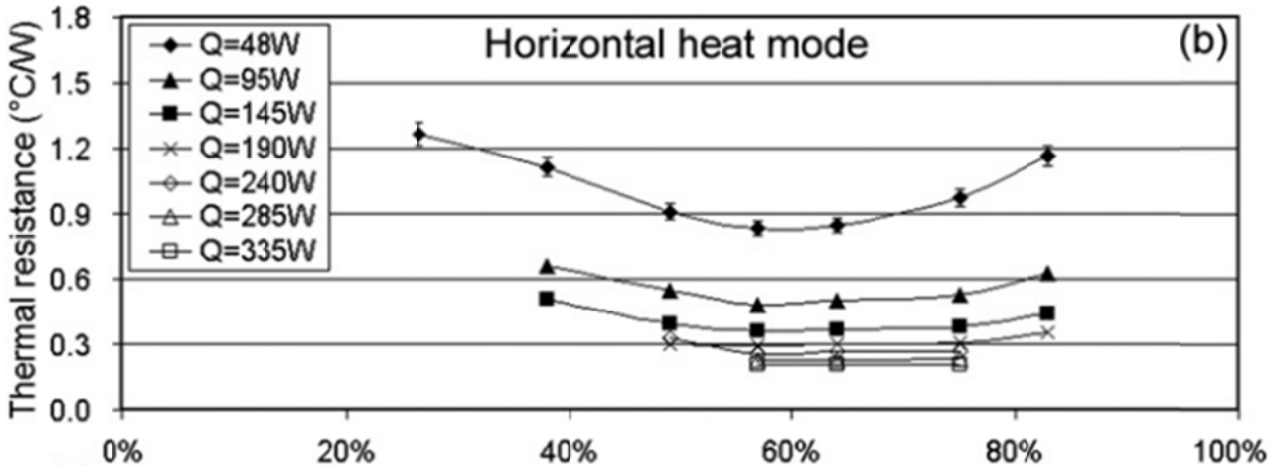

Figure 4: Plot of thermal resistance vs. fill ratio at various heat loads for a 40 turn, flat plate ethanol PHP [8].

2.2.2 Heat Input

While some PHPs are investigated for their ability to be used for a certain application, the majority of the research currently being conducted is intended to understand how PHPs work. Whether it be a room temperature or cryogenic PHP, during testing heat loads are typically applied using electric heaters. This allows the researchers to carefully control the heat loads during testing so that performance versus heat load can be quantified. The performance of the PHP varies based on the amount of heat applied to the evaporator section.

Many researchers have discovered that there exists a minimum heat flux necessary for a PHP to begin working properly. If the heat applied is too low, not enough vapor bubbles are created and slug-plug flow will not initiate. Furthermore, even if heat greater than a critical value is applied, the PHP still does not perform ideally. Hua et al. showed that for a rectangular channel deionized water PHP the start-up process of the PHP varied with heat input. Two contrasting scenarios are plotted together in Figure 5 to show the chaotic behavior of low heat input (80 W) compared to the more direct and composed start-up of a higher heat input (280 W)

[9]. The evaporator temperatures of each case over time, as shown in Figure 5, are used to make this point.

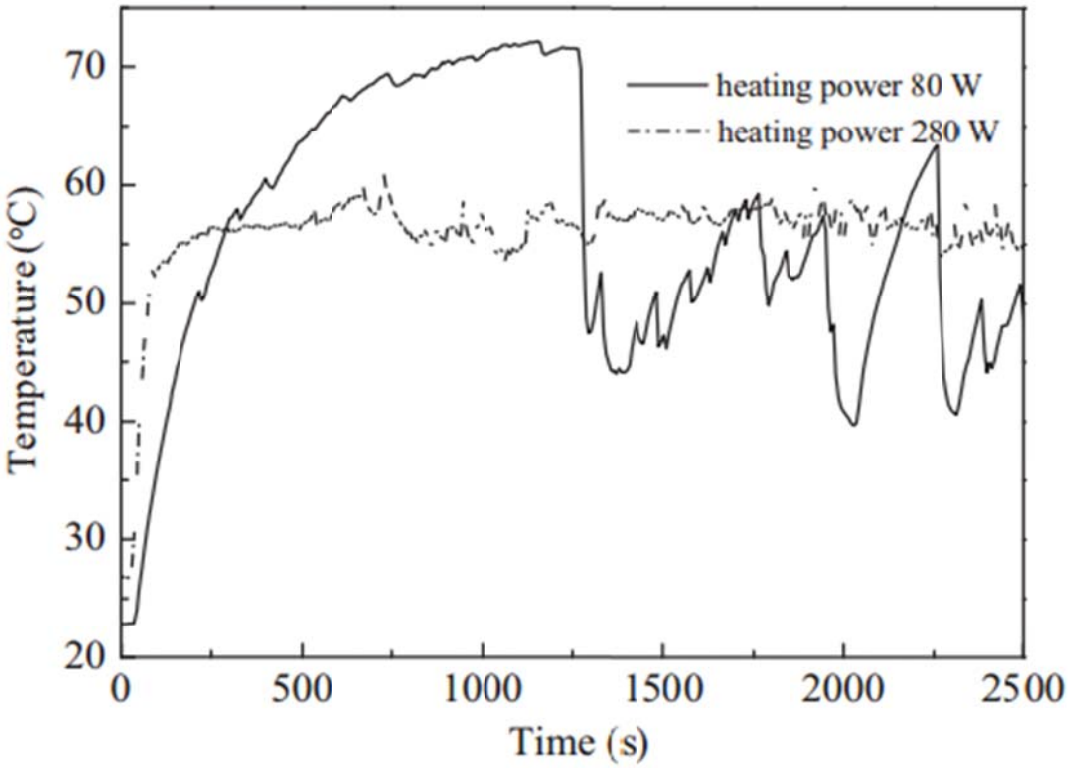

Figure 5: Plot of evaporator temperature vs. time for the start-up process of a rectangular cross-section deionized water PHP at 80 W and 280 W heat input [9].

While this PHP is able to transfer heat to the condenser, the temperature of the evaporator varies ~25 C during operation, which may not be acceptable for some applications of PHPs. In addition to the quality of the heat transfer at higher heat loads, looking again at Figure 5, it is evident that the start-up time is much shorter than the low heat input case. The concept of start-up is explored further.

In 1976 P. Saha et al. looked at thermally induced flow oscillations in two-phase flow. Their experimental procedure was intended to determine the effect of multiple parameters on the

thermally induced flow in a two-phase mixture of Freon-113. The data they collected comparing heat input to flow amplitude in their test section is of particular interest to the author. According to Figure 6, as heat input increased, the flow oscillations of F-113 began to show increasing order and amplitude. Figure 6 shows the amplitude of mean flow oscillations versus the power supplied to the test section. At a certain power input, the amplitude of the flow oscillation starts to increase rapidly, characterizing an onset power [10]. The pressure of two-phase flow induced by heat input reaches a point where the amplitude of flow oscillations dramatically increases. This onset power is similar to the start-up power described my many PHP investigators.

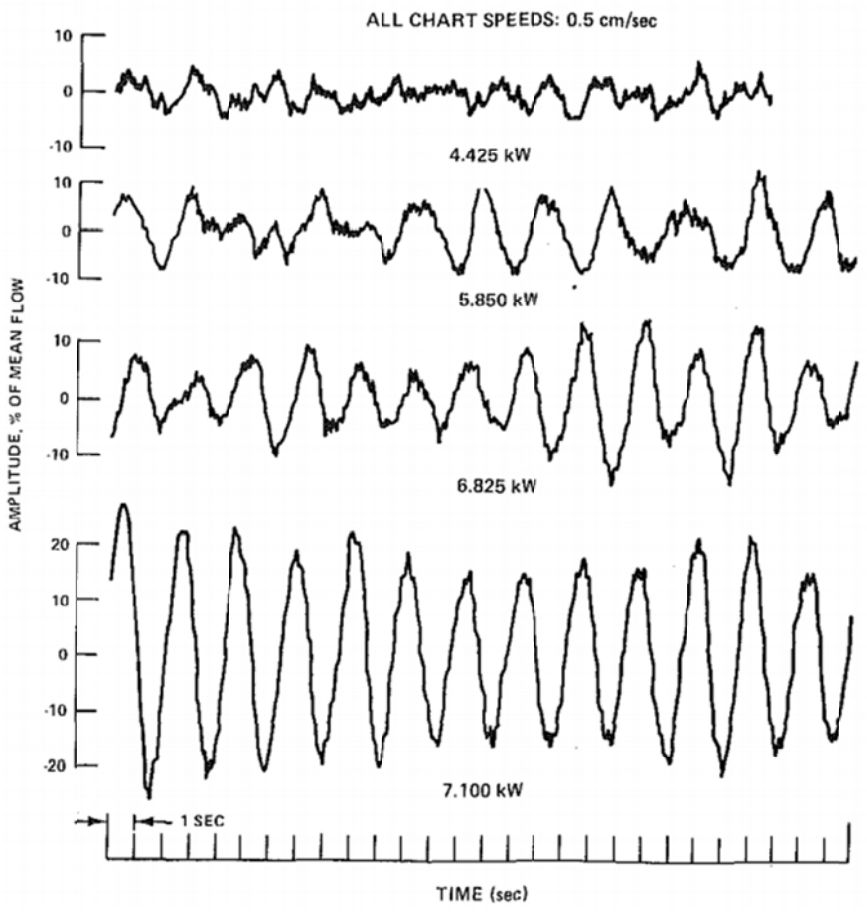

Figure 6: Flow oscillation amplitude of Freon-113 (represented as a percentage of mean amplitude) vs. time for increasing heat load [10].

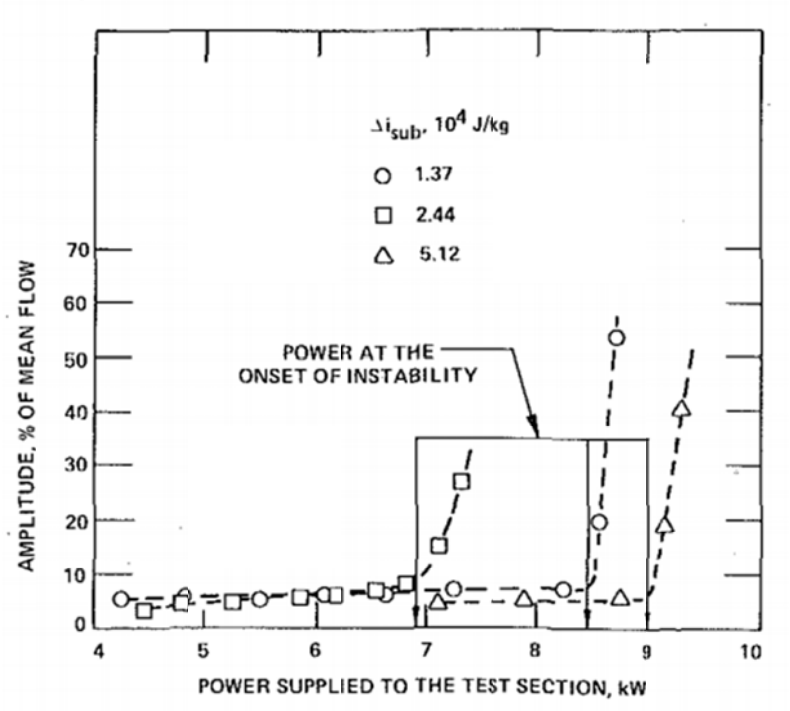

Figure 7: Flow oscillation amplitude of Freon-113 (represented as a percentage of mean amplitude) vs power applied to the test section as a function of inlet subcooling [10].

2.2.3 Orientation

Orienting a PHP at various angles relative to gravity has a significant effect on its operation. If oriented vertically, that bubbles created in the evaporator section have a natural buoyancy. Known as bottom heating mode (BHM), placing the evaporator at the bottom of a PHP has proven to have the best performance. Natsume et al. tested a PHP filled with hydrogen and neon in order to determine the orientation dependence of PHP performance [11]. Both fluids exhibited peak performance in BHM independent of fill ratio. For neon, this phenomenon was less pronounced at lower heat inputs (Figure 8).

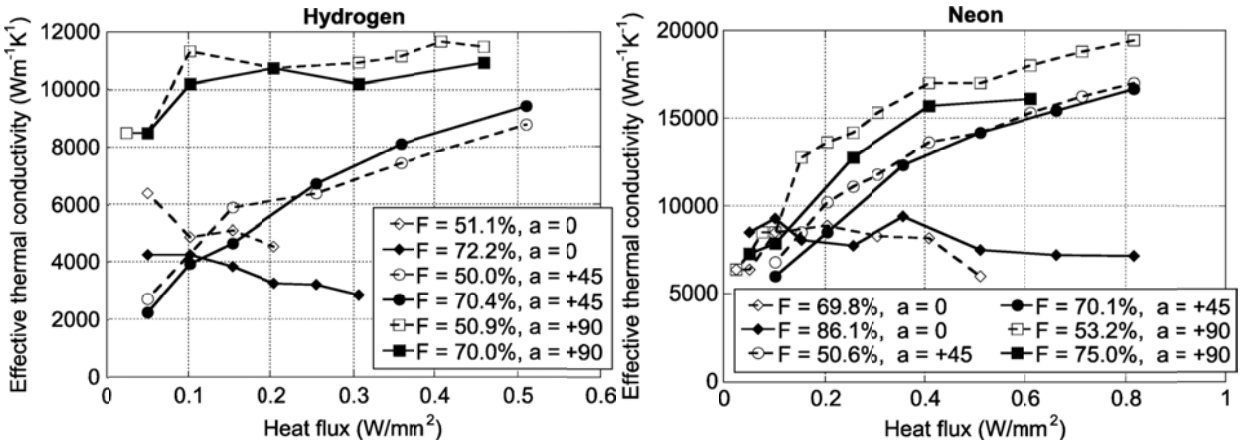

(a) (b)

Figure 8: Effective thermal conductivity vs. heat flux for (a) hydrogen and (b) neon at different fill ratios and orientations. +90 represents BHM [11].

Li et al. also proved BHM is superior to other orientations. Using a nitrogen PHP this group showed the thermal conductivity is maximized when operation in BHM (See Figure 9).

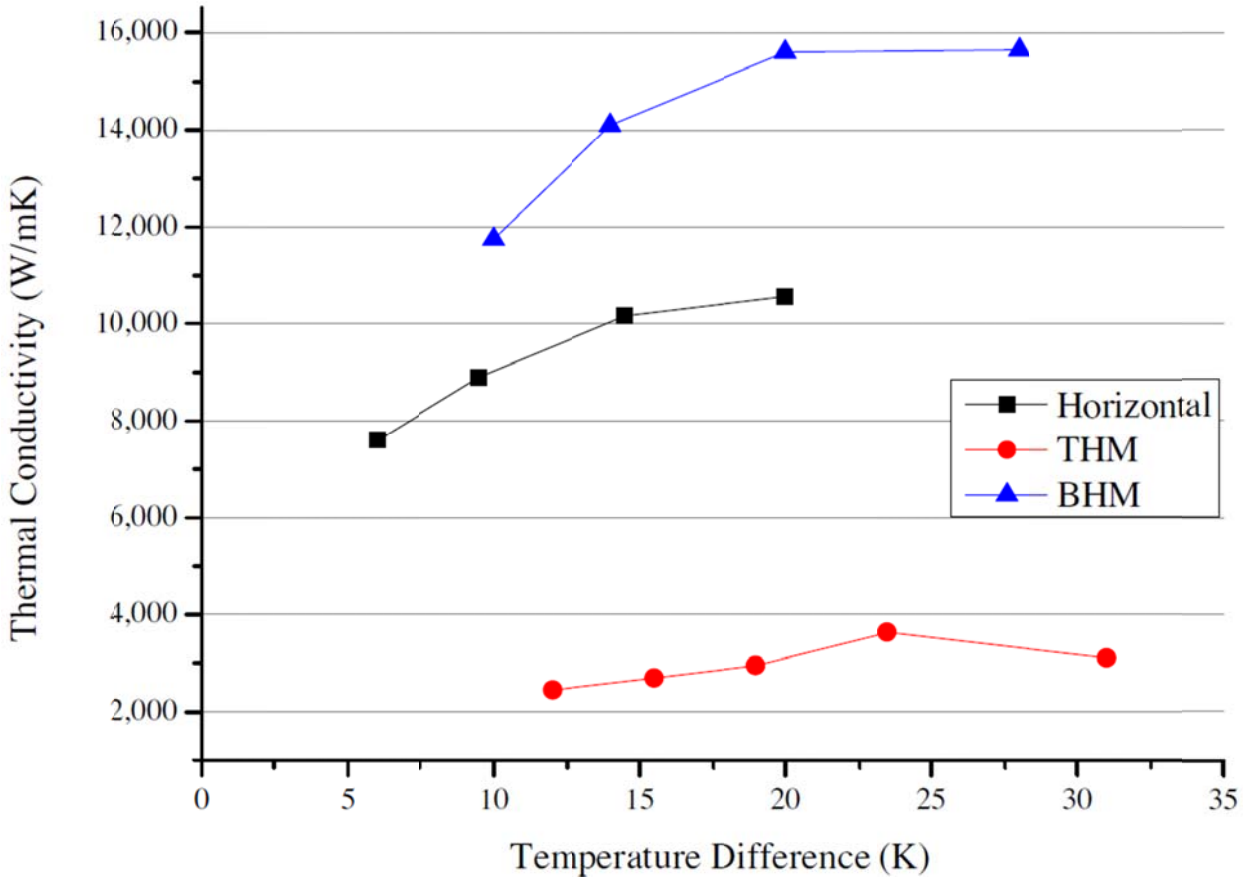

Figure 9: Effective thermal conductivity vs. evaporator/condenser temperature difference for a nitrogen PHP at different orientations [12].

2.2.4 Thermal Conductivity

The metric commonly used to determine the quality of performance is effective thermal conductivity, derived from Fouriers law:

$$K_{eff} = \frac{\dot{Q}L}{A\Delta T}$$

Equation 2: Effective thermal conductivity.

Where Q is the heat input to the evaporator section, L is the Length of the adiabatic section, A is the total area of heat transfer (number of turns times cross-sectional area of tubes), and ΔT is the temperature difference between the evaporator and condenser sections. The units of K_{eff} are

W/m-K. Thus, effective conductivity is calculated at each fill ratio and an optimum fill ratio is found. Other investigators such as Yang et al. define an optimal fill ratio as the fill ratio where maximum heat throughput is achieved without evaporator dry-out [13].

It is important to notice that normalizing by ΔT makes this method the same as the first method described. The author recognizes that effective thermal conductivity does not entirely capture the conductance per mass for PHPs. However, it is the standard valve reported in the literature for these devices and does provide some indication of the relative performance between PHP designs.

This brings us to an important characteristic of PHPs: dry-out. As described above, dry-out occurs when the heat flux of the evaporator section causes an excess amount of vapor to exist in the evaporator section and the thermo-hydraulic heat transfer method of the PHP ceases. If the liquid film at the wall evaporates and is not replenished, the temperature in the evaporator increases. At lower fill ratios, dry-out tends to happen at lower heat loads than at higher fill ratios due to a lack of sufficient liquid to replenish the evaporated liquid at the wall. Virtually all investigators including the author have observed this phenomenon. The opposite of dry-out can occur at very high fill ratios. At fill ratios above 80%, investigators have seen PHPs behave like thermosiphons. Khandekar et al. found that their PHP actually performed better at 100% compared to 85% due to the single-phase thermosiphon mode present at 100% fill [6].

2.2.5 Capillary Tube Dimensions

The capillary tubes are the most important part of a PHP because they are the path for heat transfer between the evaporator and condenser. The dimensions of the tubes is very important to ensure successful operation of the PHP. Holding all other experimental factors

constant, decreasing the tube diameter from a critical value has a negative effect on the performance of a PHP. Also, a smaller diameter tube results in less liquid in the system, which decreases the amount of available sensible heat transfer [14]. As previously mentioned, a great property of PHPs is their ability to work without the requirement of a pumping system. The heat input to the device and the constant cooling of the condenser provide the necessary input power for the thermally driven oscillations. While it is generally beneficial to have relatively large tube diameter, the dominant forces on the bubbles and liquid slugs in a PHP system needs to be surface tension forces rather than buoyancy forces in order for the thermo-hydrodynamic oscillations of a PHP to work in any orientation. Thus, each tube needs to be of sufficiently small diameter to facilitate operation in any orientation as depicted in Figure 10 [6].

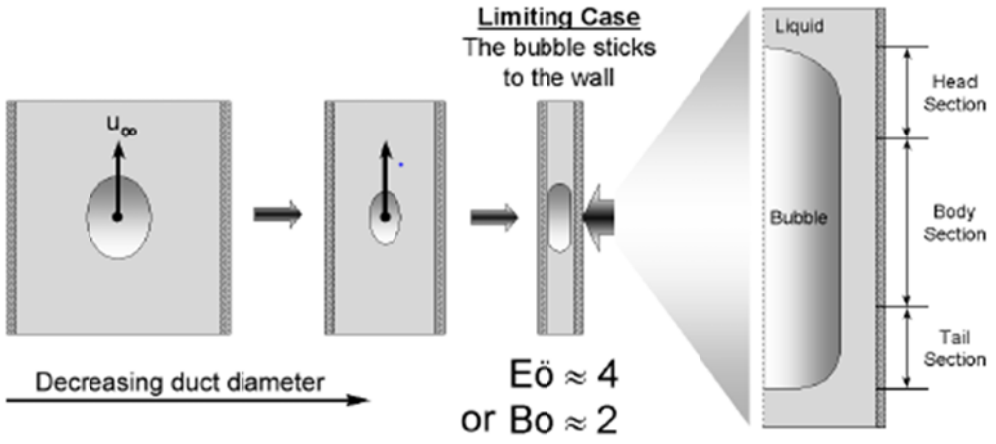

Figure 10: Depiction of bubble velocity dominated by surface tension rather than buoyancy [6].

The buoyancy force and other forces acting on the bubble govern the velocity with which a bubble moves through a tube. The following non-dimensional numbers represent these force balances:

$$\text{Froude Number} = Fr = \frac{\rho_{liq} \cdot u_{\infty}^2}{Dg(\rho_{liq} - \rho_{vap})} = \frac{u_{\infty}^2}{Dg} \qquad \text{if } \rho_{liq} >> \rho_{vap}$$

$$\text{Poiseuille Number} = Ps = \frac{(u_{\infty} \cdot \mu_{liq})/D}{Dg(\rho_{liq} - \rho_{vap})} = \frac{(u_{\infty} \cdot \mu_{liq})/D}{Dg\rho_{liq}} \qquad \text{if } \rho_{liq} >> \rho_{vap}$$

$$\frac{1}{\text{Eötvös Number}} = \frac{1}{Eö} = \frac{(\sigma/D)}{Dg(\rho_{liq} - \rho_{vap})} = \frac{(\sigma/D)}{Dg\rho_{liq}} \qquad \text{if } \rho_{liq} >> \rho_{vap}$$

Equations 3-5: Non-dimensional numbers useful in PHP capillary tube design.

The internal diameter of the tube is the characteristic dimension represented in each of the above equations. The Froude Number is relevant when viscous forces and surface tension can be neglected. When viscous forces dominate, the Poiseuille Number is relevant. The case of interest for a PHP is when surface tension dominates, thus the Eötvös Number is relevant. However, velocity is not present in the Eötvös number so this number cannot be used directly to find the dependence of velocity under surface tension dominant systems. Since the three aforementioned non-dimensional numbers represent the general solution to a force balance on a bubble, a fourth number can be conveniently used to facilitate an analytical solution [15]:

$$\text{Property number} = Y = \frac{g \cdot \mu_{liq}^4}{\rho_{liq} \cdot \sigma^3} = \frac{Ps^4 \cdot Eö^3}{Fr^2}$$

Equation 6: Property number governing PHP bubble flow.

Through an analytical solution by Bretherton et al., it was shown that as tube diameter decreases the Eötvös number should tend to zero and the bubble rise velocity should follow this trend and approach zero [15]. Experimental observations by Beardmore et al. contradict this analytical solution. Figure 11 below shows the results of an experiment carried out by Beardmore et al. in which the properties of various fluids were measured in order to calculate the non-dimensional numbers shown in Equations 3-5. The main conclusion of interest is that the Froude number, and in turn the terminal velocity of the bubble, does not equal zero when the Eötvös number is zero. It is actually equal to zero when the Eötvös number is equal to ~4. Thus a critical diameter, below which surface tension dominates the bubbles movement, can be found using Equation 6 [16].

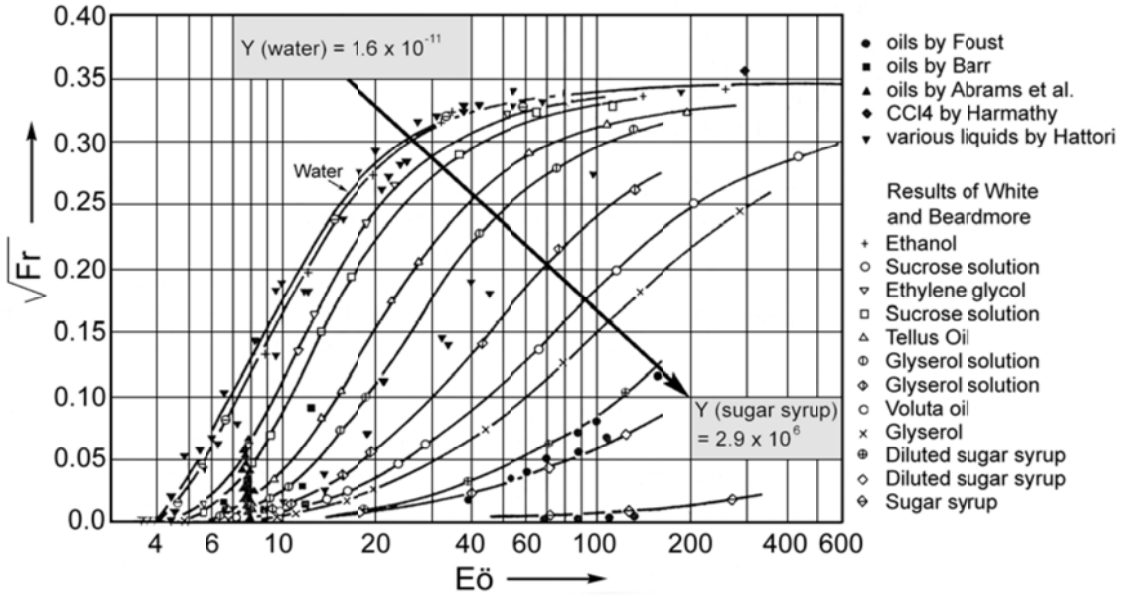

Figure 11: Results for cylindrical air bubbles rising in vertical tubes. Square root of Froude number (proportional to velocity) is plotted against Eötvös for various fluids represented by their property number (Equation 6) [16].

$$(\text{Eö})_{crit} = \frac{D_{crit}^2 \, g \, (\rho_{liq} - \rho_{vap})}{\sigma} \approx 4 \text{ or } D_{crit} \approx 2 * \sqrt{\frac{\sigma}{g \, (\rho_{liq} - \rho_{vap})}}$$

Equation 7: Critical diameter of capillary tubes.

For nitrogen at its ambient pressure saturation temperature, Dcrit = ~ 2mm. As mentioned above, it would be beneficial to have an internal tube diameter that is as close to this dimension as possible to increase the amount of heat transfer between the two ends of a PHP. However, some investigators aim to test multiple fluids with their PHP so it is necessary to choose a diameter that suits the properties of each fluid.

As long as the capillary dimension is below the critical value the PHP will operate, but the conditions and quality of performance can still vary with tube diameter. Yang et al tested two R123 PHPs with tube internal dimensions of 1 mm and 2 mm. The thermal resistance of the two PHPs varied with orientation according to Table 1 below. The thermal resistance of the 1 mm ID PHP was consistently higher than the 2 mm PHP. Furthermore, while the performance of the 1 mm ID PHP was not as good as the 2 mm, the 1 mm exhibited almost no orientation-dependent performance. [28]

Table 1: Minimum thermal resistance (K/W) for both 1 mm and 2mm ID R123 closed-loop PHPs (CLPHPS) in horizontal heating mode with fill ratio =30%, 50% and 70% [28].

Filling ratio (%)	ID = 1 mm	ID = 2 mm
30	0.59 (Q = 75–110 W)	0.36 (Q = 230–350 W)
50	0.42 (Q = 250–360 W)	0.36 (Q = 250–400 W)
70	0.50 (Q = 150–250 W)	0.41 (Q = 120–300 W)

Not only does diameter of the tubes have an effect on performance, their shape is also significant. Hua et al. studied the influence of tube geometry on performance by testing circular and rectangular tube geometries. This study showed that the start-up process of a rectangular PHP shifted from a "sudden start-up" to a "smooth start-up" with increasing heat load, as seen in Figure 5. The start-up heat flux of a rectangular tube PHP was 1.5-2 times greater than the circular tube PHP. Furthermore, the thermal resistance of the rectangular tube PHP was 30-40% lower than the circular PHP [9].

3 Need for technology

3.1 Cryopropellant Thermal Management Systems

PHPs have been the subject of several studies to determine their performance in microgravity. Gu et al. flew a micro pulsating heat pipe in reduced gravity and saw improved performance compared to orientation dependent performance under normal conditions [17]. Mameli et al. proved that the orientation dependence of a PHP still exists in microgravity and thus ground-based tests can be successfully extrapolated to represent PHP performance in

microgravity [18]. When operating in horizontal mode, Mangini et al. tested a Thermosyphon/Pulsating Heat Pipe with a diameter larger than the critical limit and showed that while their device performed strictly as a thermosyphon in normal gravity conditions, in microgravity the device exhibited PHP behavior [19]. This group also showed that the hyper-gravity portion of a parabolic flight was able to eliminate partial dry outs.

Reduced-boil off cryogenic propellant systems have become a concept of interest to NASA engineers as more rigorous and lengthy space missions are proposed. Current methods will eventually be irrelevant for proposed missions to Mars or other low-earth orbit tasks. Reducing the boil-off of a cryopropellant allows for longer mission durations by conserving fuel. Analytical and experimental methods such as those presented in Platcha et al. and Feller et al. aim to justify the added mass and complexity of an actively cooled system. Platcha et al. showed that compared to passive-only methods, a helium chilling boil-off reduction system begins to reduce system mass if mission durations are as low as 40 days for LH_2 and 14 days for LO_2 [20]. Experimentally, Feller et al. showed that actively cooling a thermal radiation shield using a Stirling type cryocooler could reduce the heat leak to a LN_2 tank (a propellant tank simulator) by 82% [21].

To date, there has not been any research done using a PHP as a distributed cooling system for any application including spacecraft. It is necessary to prove a PHP with multiple heat pick-up points can operate successfully in the laboratory. The technology will need to be adapted for multiple heat pick up points if it is to be used as a distributed cooling system for cryogens in space. The intention of this work is to prove that a PHP can operate with multiple evaporators as a first step toward implementation in distributed cooling and heat spreading applications.

3.2 Distributed Cooling for Server Rooms

While the focus of this research is on cryogenic PHPs, it is important to note that the findings of this thesis could be extrapolated to room temperature PHP systems. PHPs have been investigated for use as a distributed cooling system for servers. Recently the increased demand for data processing, data storage, and digital telecommunications have brought about dramatic growth in the data center industry. Energy statistics indicate that, worldwide, the data center industry is responsible for 1.3% of electricity consumption. Furthermore, 25-30%, or 30 Billion Watts, of the worldwide consumption of power for data centers comes from U.S. users [22]. Data centers consume a lot of power, but they are not very efficient. Green Grid is an association of IT professionals seeking to improve the energy efficiency of data centers by proposing short and long-term solutions. They define a metric called power usage effectiveness (PUE), which they use to determine how much of a facilities power (all power required including cooling systems) goes to IT equipment power (load associated with all IT equipment); a number near one is desirable. Currently many data center have PUEs near 3.0, but with proper design, a value of 1.6 can be attained [23].

Cooling systems consume 30% of the facility power at data centers [24]. Thus, one way data centers can improve their PUE is to improve cooling systems. Current conventional methods of cooling servers are called computer room air conditioning (CRAC) and computer room air handler units (CRAH). Figure 12 shows an air-cooled data center. The cold side and warm side of server racks face each other and chilled air is introduced to the cold side through vents in the floor. The air passes through the server racks and the warm side air is recirculated into an air-chiller system. There are many documented issues with cooling servers using this method as outlined by Khandekar [25]:

1) The poor thermal properties of air result in a low convection heat-transfer coefficient and the low specific heat of air results in a large temperature rise of the air. This can cause up to a 30-degree temperature gradient across the server.
2) Localized hot spots can cause the temperature in a specific location to reach dangerous levels. To combat this the air temperature needs to be set unnecessarily low as not exceed manufacturer specified maximum equipment temperature.
3) The cooling system needs to operate at all times regardless of outdoor conditions.
4) This type of cooling system is inherently indirect because the heat picked up from the equipment is circulated throughout the server room and recycled.

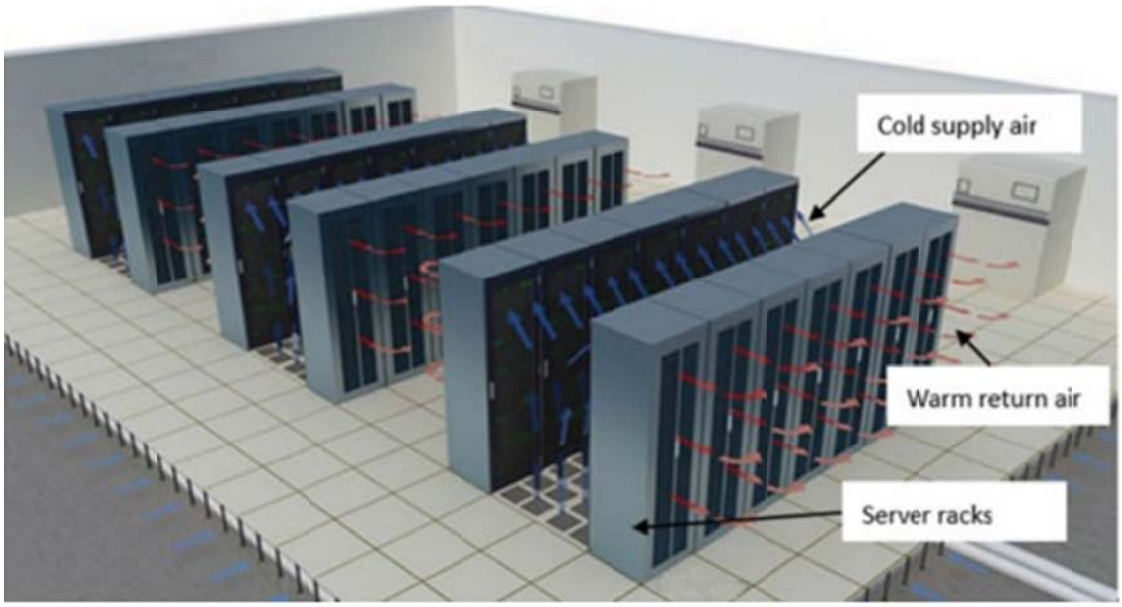

Figure 12: Depiction of a computer room air-handler (CRAH).

Various methods such as single and two-phase cold-plate based liquid cooling systems, integrated microchannel cold plates and heat-pipe-based systems have been investigated. The system that is best suited to this project is distributed heat-pipes.

Multiple investigators have researched a distributed cooling system using heat pipes. Tian et al. investigated a theoretical distributed heat pipe system, which utilizes chilled water to cool multiple loop heat pipes (LHPs) connected to server racks. Figure 13 shows the cooling system. The theoretical analysis showed that facilities PUE could be reduced from 1.6 to 1.35 [25]. Qian et al. also investigated this same distributed heat pipe system and concluded that it could reduce energy costs by 26.8% when compared to a CRAH system [25].

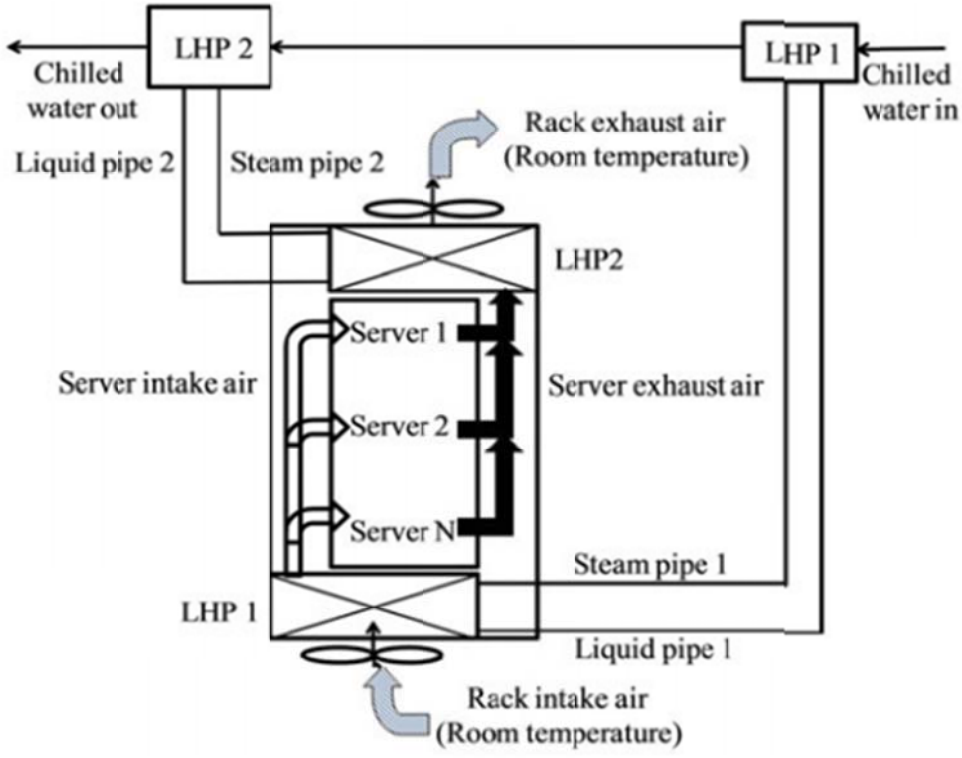

(c)

Figure 13: Diagram of a theoretical analysis on a distributed loop heat pipe system (LHP). LHP 1 precools the air and LHP cools the air re-entering the room. Both LHPs are cooled by chilled water [25].

In an attempt to combat the localized hot-spot issue with CRACs, Zheng et al., conducted an experimental study using heat pipes mounted in the back of server racks. The heat pipes were

cooled outdoors by chilled water and picked up heat by forcing air to each server rack individually. This type of system could be called a “cooled-directly-in-rack” system due to its minimal interaction with room air. Pictures and schematics of the cooling system can be seen in Figure 14. This system reduced the energy consumption of a CRAC system by about 18% when used in the summer [25].

(a)

(b)

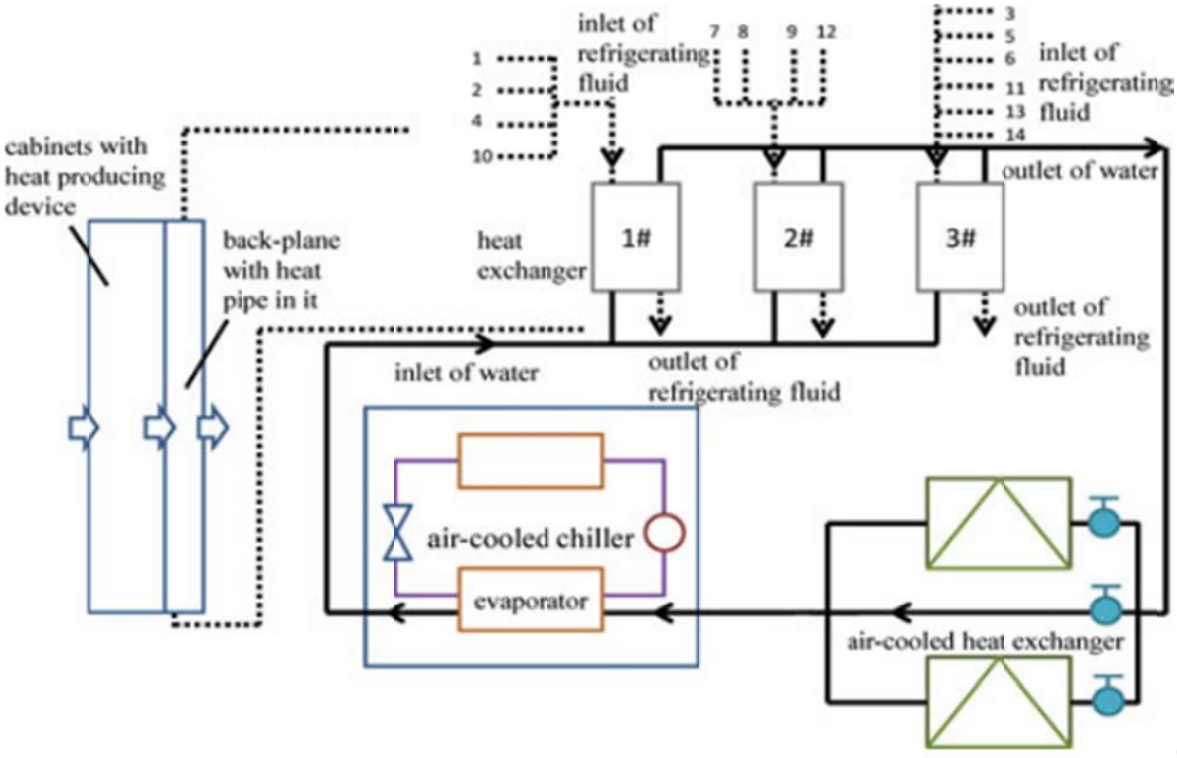

(c)

Figure 14: (a) Picture of heat pipe system mounted on the doors of server racks. (b) Cooling system for heat pipes. (c) Schematic of entire layout [25].

Ohadi et al. investigated another method of cooling. This group aimed to compare air, liquid and two-phase cooling of data center. Through CFD analysis, it was shown that a water or dielectric fluid cooled system could reduce the thermal resistance of the cooling system by up to 79% compared to an air-cooled system. The group also showed that thin film microchannel cooling using a two-phase refrigerant could reduce the thermal resistance of a system by up to 95% with a drastically reduced pressure drop compared to liquid cooled systems [26]. Two-phase refrigerant cooling can also eliminate the use of chilled water and the equipment necessary to chill the water.

The methods outlined above show that there is a need for improvement in server cooling to decrease costs and reduce the burden that server cooling imposes on the power grid. A pulsating heat pipe system could also be used as an alternative method to CRACs. Lu et al. studied the ability of a pulsating heat pipe to cool a server rack. This type of cooling is rack-level cooling compared to room-level cooling associated with air-cooled systems. Lu et al. made a rack with heaters to replicate the thermal load of servers, forced air, an R600a plate pulsating heat pipe and a chilled water system to cool the PHP. A schematic of the experimental setup is showing in Figure 15. These investigators do not offer much in terms of performance capabilities other than comparing the influence of changing chilled air velocity and heat load [27]. Nonetheless, it shows that the technology of server cooling can be influenced using pulsating heat pipes.

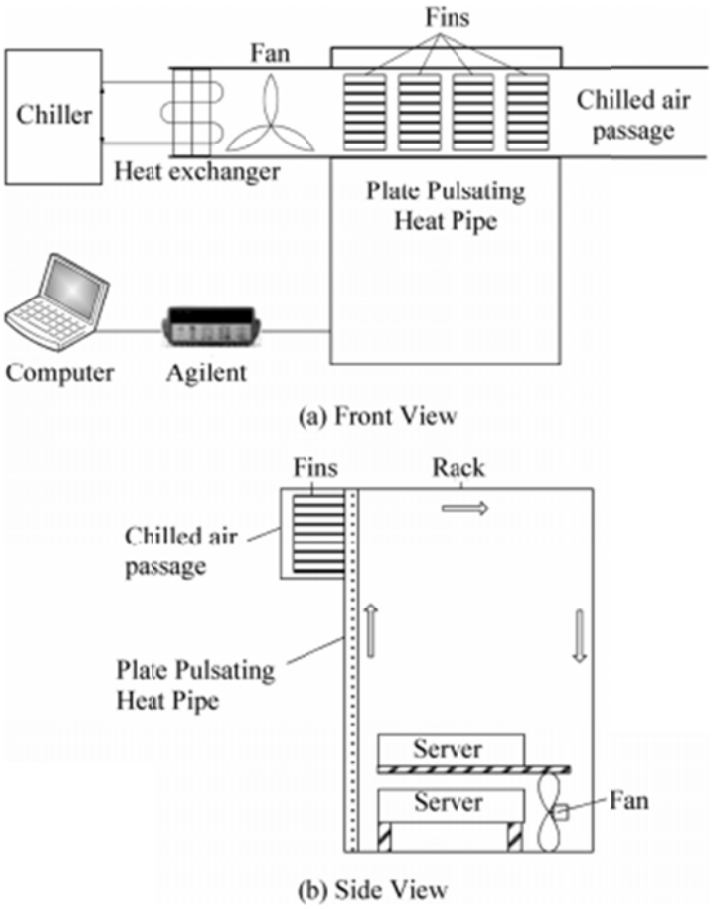

Figure 15: Layout of PHP server rack cooling system by Lu et al. air is forced over the server rack and absorbed in the back by a water-chilled PHP [27].

One cannot help but imagine a distributed cooling system using pulsating heat pipes to cool a server rack. The advantages such a system would have over the aforementioned systems are abundant. The proximity of water to server racks is eliminated, latent heat provides additional cooling, no pump would be required, the small diameter of PHP tubes could work nicely with microchannel-cooled racks and reduced interaction with room-air and PHP tubes would not be limited by the capillary limit like a standard heat pipe. Thus, it has been shown that investigating PHPs as a distributed cooling system is justified.

4 Experimental Setup

4.1 Intent of Experiment

In sections, 2 & 3 the work that has been done to demonstrate how PHPs operate and under which conditions they perform best has been summarized. Something that hasn't been done previously is demonstrating a PHP can operate with multiple evaporator sections and just one condenser. To do this, a 3-evaporator, 42 turn, cylindrical PHP was fabricated for operation with nitrogen at cryogenic temperatures. The capillary tube of the PHP meanders between the three evaporators and one condenser in a continuous loop similar to the schematic shown in Figure 16. Rather than having three separate PHPs, this configuration takes the multiple PHP concept one-step further and allows each PHP to interact with one another through the condenser. This arrangement simplifies assembly by maintaining one fill line and valve to room temperature. It is also possible to study the effect of heat spreading between the three sections, a concept that would lend itself to improved performance of a cryopropellant tank PHP system. The design, fabrication, assembly and instrumentation of the multiple evaporator PHP is discussed in detail in this chapter.

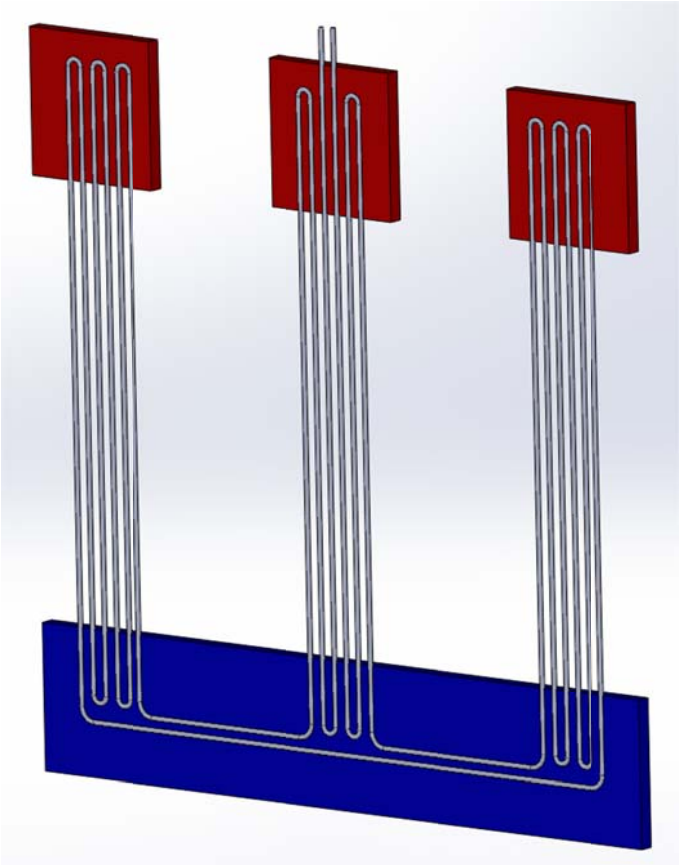

Figure 16: SolidWorks model of simple PHP schematic intended to show general concept of the relationship between each section of the PHP. Condenser shown in blue and three evaporators in red.

4.2 Preexisting Dewar

The PHP was constructed and installed in a preexisting Dewar developed by Luis Diego Fonseca to house his single evaporator nitrogen PHP. Therefore, the design of the multi-evaporator PHP needed to adhere to dimensions of this Dewar. It was also important to compare the performance of the single evaporator PHP with the split evaporator PHP so it was crucial to keep the dimensions relatively consistent. Furthermore, in the interest of time the original suspension system, fill line, cryocooler, thermal strap to the cryocooler, thermal jacket and MLI

from the single evaporator PHP test facility were used. A Creo model of the test facility is shown in Figure 17.

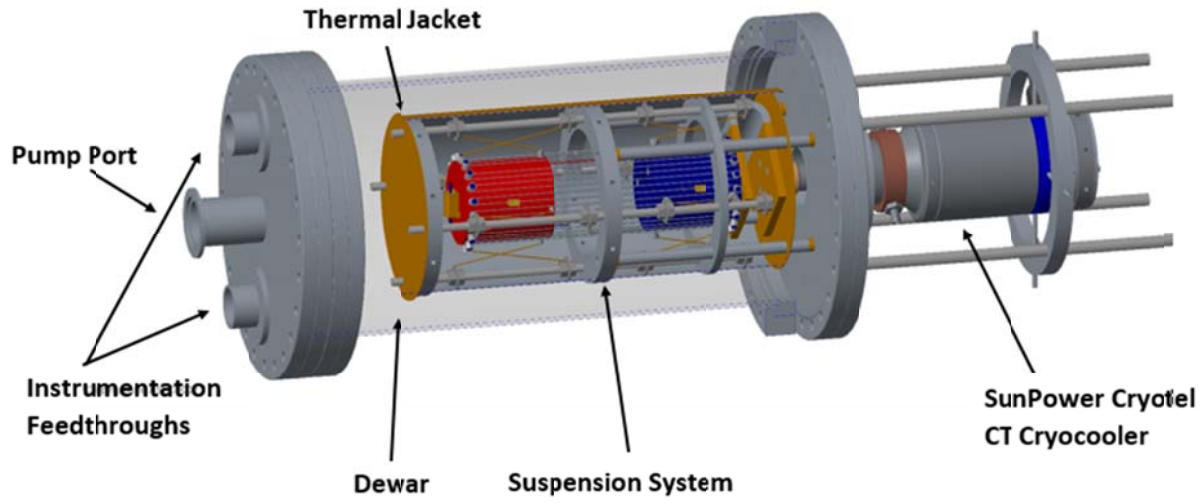

Figure 17: Creo model of test facility created by Luis Diego Fonseca.

4.3 Design considerations

4.3.1 Dimensions

As mentioned above, the dimensions of the PHP were chosen so that the PHP would fit into the preexisting Dewar. As seen in Figure X: $L_{evap} = L_{cond} = 70$ mm , $L_{adiabatic} = 80$ mm, for a total length of 220 mm as shown in Figure 18. A major design characteristic of PHPs is the number of turns between the evaporator and condenser sections. To keep the number of turns on each evaporator section equal, a number of turns that is even and divisible by three was chosen. Thus, to keep relatively consistent with the number of turns on the single evaporator PHP (40) 42 turns was chosen. The diameter of the evaporators and condenser,$D_{evap,cond} = 67.8\ mm$, was

set to effectively hold all 42 turns (21 on each side) while keeping in mind a minimum capillary tube bending radius of 2 mm.

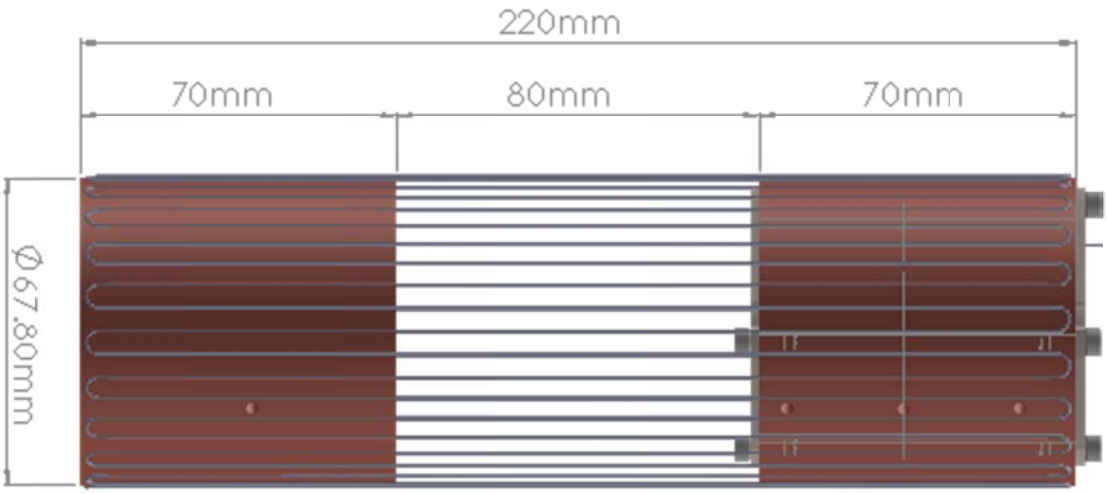

Figure 18: Orthographic view of SolidWorks model of PHP showing dimensions.

4.3.2 Evap/Condenser Design

The thickness of the evaporators and condenser section was minimized to reduce cool down time. However, this thickness needed to be sufficiently thick because the sections needed to be isothermal and heat applied to each evaporator section and the heat received by the condenser section needed to be distributed uniformly across the entire section. It was decided that four equally spaced heaters would be attached to the backside of each evaporator section and wired together in series as seen in Figure 19. A $1/16^{th}$ symmetry 2-D finite difference model was implemented in Engineering Equation Solver [32] to determine the proper thickness to ensure each section was isothermal. Figure 20 shows a contour plot created with the model and shows that the maximum temperature difference across each evaporator and condenser section is 0.2 K

for a thickness of 6mm. This temperature gradient was deemed to be acceptable. The details of this model can be seen in Appendix D.

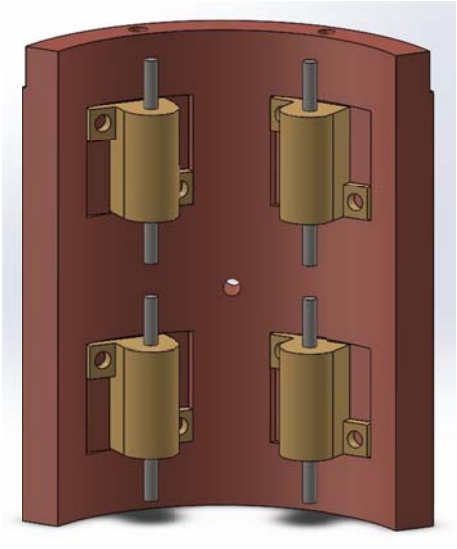

Figure 19: SolidWorks model of one evaporator section displaying four 30 ohm heaters on the backside.

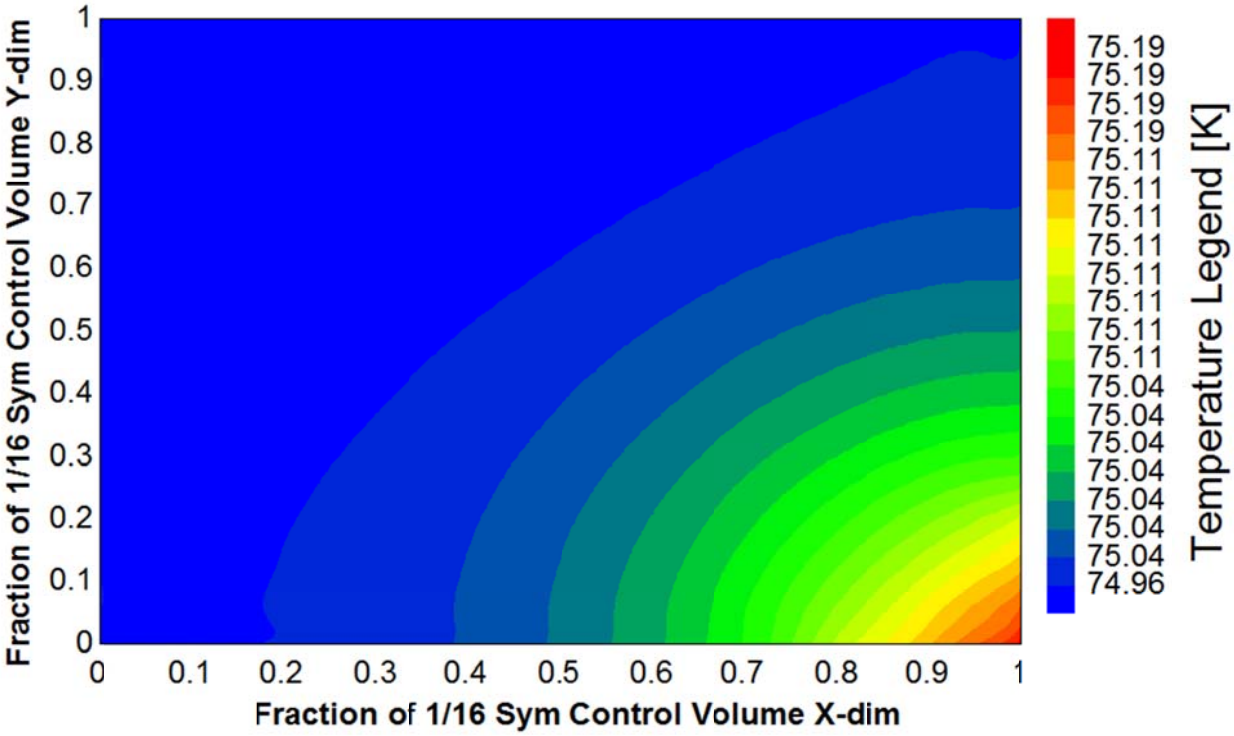

Figure 20: Result of 2-D finite difference model of evaporator section. Maximum temperature gradient is ~0.20 K.

To maintain structural rigidity, laser-cut stainless steel supports were made to hold the evaporator sections together while keeping each evaporator section thermally isolated from the others. The heat leak between each section was calculated to be only 1% of the input load at a heat load of 2 W. These supports are henceforth referred to as “spokes” and are shown below in Figure 21. The spokes were laser-cut out of 304 stainless steel by GenMet Corp in Menomonee Falls, WI.

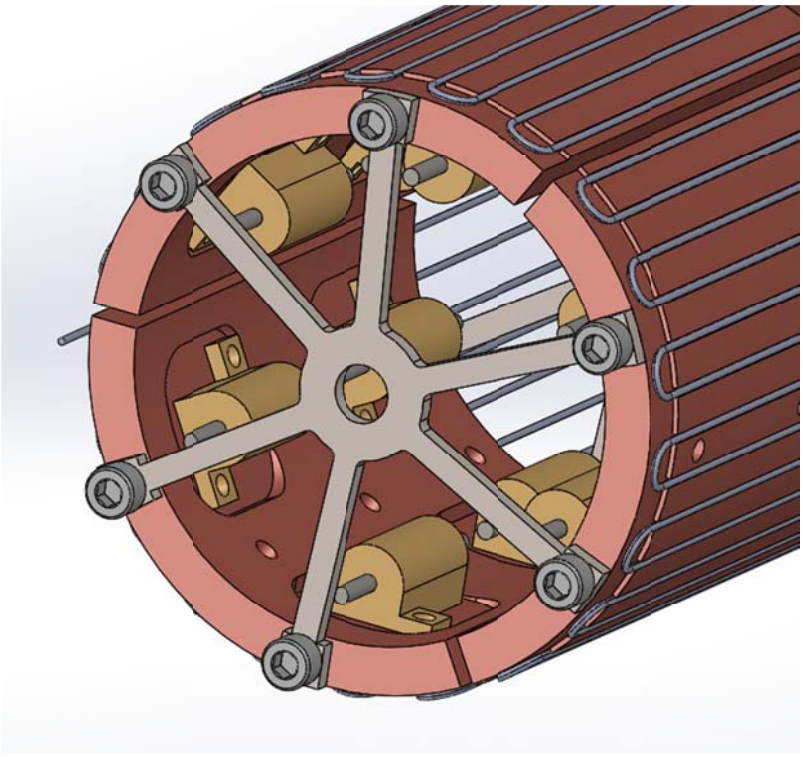

Figure 21: SolidWorks model showing evaporator sections held together by stainless steel spokes.

4.4 Fabrication

4.4.1 Connecting Capillary Tubes

An important design feature of the PHP is grooves cut into each section intend to increase the contact area between the capillary tubes and the evaporator and condenser sections. Due to the complicated machining procedure and the difficulty involved with soft soldering small capillary tubes, a test piece was made to prepare for the actual machining process and soldering procedure. This test piece was also used to test different soldering methods. Shown in Figure 22, grooves were cut into the copper test piece using a 1 mm thick slitting saw and three different soldering methods were tested. The best method involved applying solder to the capillary lines, laying them in the grooves, heating the test piece and applying more solder to ensure maximum contact area. This method was used when soldering the actual PHP and will be discussed in more detail below.

Figure 22: Test piece used to practice machining and soldering techniques.

For the actual PHP parts, 0.9 mm deep grooves were cut into the face of each section using a 1 mm thick slitting saw. In total 84 grooves were cut. Once all the grooves were cut at 8.57-degree increments, the evaporator section was cut into three pieces using a larger slitting saw. Two holes were drilled and tapped on each evaporator section as attachment points for the suspension system. Six holes were added to the condenser section for the same purpose. Four flats were milled into the back of each evaporator section to create a surface for the four heaters that would eventually be attached to each section. Figure 23 below shows the evaporator and condenser sections post-machining and pre-soldering.

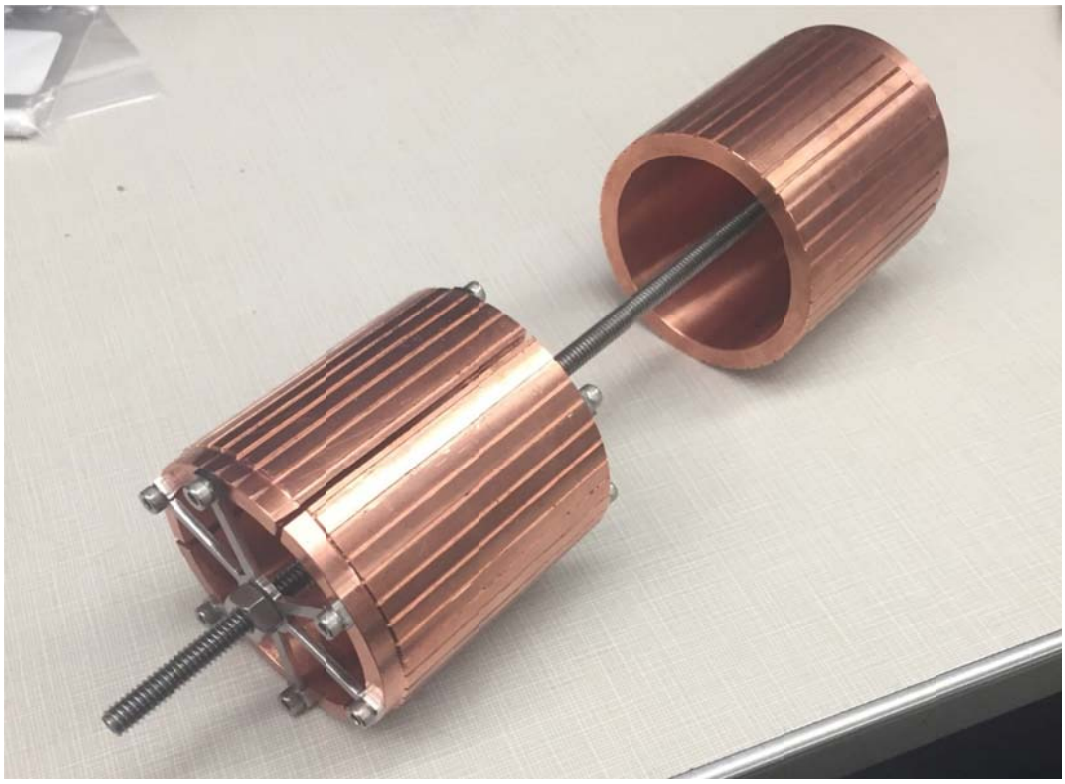

Figure 23: PHP post-machining

The three evaporator sections were held together using the laser-cut supports fastened to the top and bottom of each section. A threaded rod was inserted and fastened through the center of the condenser and evaporator sections to maintain alignment and rigidity during soldering.

One method for bending the capillary tubes that previous investigators have used is tapping holes on the evaporator and condenser sections and using shoulder screws to bend the tubes directly on the PHP. Instead of doing this, a fabrication jig was made to bend each of the 1.5 m, .5 mm ID, .8 mm OD capillary tubes. As seen in Figure 24, 5 grooves of the same dimensions of the PHP grooves were cut along the length of a 220 mm aluminum tube. 5 mm shoulder screws were turned down to 4.1 mm and threaded into the edges of the jig to provide turnbuckles for bending. A holding screw was tapped into the face of the jig to hold the tubes while bending. Since each length of capillary tubing was only 1.5 m, 7 sections needed to be bent and soldered together in the adiabatic section of the PHP. At each interface .85 mm ID copper tubing was used to couple the end of the capillary tubes. The jig was also used for spacing when soldering all the sections together.

Figure 24: Bending and soldering jig used to simplify PHP fabrication.

Once all the tubes were bent, acid flux was applied to the necessary areas of the tubes and rosin core solder was applied using a soldering iron. The tubes were fastened to the evaporator and condenser sections and held in their desired position using large hose clamps. Each side of the PHP was heating using a propane torch and solder was applied to the entire section while being sure to get as much solder as possible around the tubes and in the grooves. Rectangular thermometer posts were soldered to each evaporator section and the condenser section to house Lakeshore PT-103® platinum resistance thermometers [33]. The final product can be seen below in Figure 25.

Figure 25: PHP post-soldering. Notice copper joints, thermometer posts and heaters.

Next, Swaglok VCR® connections [34], shown in Figure 26, were brazed to the ends of larger stainless tubes with an internal diameter of 1 mm. These tubes were then brazed to the loose ends of the capillary tubes protruding from the PHP. These VCR® connections were used to fill the PHP by through a VCR® tee. This assembly and connection will be discussed further below.

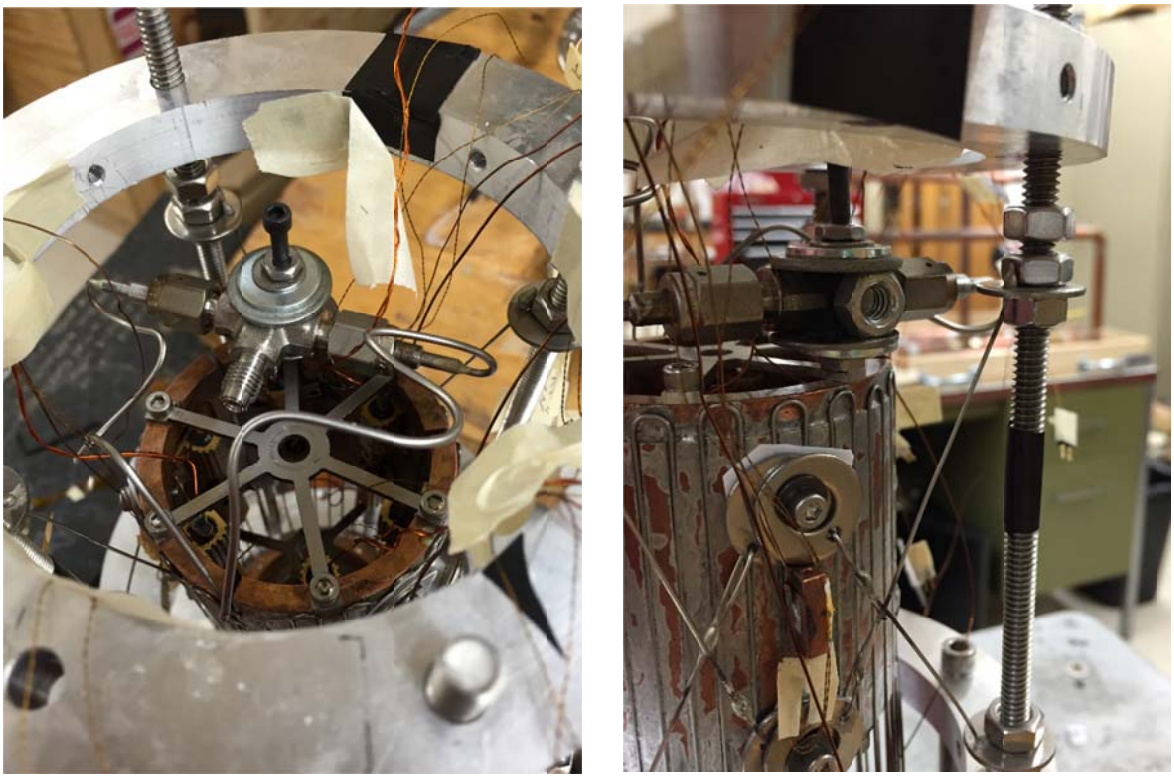

Figure 26: (left) Top view of PHP. Note VCR® tee. (right) Rear view of tee. Notice the attachment method which inherently interferes with evaporator section 1.

With the PHP soldered together and leak-tight, the 12 heaters were installed on the back of each evaporator section. Four 30-ohm aluminum heaters were connected in series by soldering copper wire between each heater. The ends of the series connection were then soldered to two different sets of leads: copper leads for delivering power to the heater circuit and stainless steel wires for measuring the voltage drop across the circuit. The assembled circuits were then attached to the back of each evaporator section using Stycast 2850® epoxy [35]. The top spoke was removed, a thin layer of the epoxy was applied to the back of each heater and the heaters were pressed into place and allowed to cure. The heaters can be seen in detail in Figure 27.

Figure 27: Close-up of heaters positioned on the back of each evaporator section.

4.5 Installation

At this point, the PHP was ready to be installed into the Dewar. The PHP was carefully lowered into the support structure and the condenser section was attached to the thermal strap that is attached to the cryocooler cold head. The stainless steel support wires were attached to the threaded holes on each section of the PHP. These wires were attached using washers and Teflon® to prevent the washers from damaging the capillary tubes once clamped down. The

support wires were tightened and the PHP was leveled using the support system designed by Luis Diego Fonseca.

To maintain rigidity the fill line tee was attached to evaporator section using a long fastener and a series of washers as seen in Figure 26 above. It is important to note that attaching the fill line in this manner is not ideal and creates an additional heat leak on section 1. This issue was addressed in a revised design that was implemented in the fall of 2016. The components of the redesign, shown in Figure 28, aimed to accomplishes few things: better thermal contact between the tee and the PHP, a smaller tee volume, a more direct path between the inlet and outlet, a comparably better conduction path from outlet-to-inlet and to heat sink the fill line to the thermal jacket. This was accomplished by fabricating the miniature copper tee shown in Figure 28, adding a 1.5 m section of 0.5 mm ID capillary between the PHP and the room temperature plumbing (spiraled and clamped under an aluminum plate) and soldering the fill line to the thermal jacket (covered in epoxy). These three changes can be seen in situ in Figure 29.

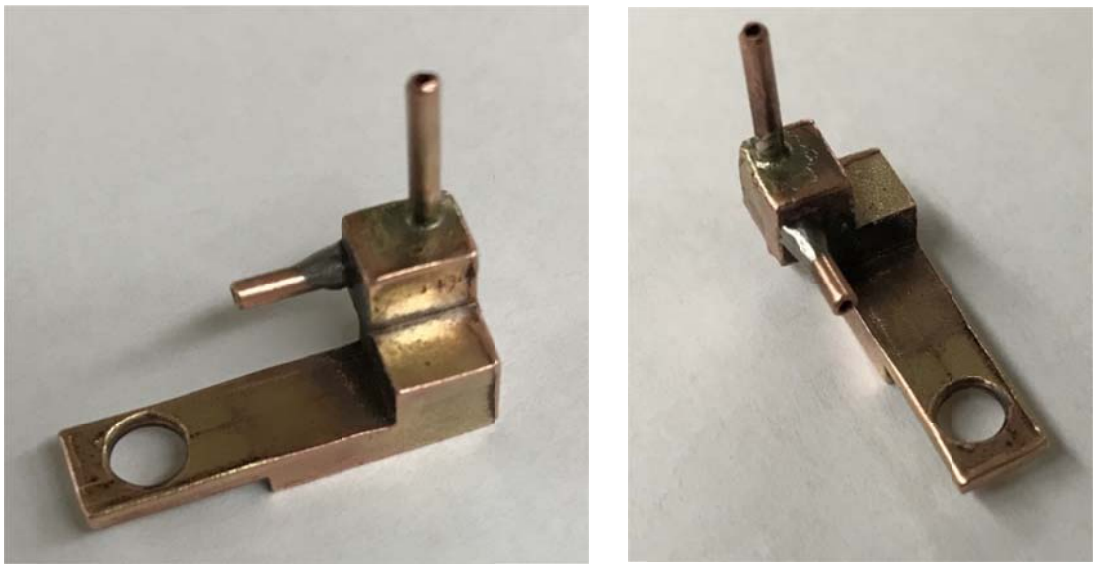

Figure 28: Miniture copper tee made during fill line redeisn of fall 2016. Dimentions are ~16 mm x 10 mm x 6 mm.

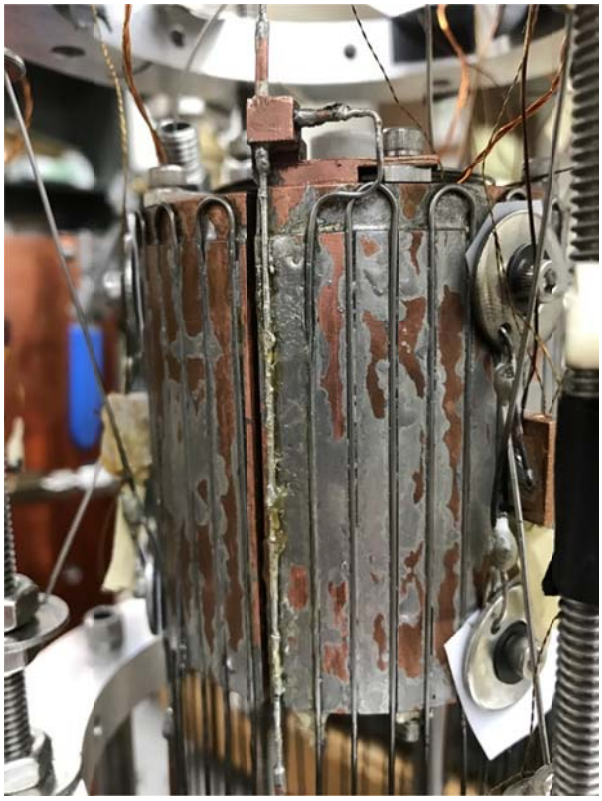

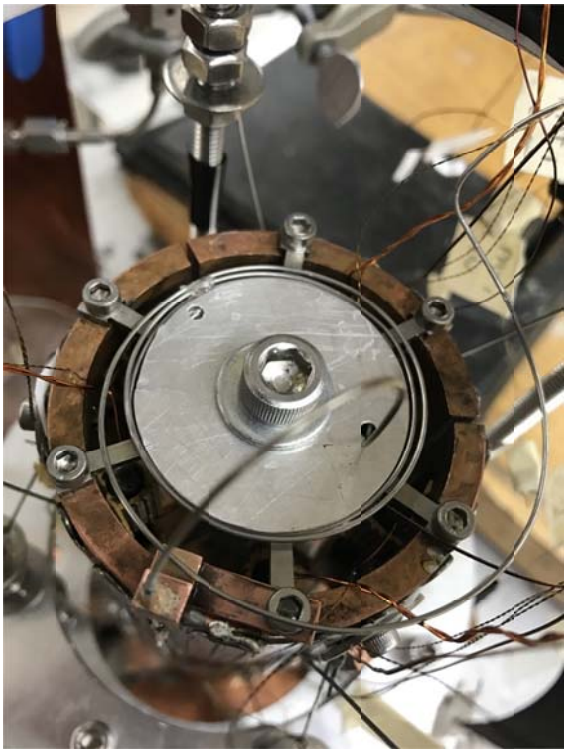

Figure 29: Results of fill line redesign of fall 2016. (top) New tee attached to evaporator sectoin 2. (left) Extended fill line campled (heat sunk) to spokes by aluminum plate. (right) Fill line soldered an exopxied (heat sunk) to thermal jacket.

4.6 Instrumentation

4.6.1 Thermometry

Five Lakeshore PT-103 platinum resistance thermometers [33] are used in this experiment along with one type-T thermocouple. Each evaporator section has a PRT fitted into its thermometer post, the condenser section contains one PRT (directly aligned with PRT on section 2) and the fifth thermometer is attached as close to the cold head as possible. Each thermometer location can be seen in Figure 30 below. The thermometers were fabricated using a 4-wire measurement method where one side of two sets of stainless steel leads were attached to each thermometer lead using acid flux and rosin core solder. The thermometers were inserted into their posts using a small amount of Apiezon N ® thermal grease [36]. The leads of the thermometers are heat sunk, according to Lakeshore standard [29], to their post using cigarette paper and GE varnish. This can clearly be seen in Figure 30.

Figure 30: (left) Thermometer post located on each evaporator section. (right) Thermometer post on condenser (directly aligned with PRT on evaporator section 2). (middle) Thermometer near cold head.

The five thermometers were calibrated after all data was collected. The desired quantity for this experiment is the temperature difference between each evaporator and the condenser. All thermometers were calibrated according to the method outlined in Appendix A to find the offset to apply to each temperature measurement. Once this value was found, it was offset from all data before analysis.

The thermometers are powered using a Lakeshore 120 [33] current source with the exception of PRT5, which is intended to represent the cold head temperature of the cryocooler. This thermometer is powered using the current output of the cryocooler controller that has a nominal value of 1 mA. In addition to being supplied to LabVIEW, the voltage measurement of this thermometer is also fed back to the cryocooler controller to allow temperature control of the cold head. A breadboard is used to connect PRTs 1-4 in series with a nominal current output from the Lakeshore 120 of 1 mA as seen in Figure 31. Each thermometer voltage was read and the temperature was computed using the ratio of polynomials equation for RTDs shown below in Equation 8 [38].

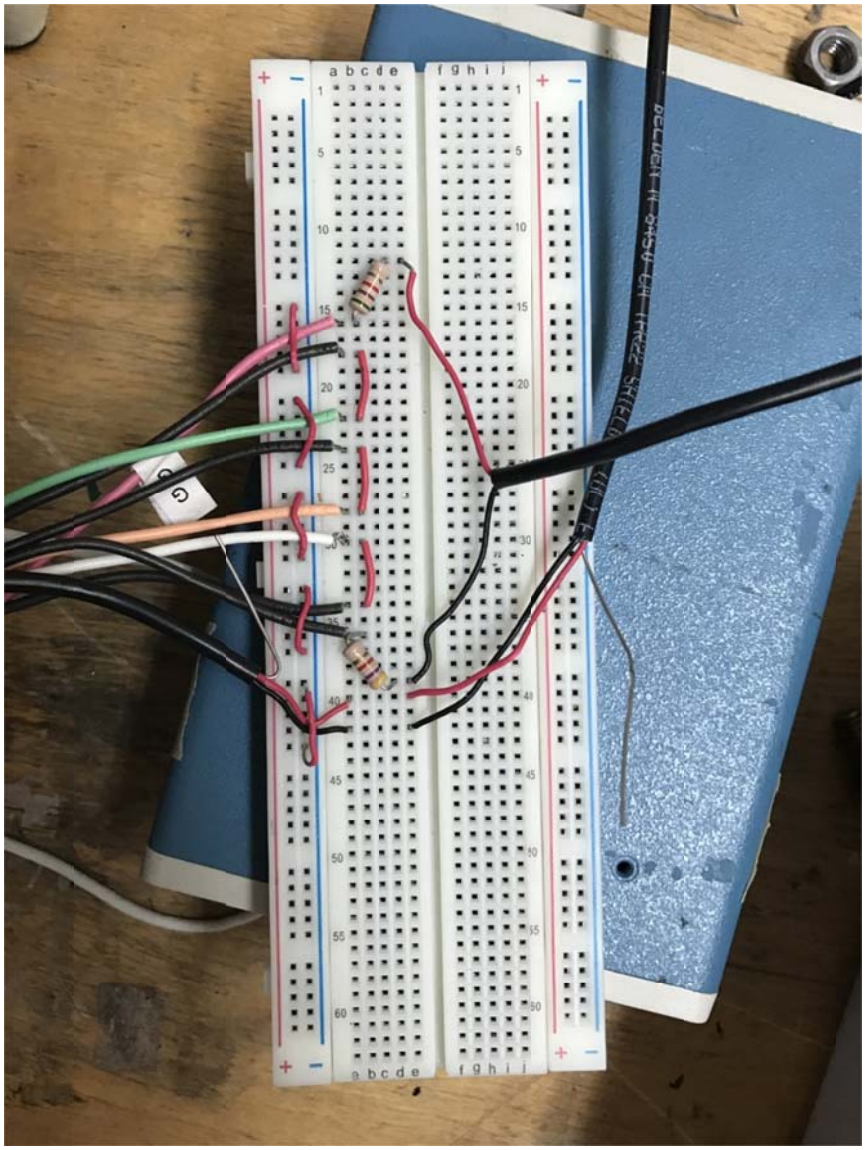

Figure 31: Circuit supplying current to all 5 thermometers.

$$T = c_0 + \frac{R\left(c_1 + R\left(c_2 + R\left(c_3 + c_4 R\right)\right)\right)}{1 + R\left(c_5 + R\left(c_6 + c_7 R\right)\right)}$$

Equation 8: Temperature [C] as a function of platinum resistance [38].

Table 2: Values of coefficients in Equation 8.

c_0	c_1	c_2	c_3	c_4	c_5	c_6	c_7
-245.19	2.5293	-0.066046	4.0422E-3	-2.0697E-6	-0.025422	1.6883E-3	-1.3601E-6

The one type-T thermocouple is used to measure the temperature of the thermal jacket and is uncalibrated because the measurement is not very critical. The thermocouple is soldered to a small thin piece of copper and epoxied to the inside of the thermal jacket near the top in order to represent the highest temperature of the jacket (furthest from the cold head).

4.6.2 Heaters

The four-wire heater measurement has evolved throughout the experiment. The measurement was originally made by measuring the voltage across a 26-Ohm resistor, which was in series with the current going into the heater in order to measure that current. This current was then multiplied by the measured voltage drop across each heater circuit to get the power applied to the system by each heater. The measurements were made using two multimeters and the power was calculated by the user using a standard Texas Instruments calculator. Since fall 2016, as part of an entire measurement system overhaul, the power was measured using a more sophisticated method utilizing op amps and LabVIEW. The intention was to be able to control the power applied to the heaters using LabVIEW and to control the heat automatically by stepping through a list of powers. This has proven to be incredibly useful.

A 0-5 V signal is output from LabVIEW to a USB 6009 DAQ [37], this signal is amplified using an op amp with a gain of 2. This signal is then received by a Tenma 72-2005 [39] power supply and drives a 0-24 V voltage output proportional to the 0-10 V input signal. This signal is then sent to a control box, shown in Figure 32, where it is split into three voltage signals, one for each heater. Each signal is then run through a potentiometer to independently control the heat applied to each section. The signal is then passed through a ~2 Ohm resistor and the voltage drop across the resistor is measured to find the current going into each heater.

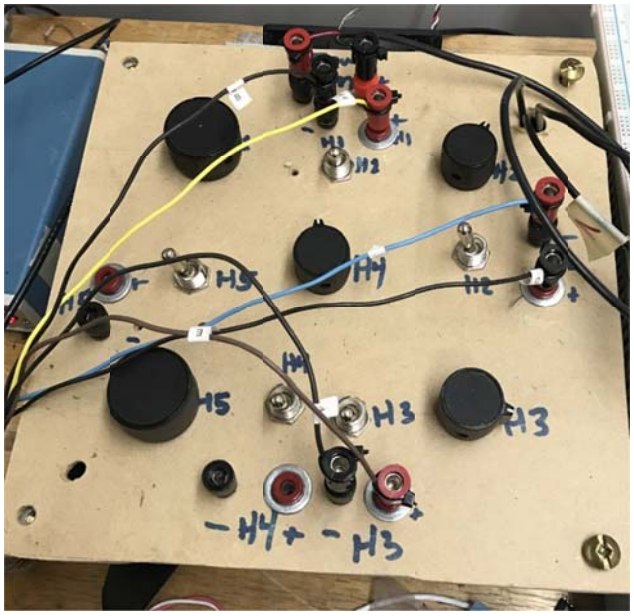

Figure 32: Heater box used to independently control the heat load on each section.

Since the + and – sides of this differential voltage measurement across each resistor can exceed the 10 V maximum analog input of the USB 6009 DAQ, differential op amps and a breadboard are used for each signal. This type of op amp simply subtracts two voltage inputs and returns the result. This voltage is then sent to LabVIEW, multiplied by the precisely measured ~2 ohm nominal resistance and Labeled as I_R. The + end of the differential voltage measurement across each heater is also too large for the DAQ to handle so this signal is reduced using op amps with a nominal gains of 0.5 and sent to LabVIEW, multiplied by the precisely measured gain and labeled as V_H. The power dissipated by each heater is then the product of V_H and I_R. The entire set up is shown in Figure 33

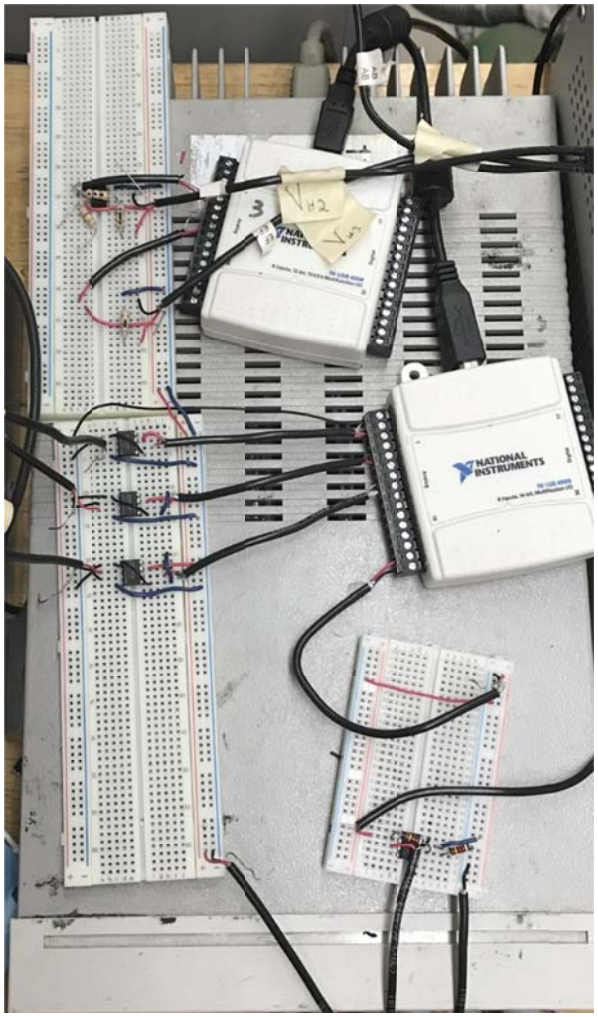

Figure 33: View of op amps, differential amps and daqs.

As it turns out this method is not a very accurate one. The current received by the heaters is accurately controlled, but the measurements of V_H and V_R and very inconsistent. Even after several hours were spent trying to improve these measurements the measurement still proved to be inconsistent. A better solution would be a so-called “magic box” in which all components are soldered together neatly and precise resistors are used. In the interest of time, heater powers are calculated using a V^2/R method: the voltage across the heaters is measured using a Hewlett Packard (HP) 34401a® [40] millimeter and divided by a measured total heater

resistance at 77 K of 118.2 Ohms. This is not the most accurate method for determining power, but it has nonetheless proven to be effective. See Appendix A for error analysis.

4.6.3 Pressure

Two different Endevco 8530B® pressure sensors [41] are used in the experimental set up. One is used to measure the pressure in the holding tank and one is used to measure the dynamic pressure of the PHP system. The excitation for both is provided by a HP 3611a DC power supply [40] set to output 10 V. The sensors that were originally absolute pressure measurement devices were calibrated to using a MKS Baratron pressure gauge [42]. The voltage output of the sensor was measured at five different pressures and compared to the pressure measured by the Baratron. The ambient pressure was recorded during this calibration. (For more accurate results, this pressure could be measured every day and subtracted from any pressure measurements to be contingent with calibration.) A linear best-fit line was applied to these measurements and the equation of this line is used in LabVIEW to calculate an absolute pressure based on the voltage measured.

The vacuum pressure is measured using a thermocouple gauge. The gauge is installed near the turbo pump and is predominantly used to determine when to turn on the turbo pump.

4.6.4 Data Acquisition

The main data acquisition device is part of the National Instruments (NI) SCXI family . The set up consists of a SCXI 1300 Module connected in series with an SCXI 1110 Multiplexer, a SCXI 1000 chassis and a USB 6363 A to D converter (All [37]). A downfall of this set up is that only one channel can be read at a time and a 0.20 second ramp up occurs when switching between channels. Thus, creative methods have to be used to acquire data using LabVIEW. At a

sampling rate of 30,000 S/s and a sample count of 15,000 the first 65% of each temperature measurement is ignored to counteract the effects of the ramp up. In addition, each time a measurement is complete, the LabVIEW task is cleared and a new task involving the next channel is created. Other things such as voltage output for slaving the Tenma 72-2005 power supply [39] and the voltage measurements for calculating heater power are done using NI 6008 and 6009 devices [37].

4.6.5 Safety Valve

A safety valve is hooked up in parallel with the room temperature fill lines and set to crack at 80 psi, which corresponds to a saturation pressure of ~95 K. This pressure allows for continued operation if the input heat flux is high enough to drive the condenser temperature to a temperature approaching 95K while protecting the system against an event where the cryocooler turns off unexpectedly.

4.6.6 Cryocooler

The cold end of the PHP is cooled with a SunPower Inc. Cryotel CT Stirling type cryocooler [43]. The warm end of the cryocooler was originally cooled with fins and forced air, but in the spring of 2017, a water jacket was fabricated to increase the efficiency of the cooler. Before the water jacket was added the cryocooler could only achieve ~5.5 W of cooling at a temperature of 79 K. After the water jacket was installed the cooler could achieve the same cooling power but at a temperature of 72 K. The jacket is cooled using a Polyscience 575 water chiller [44]. Due to complications with the water jacket, it needed to be replaced with a temporary jacket. Once these complications are solved, the original jacket should be reinstalled for maximum performance.

4.7 Experimental procedure

Fill ratio is an extremely important experimental characteristic of pulsating heat pipes. The fill ratio is defined as the volume of liquid in the PHP to the total volume of the PHP.

$$V_{fill} = \frac{V_{liq}}{V_{PHP}}$$

Equation 1 Revisited

Other investigators have had success with fill ratios ranging from 20-80% [7] with varying system performance at different fill ratios. To precisely fix the fill ratio of the PHP a system of known volumes, pressure gauges and the ideal gas law are used. A schematic of the experimental setup can be seen below in Figure 34. First, the system is evacuated to a pressure of 10^-3 Torr through the purging valve (V1). Next valves 1, and 3 are closed. This isolates the cold end of the PHP and the pumping system. A large tank of ultra-high purity compressed nitrogen provides the working fluid to the PHP. This tank is connected to a small reservoir, which contains an Endevco pressure sensor. Fluid is allowed into the reservoir and the adjacent connecting lines. Knowing the pressure, volume and temperature of the fluid in the reservoir and connecting lines allows one to determine the mass of nitrogen contained in the volume using the ideal gas law. Next, valve 3 is opened, fluid begins to condense on the cold end and the pressure in the reservoir drops continuously. At a calculated reservoir pressure, valve 3 is closed. Based on the pressure drop of the reservoir the amount of mass that has moved to the cold end can be found. Knowing the volume, temperature and mass of fluid in the PHP the fill ratio is found. A detailed explanation of this calculation can be found in Appendix B.

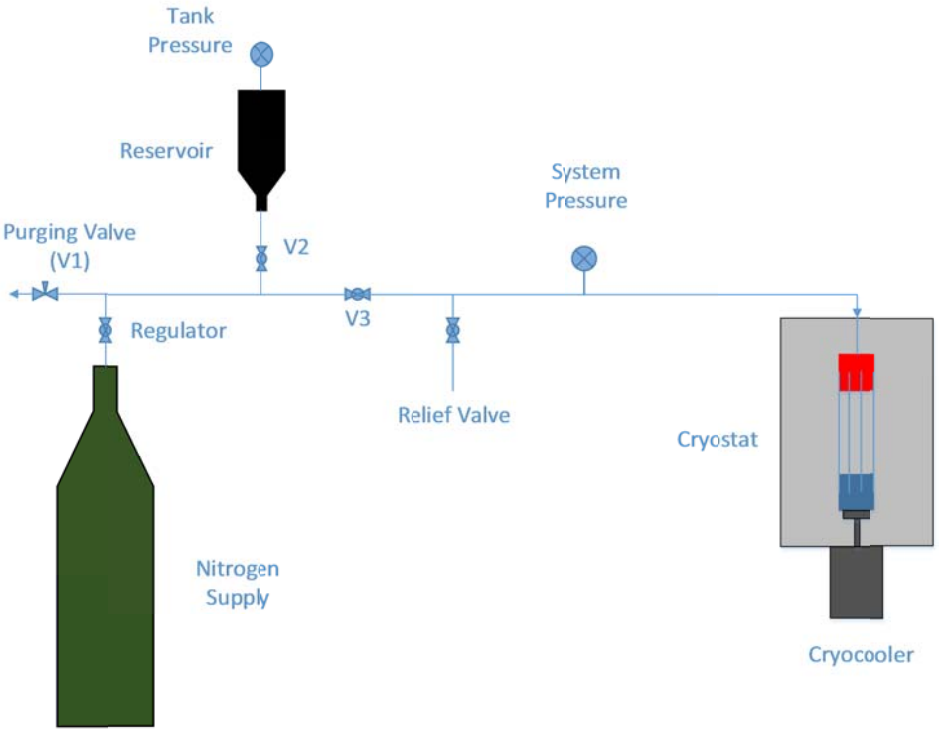

Figure 34: Schematic of PHP system.

5 Results and Discussion

The following section details the results found over the entire testing period of this project. Over this period, as the investigators understanding of how the PHP behaves grew, a myriad of result were seen and interpreted. The results in the beginning of this project were slightly misleading and confusing. As the investigators understanding of the system grew, successful operation of the PHP was eventually verified in early 2017.

5.1 Initial Results

5.1.1 Early Verification

During early tests of the PHP at a fill ratio of 80% and a heat load on each section of 1.25 W, successful operation was verified. The temperatures over time during this test are shown in

Figure 35. This run is classified as successful due to the relatively constant evaporator and condenser temperatures; however, a temperature difference between the evaporators and condenser was expected to be approximately 1 K rather than 5 K. This test proved that there was thermal communication between each evaporator and the condenser, but that under various conditions performance may improve.

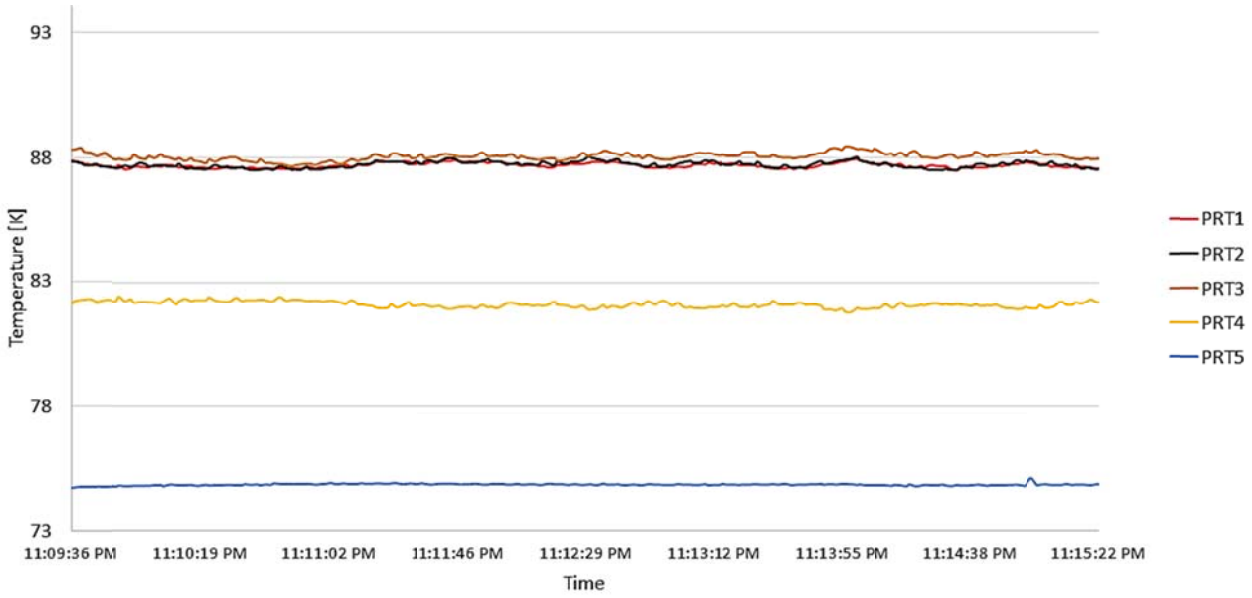

Figure 35: Temperature vs. time for run with 1.25 W on each heater and fill ratio of 80%.

5.1.2 Dry Out and Recovery

Once successful operation was proved, PHP performance with various heat loads on each section was investigated. One of the primary objectives of this project was to determine the performance of the PHP when different heat loads were applied to each evaporator section. Figure 36 shows a temperature vs. time plot for the following test. In order to observe the effect of turning off one heater, all of the heaters were initially set to 0.75 W. Once the system was stable, heater 3 was turned off while keeping heaters 1 & 2 at 0.75 W. A slight increase in the

temperatures of sections 1 & 2 and a decrease in the temperature of section 3 was observed. Also, the temperatures of sections 1 & 2 began oscillating more rapidly. This may be due to the increased vapor content of the two sections as significant amounts of liquid move to the unheated section. Once the system again came to steady state, heater 2 was turned off. This caused dry-out of section 1 due to movement of liquid to sections 2 & 3. In order to recover, heater 2 was turned back on to a comparatively low power, 100 mW. Once the system came to a steady state the power of heater 2 was cut in half to 50 mW and the system continued to pulsate. Next, the power of section 2 was reduced to 25 mW and dry-out of section 1 was observed. The results of this test indicate that there exists a minimum heat flux at which the system will operate successfully with uneven heat loads applied to at least two of the evaporator sections. Of course, the amount of liquid present in the system determines the magnitude of this heat flux. It is apparent that accurate control of the fill ratio is imperative for successful operation of the PHP.

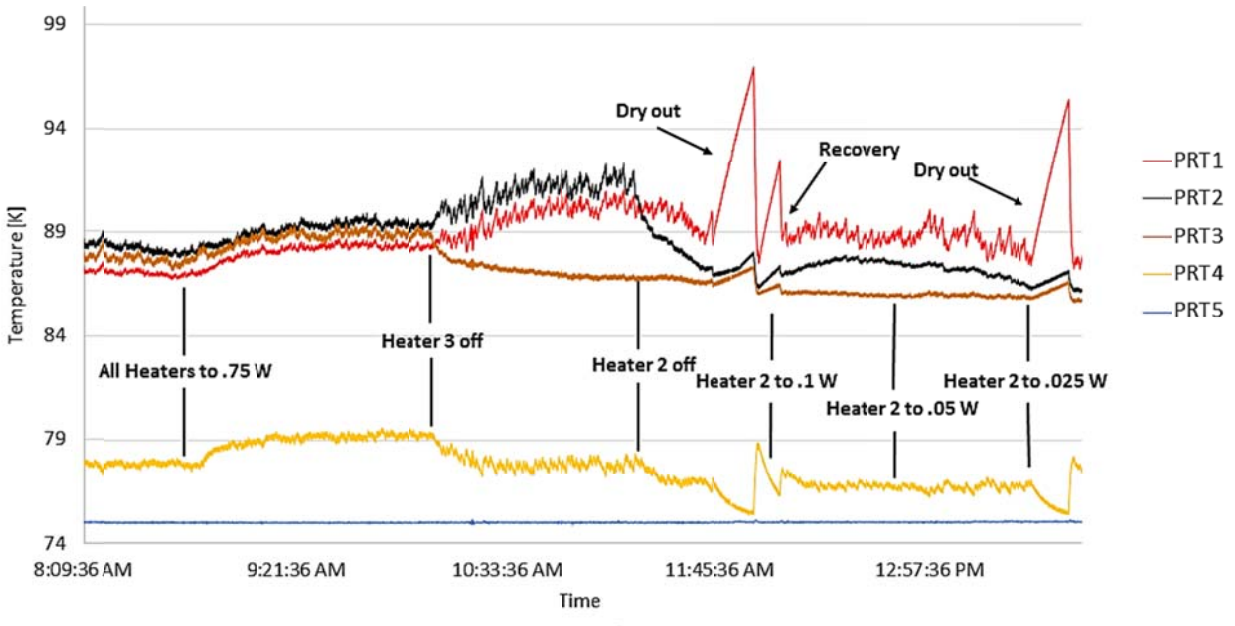

Figure 36: Temperature plot as heat load on each evaporator is changed. Effects of dry-out and recovery are indicated.

Another interesting phenomenon observed is the presence of heat spreading between the evaporator sections. Figure 37 shows that while the condenser temperature stays constant, the temperature reduction in section 2 is met with temperature increases in sections 1 & 3. This shows that the thermally isolated evaporator sections can spread heat between each other, which would be ideal in a distributed cooling system to prevent dry-out of a section.

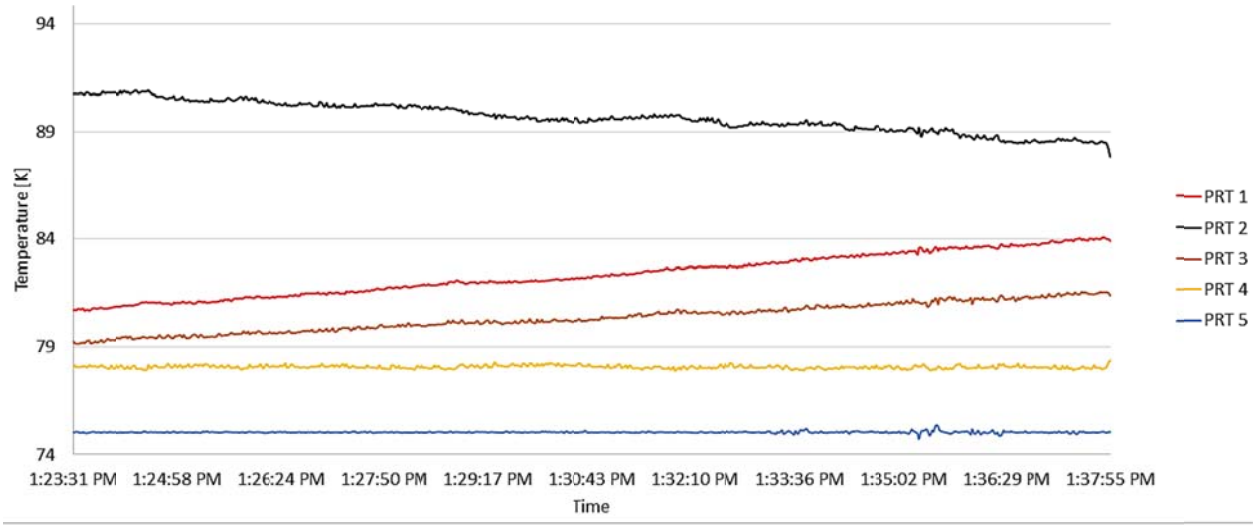

Figure 37: Example of heat spreading. The evaporator sections transfer heat to one another while the condenser remains undisturbed.

5.1.3 Moving Toward Successful Operation

Expected results such as, higher conductivities and sustained operation over time had not yet been verified. A design change was made. In the original design, as shown in Figure 26, the fluid coming in from room temperature entered a 1/8" VCR® tee and spilt to comprise the inlet and outlet (per se) of the PHP. The investigators hypothesized that the PHP did not want to "kick-in" because there was a large volume of warmer gas in the tee and the lines connecting the tee to the PHP. If the fluid tried to move in one direction, this large volume of gas interrupted the flow and it was not truly a closed-loop PHP. The redesign is discussed further in section 4.6.

The main accomplishment of the redesign was that the fluid no longer had to meander its way through the large VCR® tee volume and there was a direct path from outlet-to-inlet. With the improved fill lines, the PHP was tested again at similar conditions to those tested before the improvement. The new data showed that the PHP had significantly improved performance. A test plan was made to ensure a thorough investigation before making any conclusions about performance of a PHP with multiple evaporators. The test plan is shown in Appendix C. The test plan was designed to address various performance conditions that may affect the operation of the PHP. Running with valve 3 open proved to be unsuccessful. Continuing with the test plan, the PHP was tested at heat loads greater than the 0.25-1.25W range that was explored previously. The PHP was filled to 70% and each heater was set to 1.5 W. The PHP performed well at these heat loads.

5.2 Successful Operation

Shown in Figure 38 is a plot of temperature over time once the system reached a steady operating state. The evaporator and condenser sections settled at a mean temperature of ~88.5 K with the cold head settling at 78 K. The temperature difference between the condenser and evaporators ranged from 0.6-0.9 K with an equal heat load of 1.5 W on each section. This corresponds to effective conductivities of 47-67 kW/m-K. The PHP ran at these levels for a full 24 hours, proving that this performance was sustainable. These results were further verified by pumping out the fluid and repeating the test with the same conditions. For future reference, Figure 38 represents what will henceforth referred to as ‘successful operation’. Constant condenser and evaporator temperatures with no noticeable change in performance for a period of 2 hours characterizes successful operation.

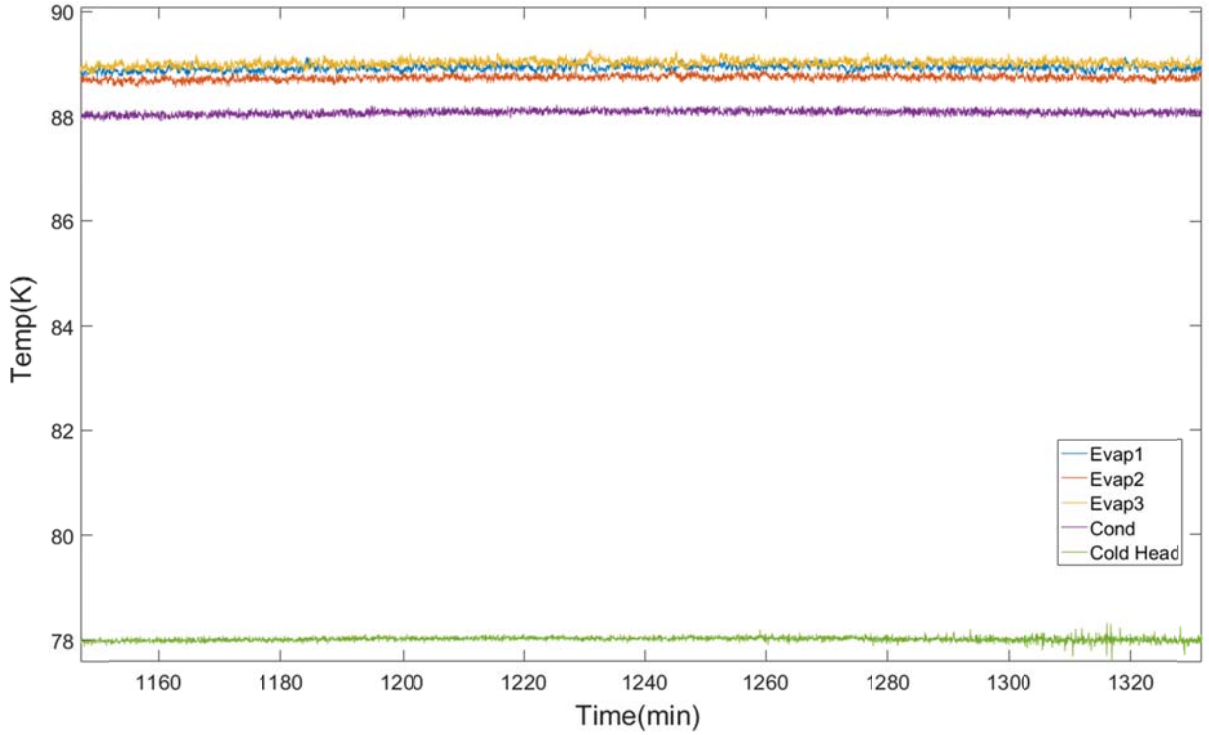

Figure 38: First successful operation of PHP at a fill ratio of 70% and each heater at 1.5 W.

It is important to note that the temperature of evaporator section 2 is noticeably lower than the temperatures of section 1 and 3. This phenomenon is present in all data collected throughout this experiment. It was originally speculated that there was a significant error with this thermometer (or with both thermometers on sections 2 & 3). After further investigation, the geometry of the PHP and thermometer placement is the cause of the discrepancy. There is only one thermometer on the condenser and it is aligned with the thermometer on section 2, as seen in Figure 39. Essentially, the same two columns of fluid pass by both thermometers causing them to read a more similar temperature compared to the other sections. This issue inflates the conductivity of section 2 in all analysis below.

Because the PHP was only tested in horizontal orientation, the following data and analysis is for the PHP in horizontal orientation.

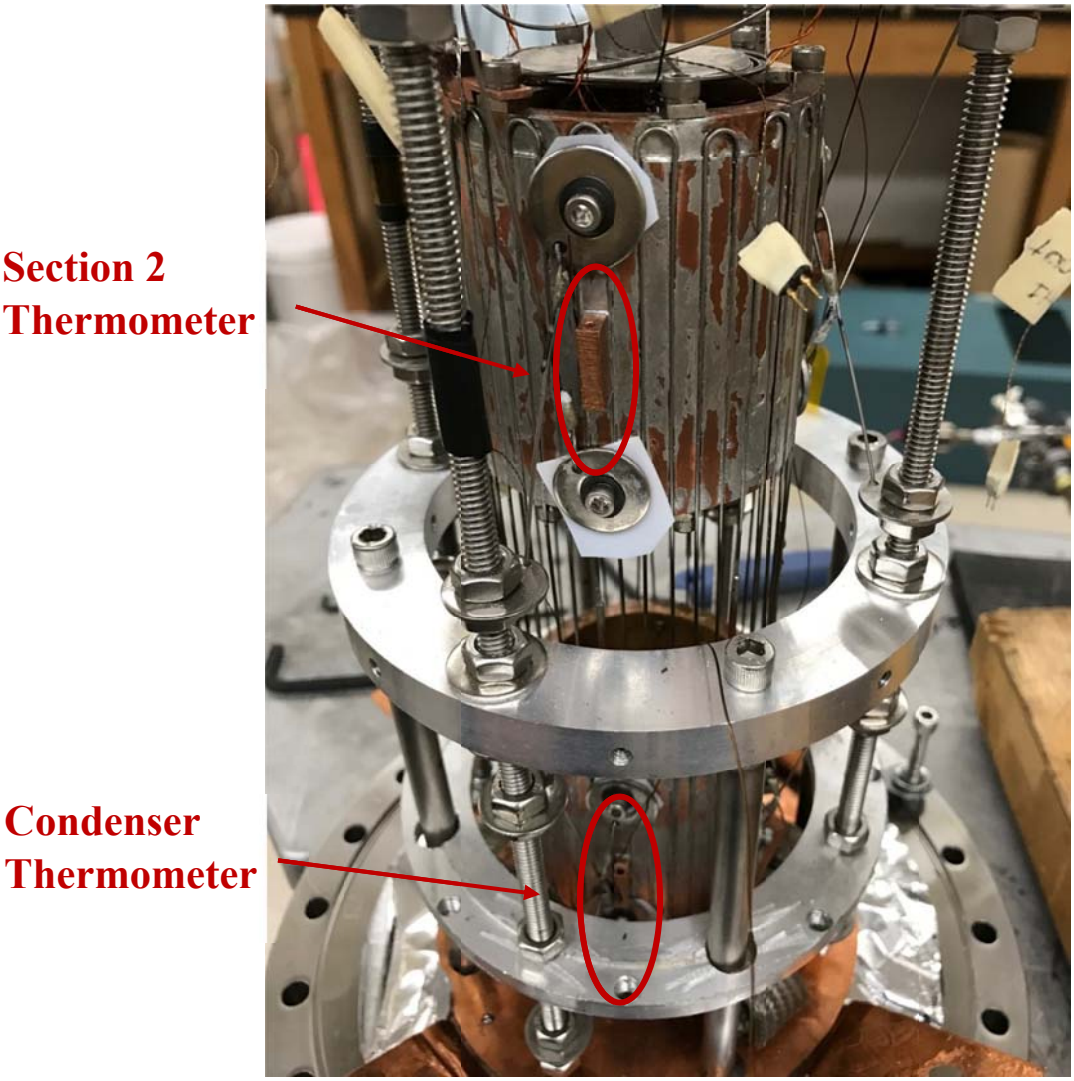

Figure 49: Picture of PHP showing the alignment of the thermometer on sections 2 and on the condenser.

5.3 Investigation of Fill Ratio

As discussed in chapter 2, other investigators have shown that there exists an optimal fill ratio where a PHP will run at the highest effective conductivity. This concept was explored with

the multiple evaporator PHP. Successful operation was achieved at fill ratios between 50% and 80% with equal heat loads of 1.5 W on each evaporator and a condenser temperature of 89 K. Figure 40 shows effective conductivity vs. fill ratio for each section of the PHP. A maximum conductivity for all sections is observed at a fill ratio of 55% with a decreasing trend as fill ratio is increased. At fill ratios below 50%, successful operation was never achieved and runs were not attempted at fill ratios above 80%.

Each fill ratio is defined based on the properties of nitrogen at 78K. All evaporators and the condenser were within 0.5 K of 78 K when filling. The filling process of the PHP is outlined in detail in section 4.7. The liquid volume fraction increases by ~5% when the condenser temperature reaches 90 K, compared to 78 K. However, for consistency sake, fill ratio is defined at 78 K.

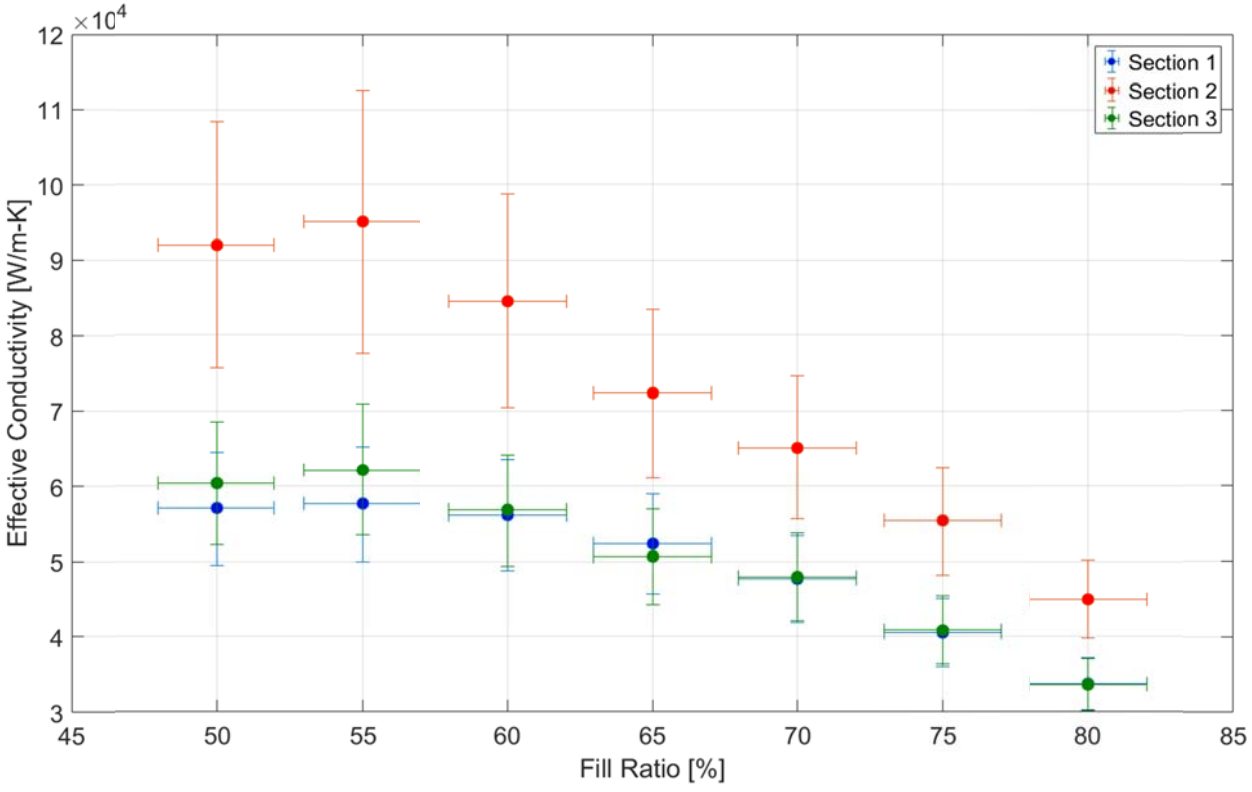

Figure 40: Effective conductivity of each PHP section vs. fill ratio.

Multiple attempts were made to run the PHP at fill ratios below 50%. Running the PHP at lower fill ratios proved to be unsuccessful even when varying the total heat load and changing the cold end temperature. It is possible that there in an insufficient amount of liquid in the system at lower fill ratios. Since the PHP is composed of three evaporators that can all be at independent temperatures, vapor can collect in one section while the other sections can work somewhat normally and still dump heat to the condenser through the normal PHP heat transfer mechanism. This phenomenon was observed multiple times. An example of run-away of section 2 and inconsistent performance of the other sections at a fill ratio of 35% is shown in Figure 41.

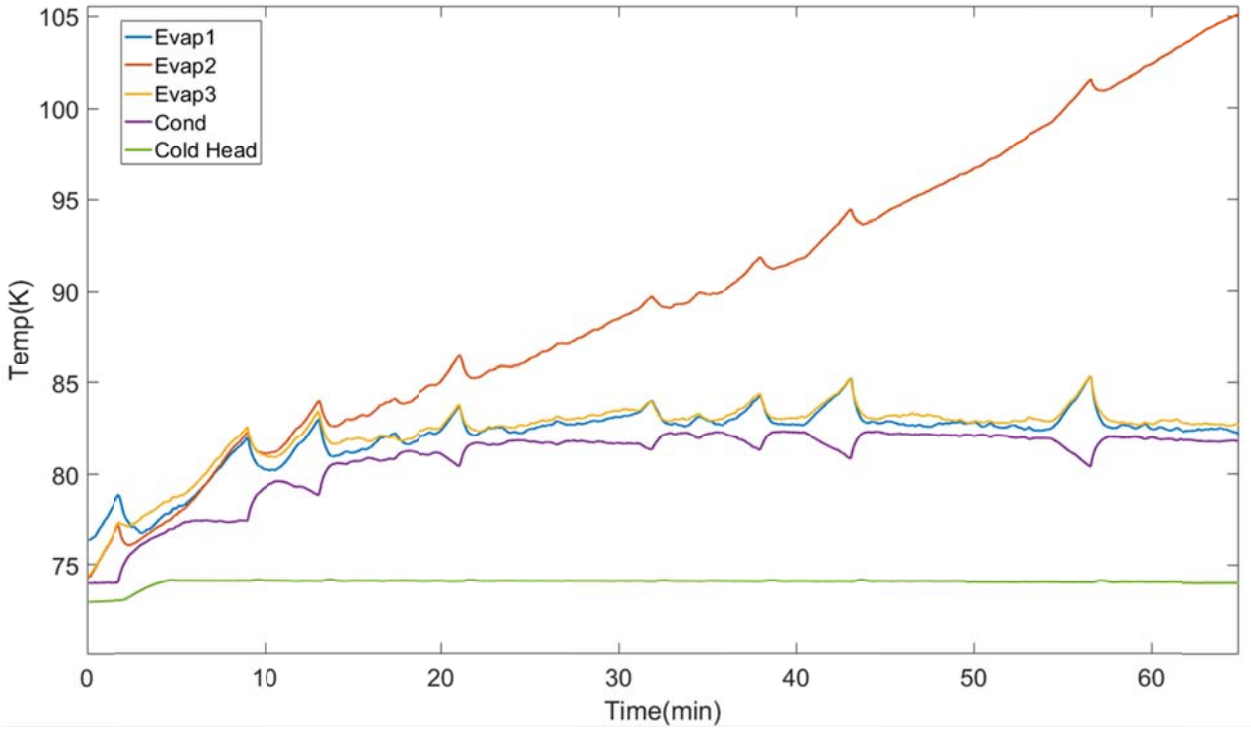

Figure 41: Run-away of section 2 when running PHP at a fill ratio of 35% and a cold end temperature of 74 K. All heat loads are 1.5 W.

5.4 Varying Heat Loads

5.4.1 Reducing All Loads Simultaneously

A PHP is expected to operate over a wide range of heat loads. As discussed above, performance was verified at various fill ratios and a total heat load of 4.5 W. By decreasing the total heat load in steps of 150 mW, performance at each heat load is compared. The conductivities of each section trend downward as the heat load applied to each section is decreased as shown in Figure 42. The temperature difference between the evaporator and condenser of each section also decreases at first, but at a total heat load at 3.45 W this difference begins to increase as shown in Figure 43. Furthermore, as the total heat load is decreased, the stability of the temperature fluctuations begins to degrade. The temperature over time as heat load is decreased is shown in Figure 44. At a total heat load of 3.6 W there is a notable change in the behavior of the evaporator temperatures. Continuing to decrease the total heat load continues to degrade the stability of the temperature fluctuations.

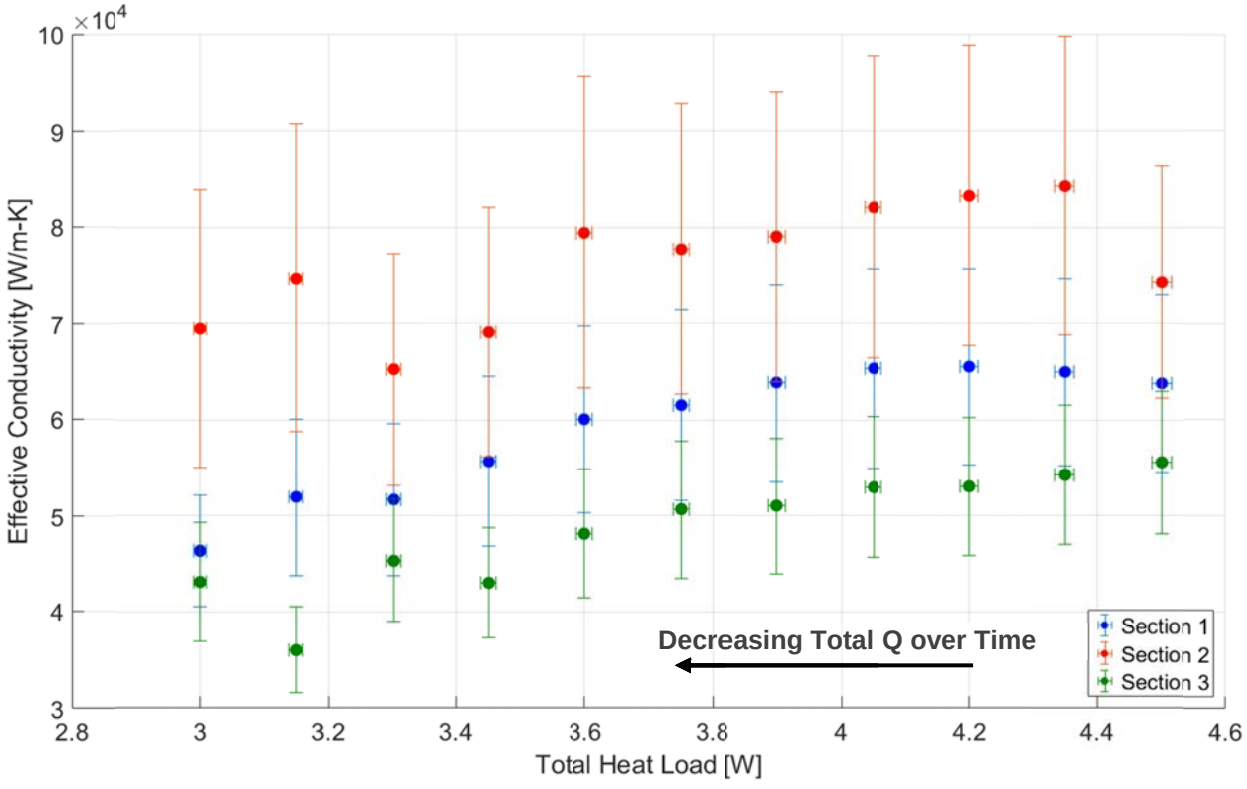

Figure 42: Effective conductivity vs. total heat load as total heat load is decreased in steps of 150 mW.

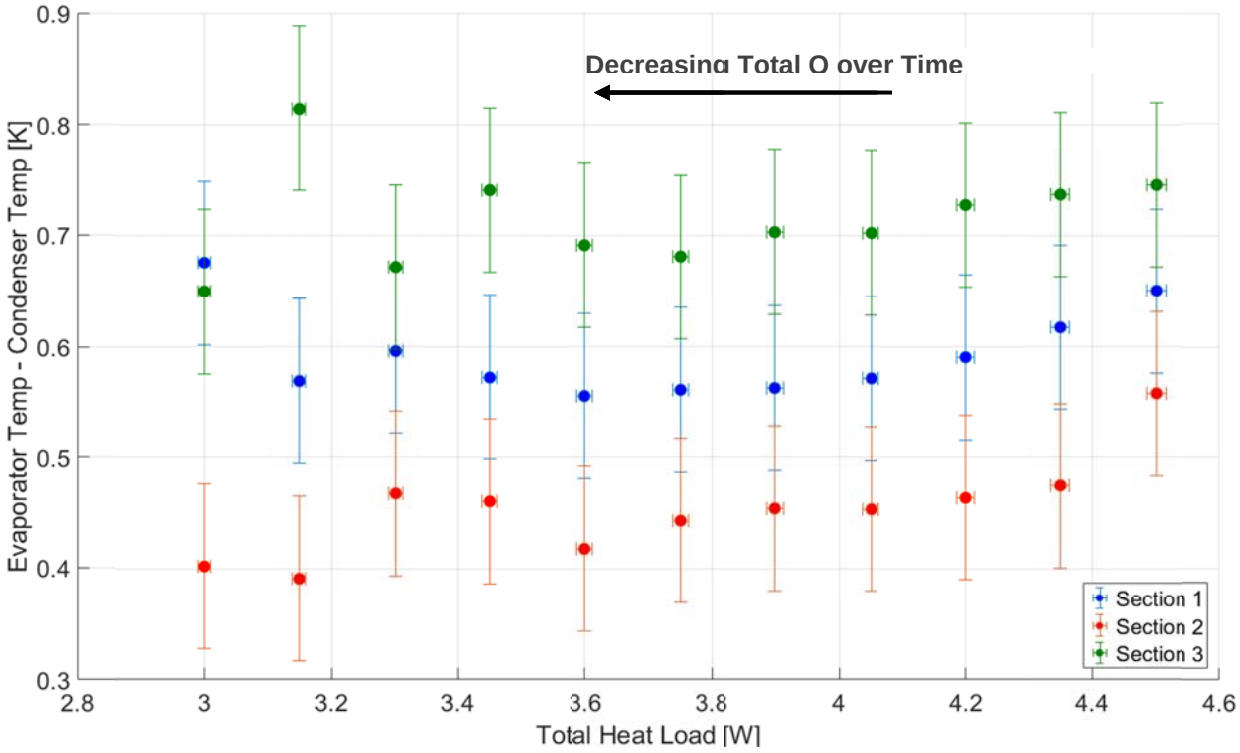

Figure 43: Temperature difference between evaporators and condensers as total heat load is decreased in steps of 150 mW.

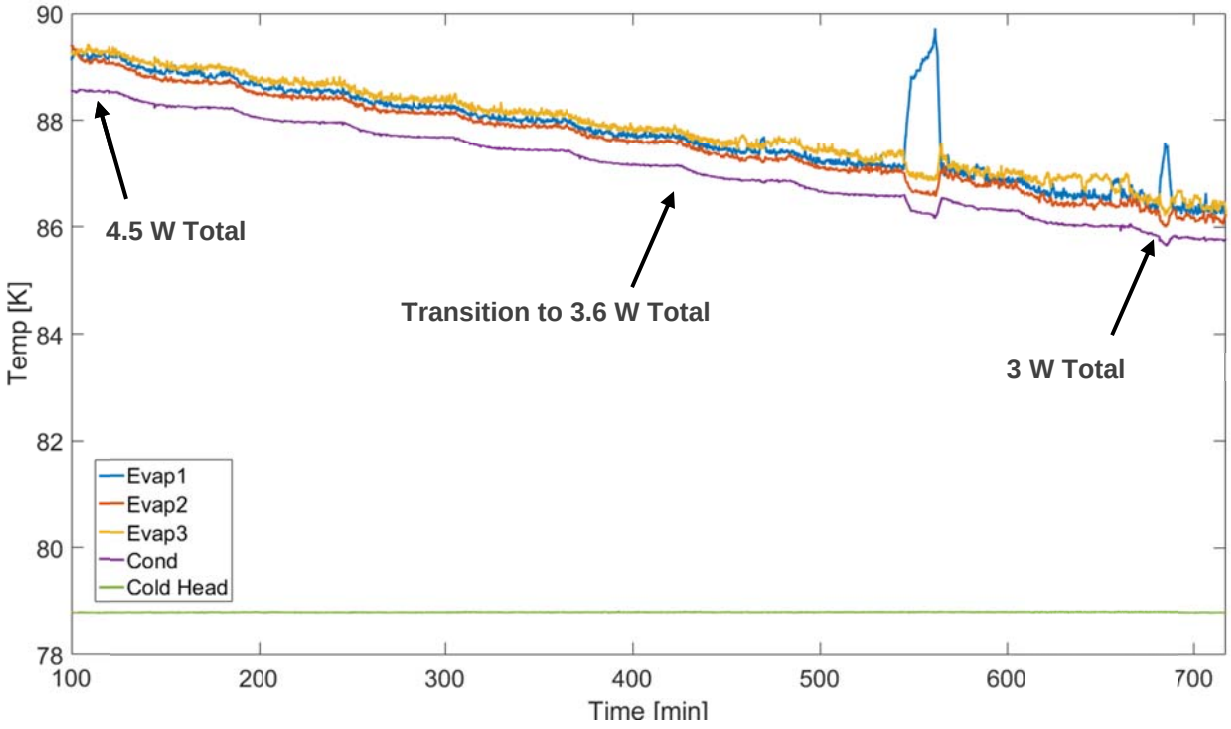

Figure 44: Temperature vs. time as total heat load is decreased in steps of 150 mW. Each dramatic reduction in temperature indicates a reduction in total heat load of 150 mW.

5.4.2 Reducing Load on One Section

The PHP worked properly with even heat loads on each section and was the first known occurrence of successful operation of a multiple evaporator PHP. Next, the heat loads on each section were varied to determine how the PHP performed with different heat loads on each section.

The heat load on section 1 (Q1) was continually decreased while keeping the heat loads on sections 2 & 3 (Q2 & Q3) constant at 1.5 W. The PHP was filled to 60%. A cold head temperature of 78.9 K and a condenser temperature of 89.2 K was observed at equal heat loads of 1.5 W. Q1 was decreased from an initial value of 1.5 W down to 0.5 W in steps of 0.1 W. When the heat load on section 1 was changed from 0.6 W to 0.5 W, the PHP stopped working.

This corresponds to a change in the total heat load of 3.6 W to 3.5 W. The PHP behaved normally throughout the test with the conductivity of each section varying according to Figure 45. The only deviation from expected performance during this run was when the total heat load was changed from 4 W to 3.9 W as shown in Figure 46 and annotated in Figure 45. The PHP seems to "adjust" to the new heat load (note: there is no user intervention during this process). Adjustment entails a slight runaway of at least one section and then recovery, but at different temperatures. The PHP appears to settle at a new quasi-equilibrium and to continue operate with good performance.

The PHP stopped working when the total heat load, or the sum of Q1, Q2 and Q3, reached a value of 3.5 W. This is a concept that is explored further below to prove a minimum total heat load (regardless of which section the heat is applied to) must be applied for the PHP to operate successfully. Figure 47 shows the temperature over time of each component once Q1 is changed from 0.6 W to 0.5 W. Normal pulsations transition to increasingly uncharacteristic behavior and eventually there is a complete disconnect between the evaporators and condenser.

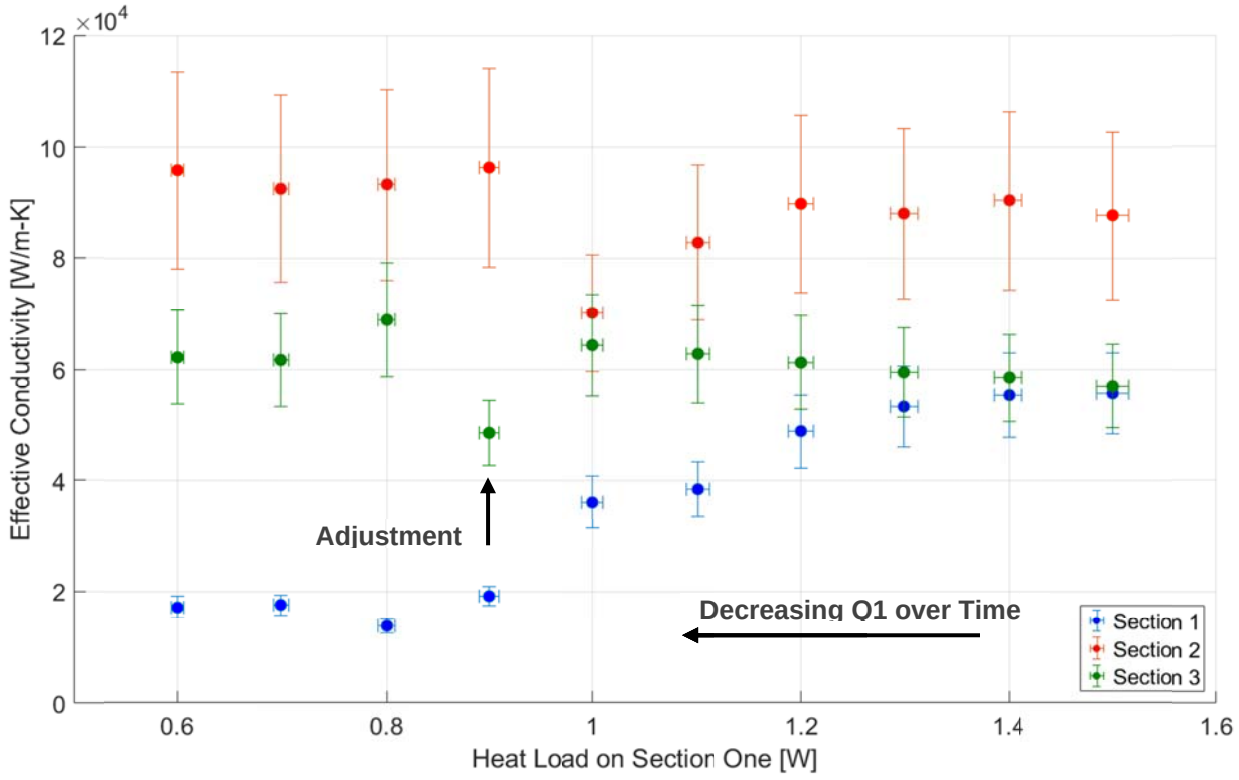

Figure 45: Effective conductivity of each section as the heat load on section 1 is decreased in steps of 100 mW. Notice the adjustment, shown in detail in Figure 47.

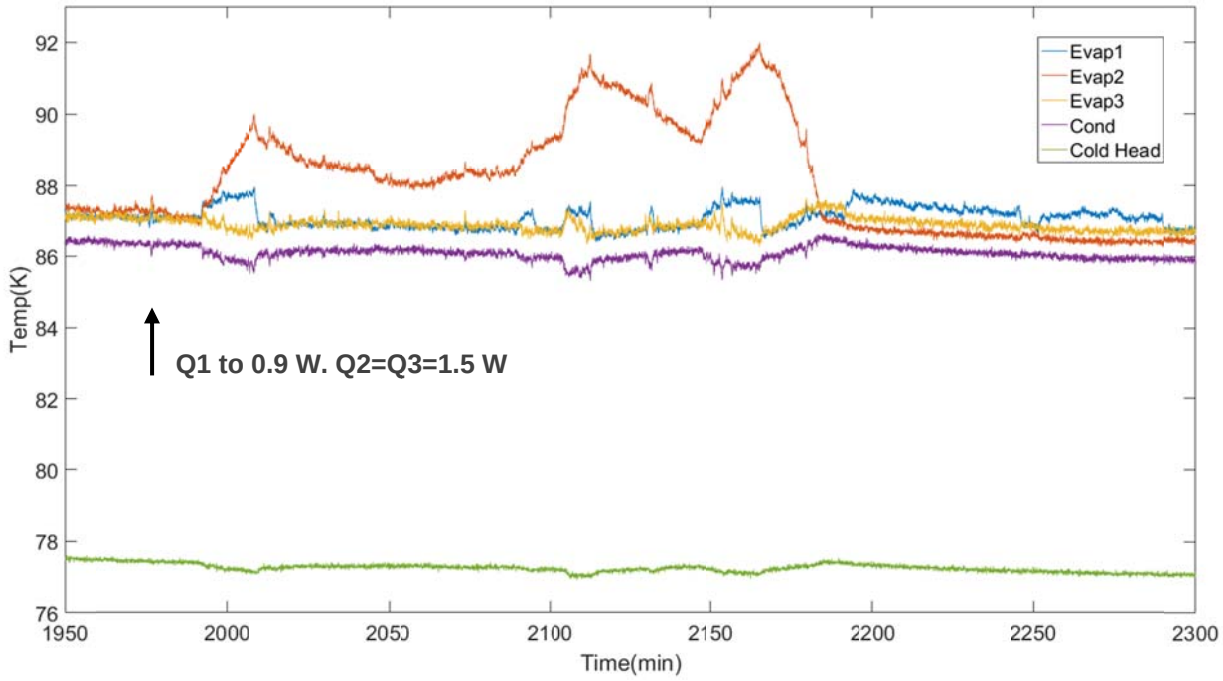

Figure 46: Adjustment in pulsations as Q1 is decreased from 1 W to 0.9 W. Q2 & Q3 constant at 1.5 W. Thus, the total heat load is decreased from 4 W to 3.9 W.

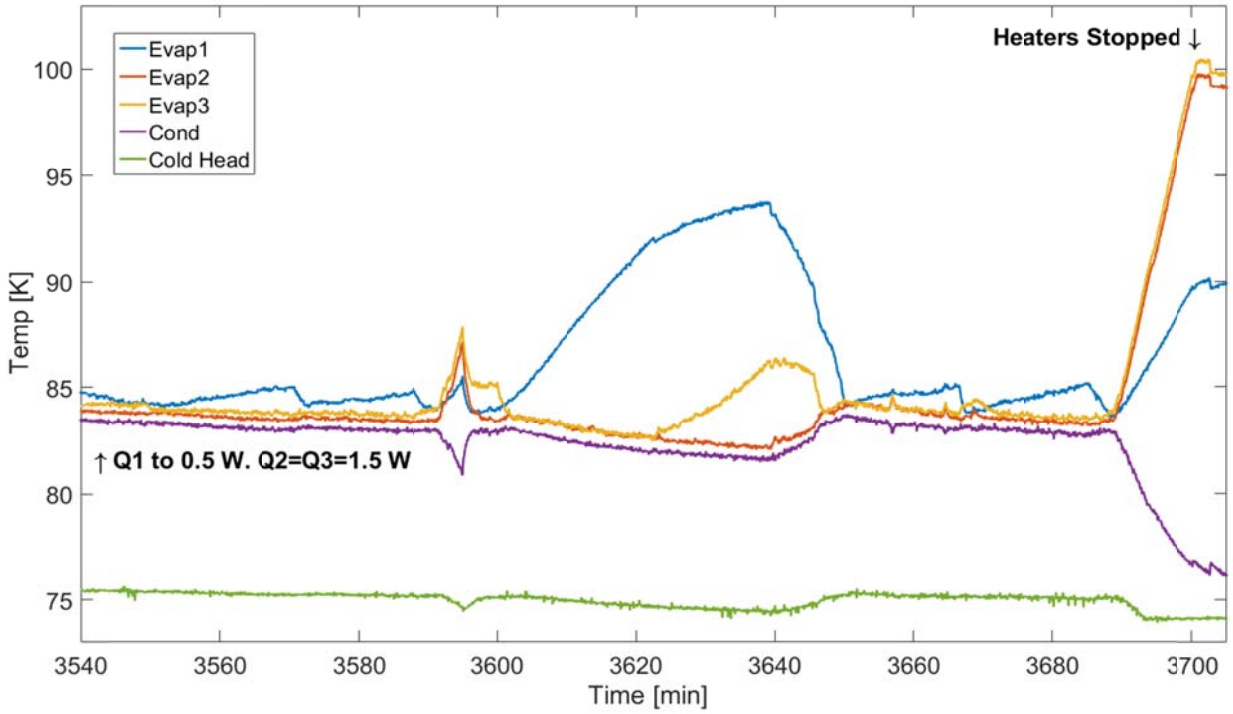

Figure 47: PHP "turning off" when Q1 is too low. Total heat load is 3.5 W.

5.4.3 Reducing Load on Two Sections

To further investigate PHP performance with varied heat loads, the heat applied to sections 1 & 3 was reduced simultaneously in steps of 100 mW from an initial value of 1.5 W while keeping section 2 constant at 1.5 W (Vfill=60%). The PHP performed well as the total heat was continuously decreased. The temperature difference between the evaporator and condenser of each section as the heat loads were reduced is shown in Figure 48. Once the total heat was reduced from 3.7 W to 3.5 W the PHP almost immediately turned off. This phenomenon can be seen in Figure 49. Again, it seems that there exists a critical total load in the range of 3.5 W.

Similar to the “adjustment” that presented itself while varying the heat load on just one section, during this test, the PHP also adjusted itself as the total heat load changed from 4.1 W to 3.9 W. This adjustment is shown in Figure 50 and annotated in Figure 48.

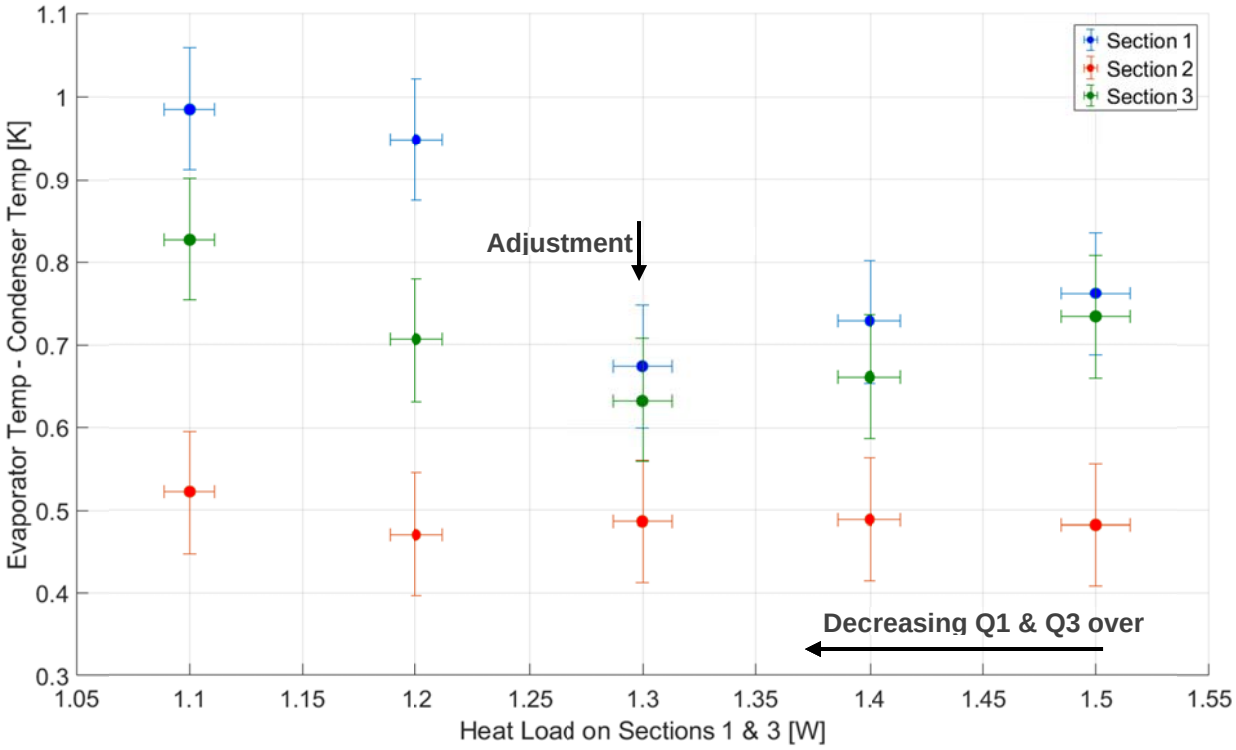

Figure 48: Temperature difference between each evaporator and the condenser as the heat load on sections 1 & 3 is reduced in steps of 100 mW. Notice the adjustment, shown in detail in Figure 51.

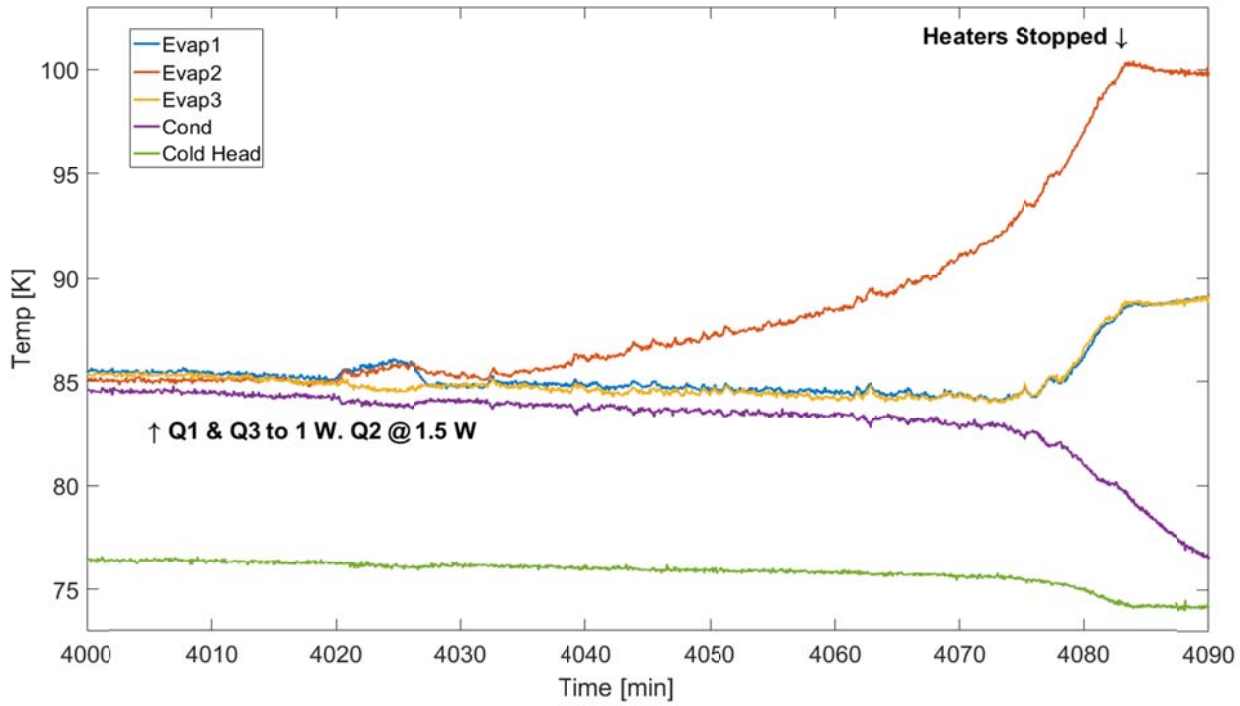

Figure 49: PHP "turned off" as total heat is reduced from 3.7 W to 3.5 W while reducing heat load on sections 1 & 3 in steps of 100 mW. Q1=Q3=**1** W, Q2=1.5 W.

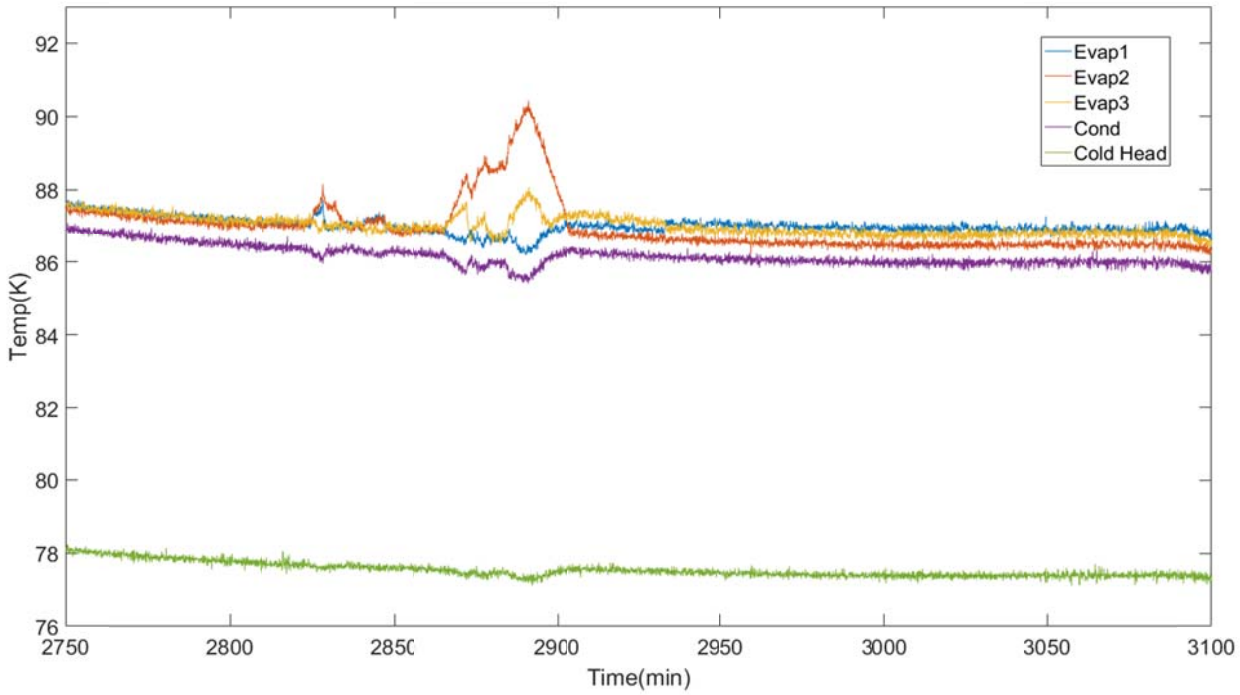

Figure 50: Adjustment as heat load in reduced from 4.1 W to 3.9 W. Q1=Q3=1.1 W, Q2=1.5 W.

5.4.4 Increasing Load on One Sectoin while Decreasing Load on Another

The degree to which the heat loads can vary across the sections of the PHP was studied. The PHP was filled to 70%. Q2 was kept constant at 1.5 W while Q1 was decreased by 100 mW and Q3 increased by 100 mW, keeping the total heat load constant at 3.5 W. The temperatures were allowed to stabilize before continuing to the next heat load. The results showed that the PHP operates successfully with heat loads as various as 0.7 W, 1.5 W and 2.3 W on sections 1, 2, and 3, respectively. The success of this test can be represented in several ways. For instance, The PHP operates successfully when Q3 is 2.29 times greater than Q1. Also valid is claiming that successful operation is possible when the maximum heat load is 51.1% of the total and the minimum is 15.5% of the total. Furthermore, it is true to claim that the PHP operates with a maximum percent difference in heat loads of 72.7%.

There were two adjustments during this run, both near the end of the test. As the heat loads were changed from (0.9, 1.5, 2.1) to (0.8, 1.5, 2.2) all three sections ran away briefly but returned to within 1.4 K of the condenser and continued to pulsate. A similar adjustment happened between (0.8, 1.5, 2.2) and (0.7, 1.5, 2.3). These two instances can be seen below in Figure 51 and 52. When the heat loads were changed to (0.6, 1.5, 2.4) the PHP turned off.

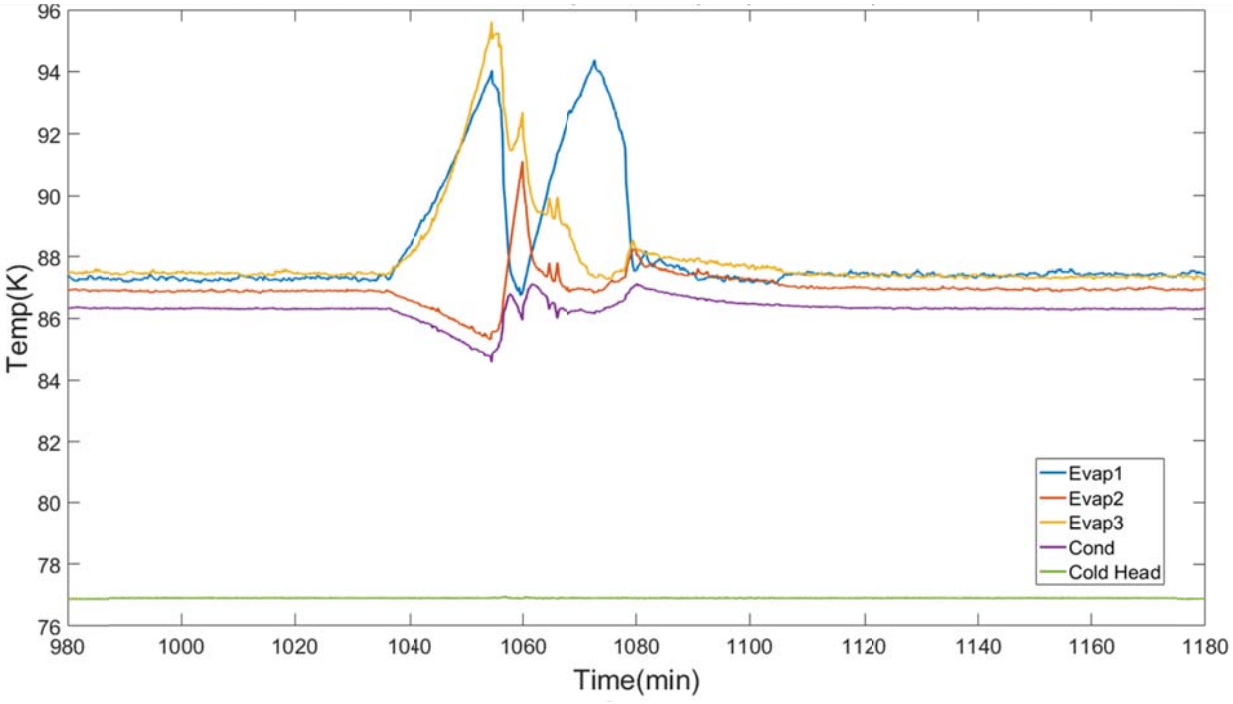

Figure 51: Adjustment during transition from (0.9, 1.5, 2.1) to (0.8, 1.5, 2.2).

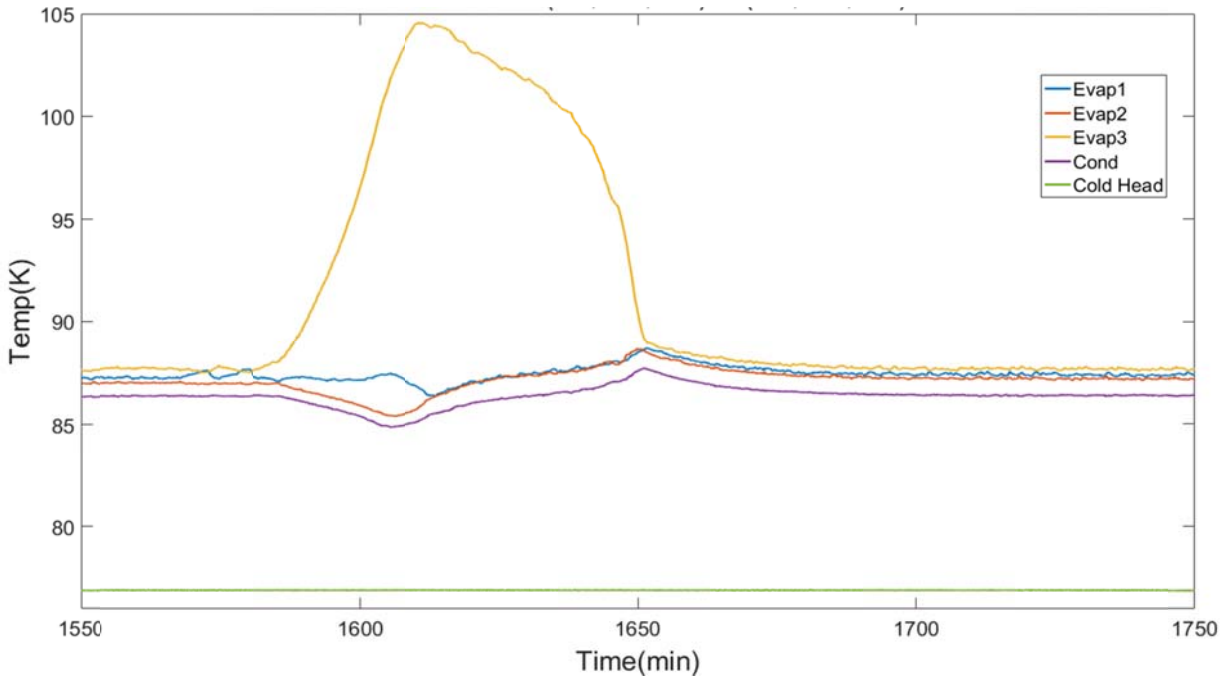

Figure 52: Adjustment during transition from (0.8, 1.5, 2.2) to (0.7, 1.4, 2.3).

The effective conductivities of each section varied according to Figure 53. Even though the individual effective conductivity of each section varies throughout the test, the sum of the conductivities, or total conductivity, remains constant as the distribution of the total heat load changes. The mean total conductivity for heat loads prior to the first adjustment is computed for comparison. According to Table 3, before the first adjustment, the total conductivity varies a maximum of 2.85% from the mean value. However, after the first adjustment, the total conductivity begins to decrease significantly even though the total heat load is constant. This indicates that the performance of the PHP begins to degrade with large differences in heat load applied to the sections until it no longer operates when the difference becomes large.

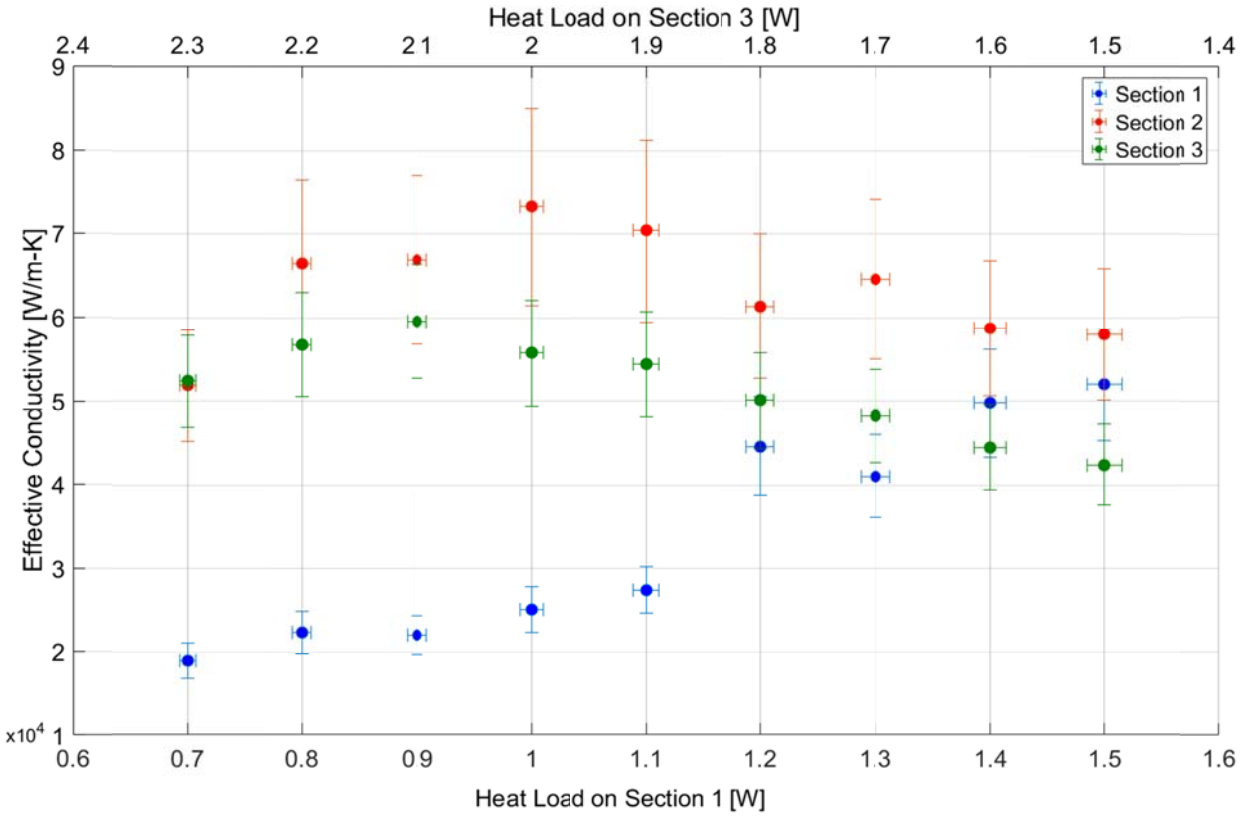

Figure 53: Effective conductivity of each section vs. the heat loads on sections 1 & 3.

Table 3: Sum of effective conductivity as the heat loads on sections 1 & 3 are varied.

Heat Load on Section 1 [W]	Heat Load on Section 2 [W]	Heat Load on Section 3 [W]	Total Heat Load [W]	Sum of Effective Conductivity [kW/m-K]	Error from Mean Before Adjustement	Percent Difference Between Max and Min Q	
1.5	1.5	1.5	4.5	152.34	0.30%	0.00%	
1.4	1.5	1.6	4.5	152.91	0.07%	6.90%	
1.3	1.5	1.7	4.5	153.80	0.66%	14.29%	
1.2	1.5	1.8	4.5	155.95	2.06%	22.22%	
1.1	1.5	1.9	4.5	152.17	0.41%	30.77%	
1	1.5	2	4.5	153.97	0.77%	40.00%	
0.9	1.5	2.1	4.5	148.44	2.85%	50.00%	
0.8	1.5	2.2	4.5	145.49	4.78%	60.87%	After Adjustment
0.7	1.5	2.3	4.5	123.12	19.42%	72.73%	After Adjustment

5.5 Pressure

The pressure of the PHP was recorded over time at various points during the term of this project. The pressure of the PHP is used to determine the period of flow oscillations in the PHP. During the test discussed in section 5.4.4, where the fill ratio was 70% and Q1, Q2, Q3 were 1.2, 1.5, 1.8, respectively, pressure was recorded and is shown in Figure 54. The mean pressure corresponds to a saturation temperature of 87.3 K for nitrogen, which represents the condenser temperature. Analyzing one oscillation reveals a period of 2.17s and a frequency of 0.46 Hz with peak-to-peak pressure oscillations of ~7kPa.

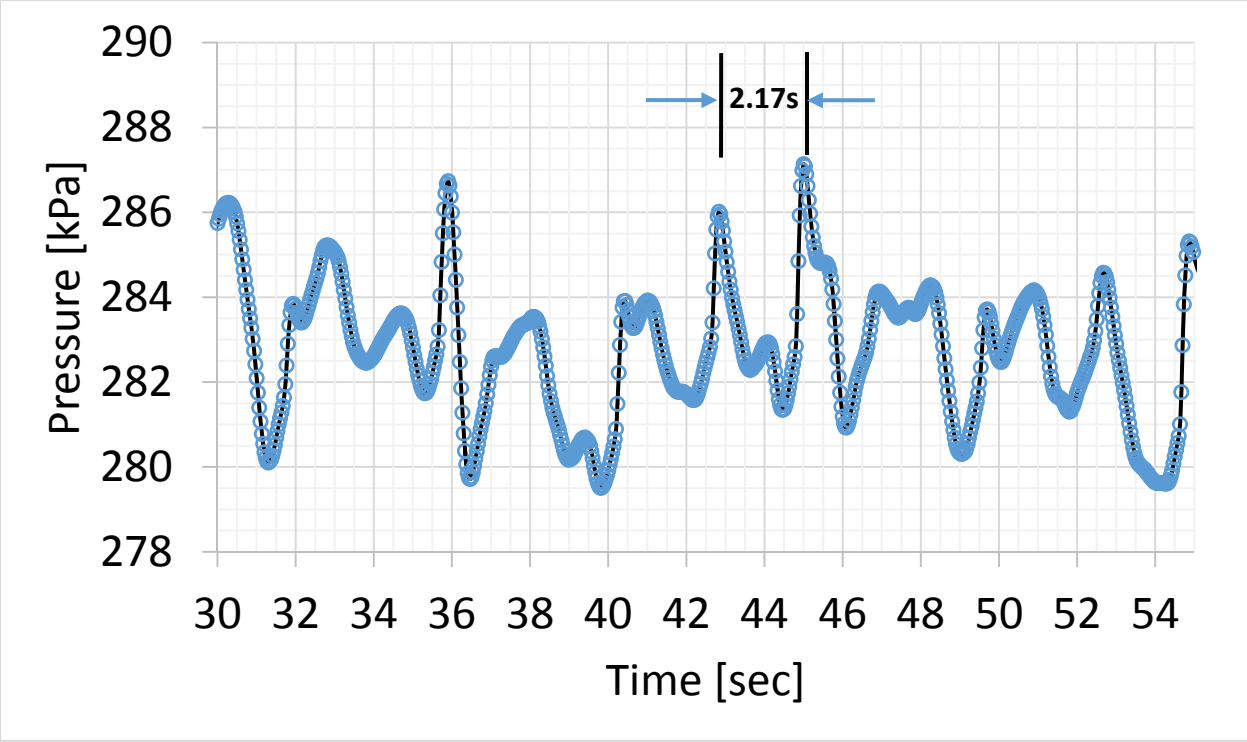

Figure 54: Pressure oscillations during stable operation.

The pressure was not measured for each test; however, the result shown in Figure 54 is used to benchmark performance by comparing to other investigators. Fonseca et al. constructed a nitrogen PHP with the same geometry as the multiple evaporator PHP, but with 40 turns and only 1 evaporator section. Their pressure data is very similar. Figure 55 shows pressure oscillations vs. time with a period of about 2 s. A power spectral density analysis of pressure for a heat load of 3 W revealed multiple peaks near 0.5 Hz with the most notable peak just below 0.5 Hz, corresponding to the 2 Hz oscillation period [31]. Comparing these results to the results of the multiple evaporator PHP helps corroborate the findings of this project.

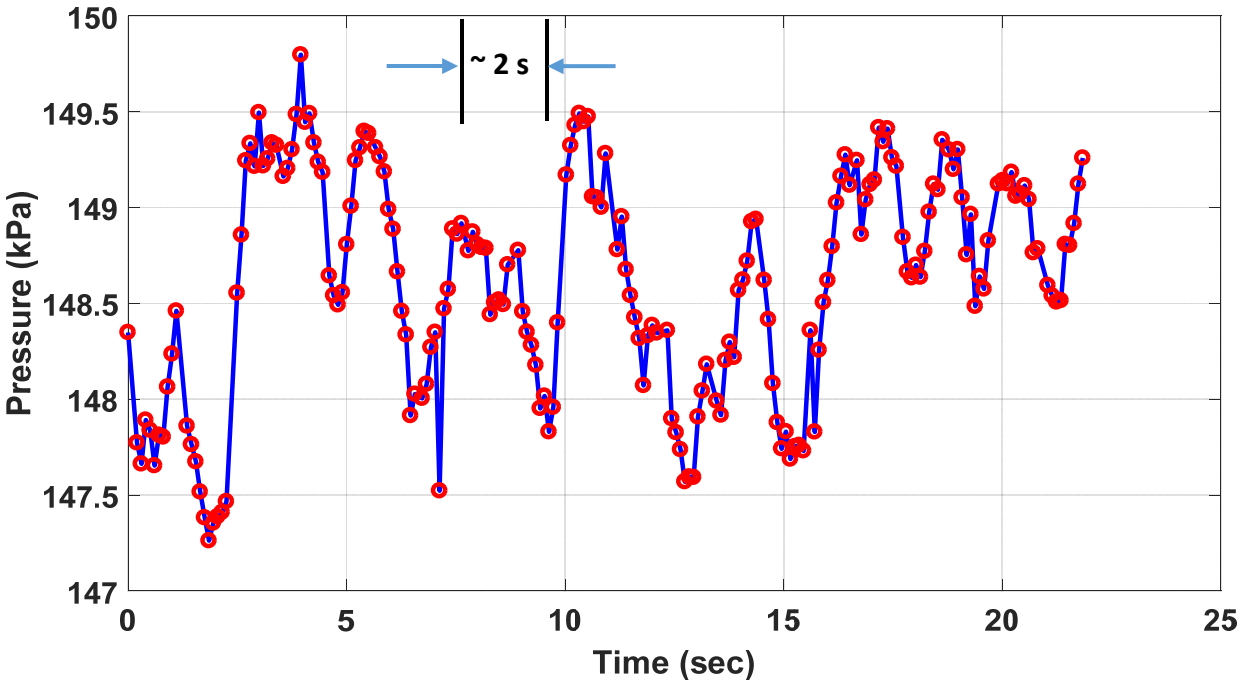

Figure 55: Pressure oscillations of nitrogen PHP tested by Fonseca et al. [source]

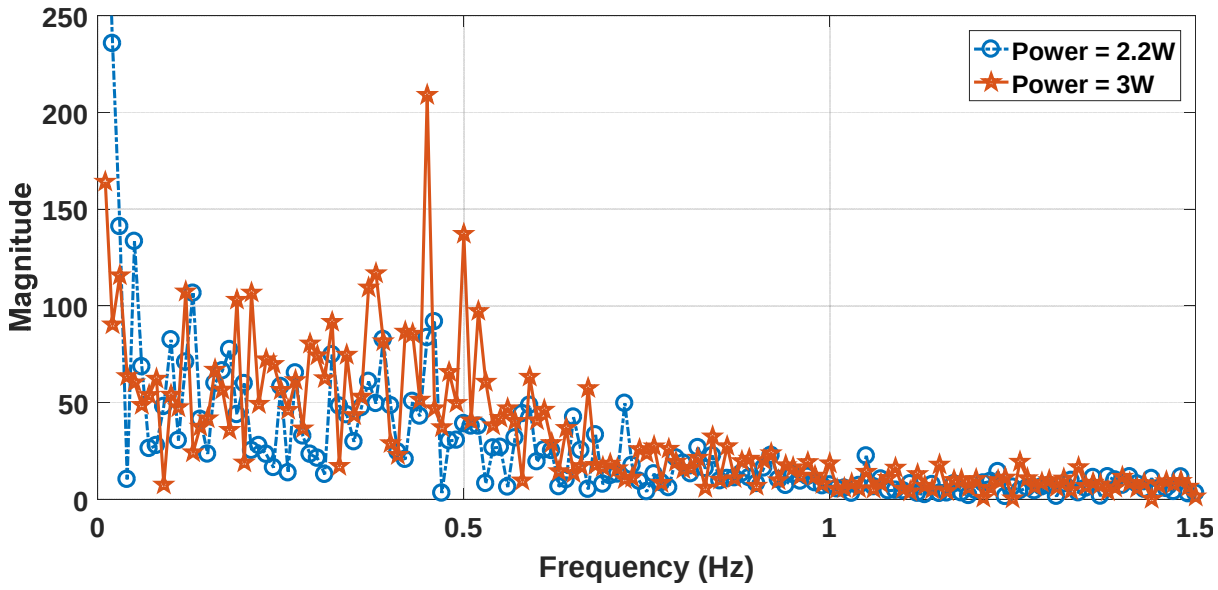

Figure 56: FFT analysis of pressure data from Fonseca et al.

6 Conclusions and Future work

6.1 Conclusions

A multiple evaporator nitrogen pulsating heat pipe was successfully designed, fabricated and tested. Results indicate that a PHP with three evaporators is able to efficiently transfer heat to one condenser over a range of heat loads. To a certain degree, the distribution of the total heat load across all evaporators has little effect on the overall performance of the PHP, making this type of system ideal for distributed cooling applications. A minimum total heat load must be applied to the evaporators in order for the PHP to operate successfully. However, the distribution of the total heat load can vary significantly across each evaporator.

Although the work required for this thesis has been accomplished, there is still an abundance of work to be done in order to develop comprehensive design tools for PHPs. The development of PHPs will continue to require the efforts of many people and organizations over many years. Continued work with this device is necessary if the application of PHPs to spacecraft thermal control systems is to be realized.

There is a notable lack of two-phase modeling tools that can adequately explain the complex operation of PHPs. The expected performance of the multiple evaporator PHP was extrapolated using the results of previous PHP experiments. As the field continues to grow, computational models of PHPs will need to be verified through experimental research, such as the work presented in this thesis. The combined efforts of members of the Cryogenic Engineering Lab at the University of Wisconsin will be essential to the future success of PHPs across all disciplines of thermal engineering.

To enhance the development of PHPs as distributed cooling devices, the multiple evaporator PHP will continue to be tested to gather meaningful data. A great deal of information has emerged from this thesis; however, there is a significant amount of testing to be done in order to characterize the multi evaporator PHP's performance entirely.

6.2 Future Work

By adjusting the orientation of the PHP, it will be possible to quantify how performance is affected by gravity and buoyancy. The data presented in this thesis is limited to horizontal orientation, but the test facility has the ability to be orientated vertically with relative ease. According to Natsume et al. and Li et al., due to the natural buoyancy of vapor, the performance of a PHP improves if the evaporator is directly beneath the condenser [11, 12].

The multiple evaporator PHP was only tested with total heat loads in the range of 2.85 W to 4.5 W. To characterize the PHP fully, it must be tested at higher heat loads. However, there are multiple factors limiting the heat that can be applied to the evaporators. First, the temperature difference across the thermal strap between the condenser and cold head of the cryocooler large due to the limited conductance of the strap. Improving the thermal strap is necessary in order to minimize the mean temperature of the PHP when running at higher heat loads. Second, the cryocooler underperforms and needs to be replaced or fixed in order to reach total heat loads above ~5 W. Finally, the heat that can be applied to each section is limited by the power supply. The following improvement will negate this issue.

Improving communication between LabVIEW and the heater system will be necessary to collect high quality data efficiently and to run at higher heat loads. The current virtual instrument can be edited to output the desired heat load to each evaporator. By using op amps, the signal

from an NI-6009 DAQ can be amplified to power each heater and the heat loads can be changed automatically according to the virtual instrument.

The water jacket used to cool the warm end of the cryocooler contains a restriction that causes the circulating pressure to exceed a maximum value set by the chiller. The water jacket should be fixed so that the PHP can be tested at higher heat loads.

7 References

[1] Schaffer, M., & Wenner, C. (2012). A Study Of Cryogenic Propulsive Stages For Human Exploration Beyond Low Earth Orbit. International Astronautical Federation.

[2] Platcha, D, W., (2015, June 24). Zero boil-off system testing. Lecture presented at Space Cryogenics Workshop in Arizona, Pheonix.

[3] Plachta, D. W., Johnson, W. L., & Feller, J. R. (2016). Zero boil-off system testing. *Cryogenics*, *74*, 88-94.

[4] Aavid Thermacore. (2017). Common Questinos About Heat Pipes [Brochure]. Author. Retrieved from http://www.thermacore.com/documents/common-questions-heat-pipes.pdf

[5] Zhang, Y., & Faghri, A. (2008). Advances and unsolved issues in pulsating heat pipes. *Heat Transfer Engineering*, *29*(1), 20-44.

[6] Khandekar, S., Dollinger, N., & Groll, M. (2003). Understanding operational regimes of closed loop pulsating heat pipes: an experimental study. *Applied Thermal Engineering*, *23*(6), 707-719.

[7] Zhang, Y., & Faghri, A. (2008). Advances and unsolved issues in pulsating heat pipes. *Heat Transfer Engineering*, *29*(1), 20-44.

[8] Yang, H., Khandekar, S., & Groll, M. (2009). Performance characteristics of pulsating heat pipes as integral thermal spreaders. *International Journal of Thermal Sciences*, *48*(4), 815-824.

[9] Hua, C., Wang, X., Gao, X., Zheng, H., Han, X., & Chen, G. (2017). Experimental research on the start-up characteristics and heat transfer performance of pulsating heat pipes with rectangular channels. *Applied Thermal Engineering*.

[10] Saha, P., Ishii, M., & Zuber, N. (1976). An experimental investigation of the thermally induced flow oscillations in two-phase systems. *Journal of Heat Transfer*, *98*(4), 616-622.

[11] Natsume, K., Mito, T., Yanagi, N., Tamura, H., Tamada, T., Shikimachi, K., ... & Nagaya, S. (2012). Development of cryogenic oscillating heat pipe as a new device for indirect/conduction cooled superconducting magnets. *IEEE Transactions on Applied Superconductivity*, *22*(3), 4703904-4703904.

[12] Li, Y., Wang, Q., Chen, S., Zhao, B., & Dai, Y. (2014). Experimental investigation of the characteristics of cryogenic oscillating heat pipe. *International Journal of Heat and Mass Transfer*, *79*, 713-719.

[13] Yang, H., Khandekar, S., & Groll, M. (2008). Operational limit of closed loop pulsating heat pipes. *Applied thermal engineering*, *28*(1), 49-59.

[14] Khandekar, S., & Groll, M. (2003, September). On the definition of pulsating heat pipes: an overview. In *Proceedings of the Fifth Minsk International Seminar*.

[15] Bretherton, F. P. (1961). The motion of long bubbles in tubes. *Journal of Fluid Mechanics*, *10*(02), 166-188.

[16] White, E. T., & Beardmore, R. H. (1962). The velocity of rise of single cylindrical air bubbles through liquids contained in vertical tubes. *Chemical Engineering Science*, *17*(5), 351-361.

[17] Gu, J., Kawaji, M., & Futamata, R. (2005). Microgravity performance of micro pulsating heat pipes. *Microgravity Science and Technology*, *16*(1), 181-185.

[18] Mameli, M., Araneo, L., Filippeschi, S., Marelli, L., Testa, R., & Marengo, M. (2014). Thermal response of a closed loop pulsating heat pipe under a varying gravity force. *International Journal of Thermal Sciences*, *80*, 11-22.

[19] Mangini, D., Mameli, M., Georgoulas, A., Araneo, L., Filippeschi, S., & Marengo, M. (2015). A pulsating heat pipe for space applications: ground and microgravity experiments. *International Journal of Thermal Sciences*, *95*, 53-63.

[20] Plachta, D. W., Christie, R. J., Carlberg, E., & Feller, J. R. (2008, March). Cryogenic propellant boil-off reduction system. In J. G. Weisend, J. Barclay, S. Breon, J. Demko, M. DiPirro, J. P. Kelley, & P. Kittel (Eds.), *AIP Conference Proceedings* (Vol. 985, No. 1, pp. 1457-1466). AIP.

[21] Feller, J. R., Plachta, D. W., Mills, G., & McLean, C. (2008). Demonstration of a cryogenic boil-off reduction system employing an actively cooled thermal radiation shield. Georgia Institute of Technology.

[22] Ebrahimi, K., Jones, G. F., & Fleischer, A. S. (2014). A review of data center cooling technology, operating conditions and the corresponding low-grade waste heat recovery opportunities. *Renewable and Sustainable Energy Reviews*, *31*, 622-638.

[23] Grid, G. (2007). The Green Grid data center power efficiency metrics: PUE and DCiE. *Green Grid report*.

[24] Pelley, S., Meisner, D., Wenisch, T. F., & VanGilder, J. W. (2009, June). Understanding and abstracting total data center power. In *Workshop on Energy-Efficient Design*.

[25] Li, Z., & Kandlikar, S. G. (2015). Current status and future trends in data-center cooling technologies. *Heat Transfer Engineering*, *36*(6), 523-538.

[26] Ohadi, M. M., Dessiatoun, S. V., Choo, K., Pecht, M., & Lawler, J. V. (2012, March). A comparison analysis of air, liquid, and two-phase cooling of data centers. In *Semiconductor Thermal Measurement and Management Symposium (SEMI-THERM), 2012 28th Annual IEEE* (pp. 58-63). IEEE.

[27] Lu, Q., & Jia, L. (2016). Experimental study on rack cooling system based on a pulsating heat pipe. *Journal of Thermal Science*, *25*(1), 60-67.

[28] Yang, H., Khandekar, S., & Groll, M. (2008). Operational limit of closed loop pulsating heat pipes. *Applied thermal engineering*, *28*(1), 49-59.

[29] Lakeshore Cryogenics. (2014). Instructions, Platinum Resistance Thermometer Installation [Instruction]. Westerville, OH: Form Number F022-00-00 Revision E.

[30] Hastings, L. J., Bryant, C. B., Flachbart, R. H., Holt, K. A., Johnson, E., Hedayat, A., ... & Plachta, D. W. (2010). Large-Scale Demonstration of Liquid Hydrogen Storage with Zero Boiloff for In-Space Applications.

[31] Fonseca, L. D., Miller, F., & John, P. (2017). Experimental Heat Transfer Analysis of a Cryogenic Nitrogen Pulsating Heat Pipe at Various Liquid Fill Ratios. Applied Thermal Engineering. Under Review.

[32] Engineering Equation Solver (EES), Fchart Software. Madison, WI

[33] Lakeshore Cryogenics. Westerville, OH

[34] Swagelok. Solon, OH

[35] Loctite Adhesives. Westlake, OH

[36] Apiezon. Manchester, UK

[37] National Instruments. Austin,TX

[38] Clifford, P. (n.d.). RTD Measurement, RTD Temperature Curve. Retrieved from http://www.mosaic-industries.com/embedded-systems/microcontroller-projects/temperature-measurement/platinum-rtd-sensors/resistance-calibration-table

[39] Tenma Corp. Japan

[40] Hewlett Packard. Palo Alto, CA

[41] Endevco-Meggitt Sensing Systems. Orange Country,CA

[42] MKS Instruments. Andover, MA

[43] SunPower Inc. Athens, OH

[44] Polyscience. Niles, IL

8 Appendix

8.1 Appendix A: Error Analysis

8.1.1 Equipment

- Lakeshore PT-103 ® Platinum Resistance Thermometers
- Lakeshore 120 ® Current Supply
- Endevco 8530B ® Pressure Sensors
- Hewlett Packard E3611A ® Power Supply
- National Instruments SCXI 1100 ® Data Acquisition System
- National Instruments USB-6363 ® Terminal Block

8.1.2 Thermometer Error

Thermometer Calibration

The error in all temperature measurements is based on the error in measured temperature differences rather than the absolute temperature of each sensor. Since effective conductivity is based on the temperature difference between each evaporator and the condenser, the uncertainty used is the uncertainty in the temperature differences. After all data was collected, each thermometer was removed from the cryostat and inserted radially into a round copper stock using Apiezon N thermal grease [36]. A Styrofoam container with a 2.54 cm thick G10 block at the bottom was used as a vessel for liquid nitrogen. The copper stock was set on the block of G10 and liquid nitrogen was poured into the container, submerging the entire copper stock. Over time, the nitrogen boiled away and the block was allowed to warm up to room temperature while continuously monitoring temperature. Each thermometer is assumed to be reading the exact same temperature. The measured temperature difference between each evaporator thermometer and the condenser thermometer in the range 85 -95 K is shown in Figure 57. This range was chosen because during successful operation, the evaporators are always in this temperature range.

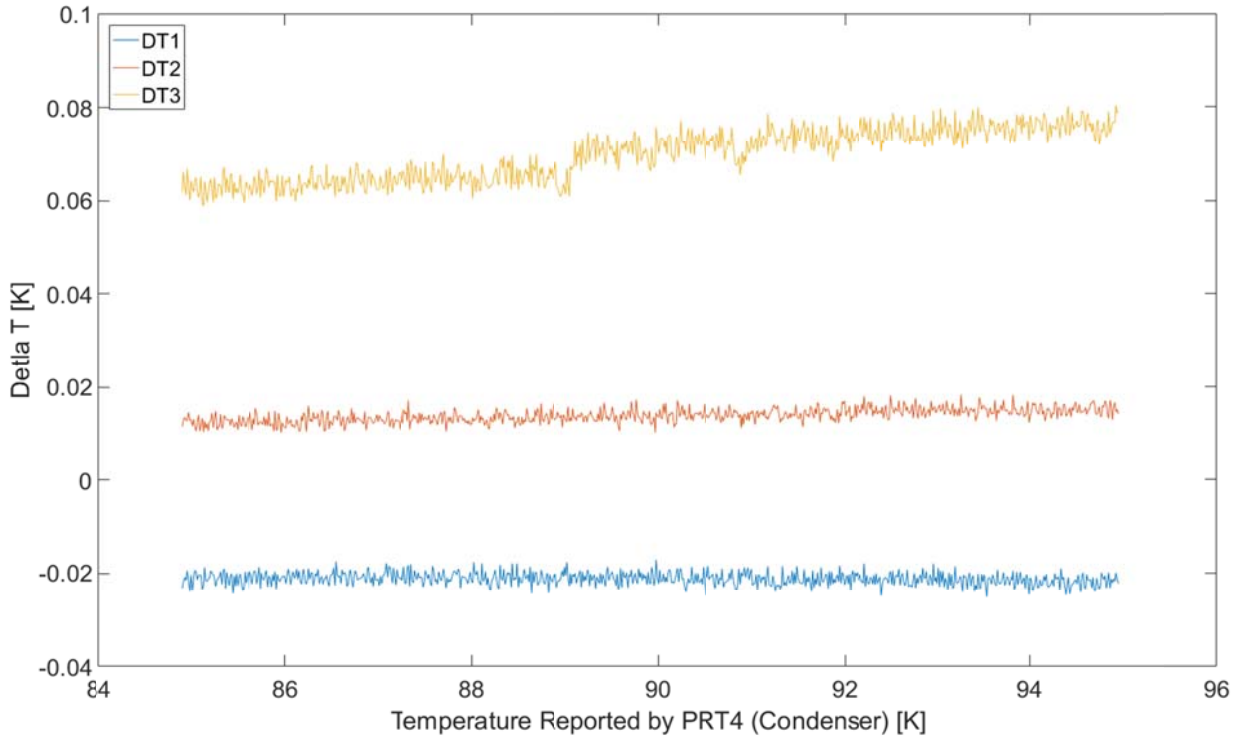

Figure 57: Temperature difference between each evaporator thermometer vs. the measured temperature of the condenser thermometer during post-calibration.

A mean value at 90 K is selected for each thermometer. This value is then subtracted from each evaporator temperature before analysis. The measured temperature difference that varied the most is that of PRT 3, the thermometer on evaporator 3. In the range of 85-95 the value increased from 60.36 mK to 81.94 mK. To arrive at an uncertainty value the following analysis was used:

$$81.94 - 60.36 = 21.58\ mK * \left(\frac{1}{2}\right) = \pm 10.79\ mK$$

This value is used for all thermometers as a worst-case scenario. The uncertainty in the applied current and voltage measurement is also considered.

Applied Current Error

The value of a resistor was measure to be 1306 ± 0.3406 Ω using a Hewlett Packard 34401a ® multimeter [40]. The voltage drop across this resistor using the Lakeshore 120 current supply [33] set to 1mA was measured to be 1.3187 V ± 59.75 μV using the same HP multimeter. Based on these two measurements the current supplied to each thermometer is 1.0972 mA ± .2673 μA.

Data Acquisition Error

Relevant errors from NI SCXI 1100 ®:

- Gain Error (0.01% of reading)
- Offset Error (5 μV)
- Noise Error (Measured Noise * $1/\sqrt{n}$)

Absolute Error = $\sqrt{Gain\ Error^2 + Offset\ Error^2 + Noise\ Error^2}$

$$= \sqrt{(0.01\% * 25\ mV)^2 + 5\ \mu V^2 + \ 0.225 mV^2 * \left(\frac{1}{15000^{\frac{1}{2}}}\right)^2} = \pm \mathbf{5.79\ \mu V}$$

Relevant Errors from NI USB 6363:

- Gain Error (Reading * 95μV)
- Offset Error (Range * 27μV)
- Noise Error(3*21μV * $1/\sqrt{n}$)

Absolute Error=$\sqrt{Gain\ Error^2 + Offset\ Error^2 + Noise\ Error^2}$

$$= \sqrt{(25mV * 95\mu V)^2 + (0.20 * 27\mu V)^2 + \left(2 * 21\mu V * \left(\frac{1}{15000^{\frac{1}{2}}}\right)\right)^2} = \pm \mathbf{8.59\ \mu V}$$

Total Data Acquisition Error= $\sqrt{5.79\mu V^2 + 8.59\ \mu V^2} = \pm$**10.36 µV**

Propagating the current and data error gives a total temperature uncertainty of **±26.54 mK.**

Reference Equation Error

The equation, which is used to find temperature based on the resistance of platinum, also has some reported error. According to Mosaic Documentation Web [38] the error involved with using Equation 8 is **±15 mK.**

Summary

Thus, the error for one temperature measurement is:

$\sqrt{26.54\ mK^2 + 15mK^2} = \pm$ **30.486 mK**

The error for a difference in temperature is then:

$$\mu(T2 - T1) = \sqrt{30.486^2 + 30.486^2} + 10.79\ mK = \pm\ \boldsymbol{53.76\ mK}$$

8.1.3 Fill Ratio Error

The error in fill ratio is due to the error in the pressure measurement used to determine the pressure change in the reservoir tank. According to Endevco the combined error in their 8530B ® pressure sensors is ±0.25% FSO (full-scale output) [41]. For a FSO of 3447 kPa, this equates to an error of ±8.6175 kPa which corresponds to a fill ratio error of ~40%. However, since the quantity of interest for the fill ratio calculation is a pressure difference rather than absolute pressure, a different error analysis is used. The change of voltage output by the transducer between two pressure values is assumed to change linearly. The manufacturer specifies that the linearity error of the sensor is 0.20% FSO. Although it is not common practice, applying the linearity error to the range of operation during the filling process (0-345 kPa) gives an error of ±**0.69 kPa.**

The data acquisition error has already been found to be ±**10.36 µV.** Using the sensor sensitivity of 0.6 mV/psi this corresponds to an error of ±0.017 kPa.

Combining these two errors gives a total error of 0.69 kPa which corresponds to a fill ratio error of **±1.97%.**

8.1.4 Heat Load Error

The error in heat load is estimated to be 1%.

8.2 Appendix B: Fill Ratio Calculation

```
"Mason Mok
Calculation of fill ratio"

"Volume Calculations"

D_swage_1=0.173*convert(in,m)                    "ID of 0.25 OD swage"
A_swage_1=D_swage_1^2/4 * pi                     "internal area of  swage"

D_swage_2=0.11*convert(in,m)                     "ID of thick wall stainless"
A_swage_2=D_swage_2^2/4 * pi                     "internal area of thick-walled stainless"

D_ss=0.035*convert(in,m)                         "ID of small stainless steel lines"
A_ss=D_ss^2*(pi/4)                               "Area od small stainless steel lines"

V_tank=3.6*convert(L,m^3)                        "volume of black resevoir"

V_1=(3+19.5+3.25+2.25)[in]*convert(in,m)*A_Swage_1 +18[in]*A_swage_2*convert(in,m)
                                                 "volume from Valve 1 to valve 3 (valve 2 closed)"
V_2=3.5[in]*convert(in,m)*A_swage_1 + V_tank     "volume from valve 2 to bottom of tank"

V_3=(11+1+4+1)[in]*convert(in,m)*A_swage_1       "volume from V3 to Dewar"
V_4=(1"T"+20+24)[in]*convert(in,m)*A_ss + 60[in]*convert(in,m)*A_cap"volume from inlet of dewar to PHP"


"Calculation of PHP volume"
V_php = ((PI*d_cap^2)/4)*L_turn*N_turn           "calulated volume of PHP"
d_cap = 0.5*convert(mm,m)                        "i.d. of capillary tubing"
A_cap=pi*(d_cap^2)/4
L_turn = 2*(L_evap + L_adiabat + L_cond)         "length of a turn = 2 legs"
L_evap = 70*convert(mm,m)                        "length of the evaporator"
L_cond = 70*convert(mm,m)                        "length of condensor"
L_adiabat = 80*convert(mm,m)                     "adiabatic length"
N_turn = 21                                      "numer of turns on PHP"

"Inputs"
F$='Nitrogen'
R=R#                                             "R_universal"
MW=molarmass(F$)                                 "molar mass of nitrogen"
T_amb=300[K]                                     "ambient temperature"
T_PHP=80[K]                                      "temperature of cold end"
P_f=p_sat(F$, T=T_sat)                           "final pressure in tank"

"properties of saturated fluid"
vol_liq=volume(F$,T=T_sat,x=0)*MW                "specific volume of saturated liquid in mol"
vol_gas=volume(F$,T=T_sat,x=1)*MW                "specific volume of saturated vapor in mol"
vol_liq_kg=volume(F$,T=T_sat,x=0)                "specific volume of liquid in kg"
vol_gas_kg=volume(F$,T=T_sat,x=1)                "specific volume of vapor in kg"
```

```
vol_liq_cond=volume(F$,T=T_cond,x=0)          "specific volume of liquid at condenser temp"
vol_gas_cond=volume(F$,T=T_cond,x=1)          "specific volume of vapor at condenser temp"

"Liquid Fill Percentage"
V_fill=V_liq/V_php                            "definition of fill ratio"
V_gas=V_PHP-V_liq                             "total volume of vapor in PHP"

"To change on parametric table"
T_cond=90[K]                                  "setting saturation temperature when in operation"
T_sat=78[K]                                   "starting temp when filling"
{V_fill=.70                                   "setting fill ratio"}

"Calculation of PHP fill ratio"
N_Down_V3=(P_fill-P_close)*(V_2+V_1)/(R*T_amb)   "number of moles on cold end once valve is closed"
N_Down_V3=N_PHP+N_lines                       "number of moles that left tank are moles in PHP and lines upstream of PHP to V3"
N_php=V_liq/vol_liq + (V_php-V_liq)/vol_gas   "numer of moles in PHP"
N_lines=P_f*(V_3+V_4)/(R*(T_amb+T_sat)/2)     "numberof moles in lines up to V3. assuming all vapor)"
P_fill=22*convert(psi,kPa)                    "Pressure to fill tank (doesnt really matter, DP is what matter"
DP=(P_fill-P_close)                           "pressure difference in tank between opening and closing V3"

"Checking fill ratio at different condenser temps based on initial fill mass"
m_PHP=N_php*MW                                "mass of nitrogen in PHP once V3 is closed"
vol_PHP=V_PHP/m_PHP                           "specific volume of PHP"
vol_PHP=(vol_liq_cond+ qual*(vol_gas_cond-vol_liq_cond))"finding quality at condenser temp during operation"
m_vap=qual*m_php                              "mass of vapor at a qaulity"
m_liq=m_php-m_vap                             "mass of liquid at a quality"
V_vap_2=m_vap*vol_gas_cond                    "volume of vapor"
V_liq_2=m_liq*vol_liq_cond                    "volume of liquid"
V_php_2=V_vap_2+V_liq_2                       "check"
V_fill_2=V_liq_2/(V_vap_2+V_liq_2)            "calculate fill ratio (verified to agree with calculation above)"

"Important pressures"
{P_close=19*convert(psi,kpa)}                 "pressure at V3 close"
{DP=3.63*convert(psi,kpa)}                    "pressure drop in tank"

"Calculation of fluid properties at different temperatures. Used to explain PHP behavior at different temperature"
mu_liq=viscosity(F$,T=T_cond,x=0)
mu_vap=viscosity(F$,T=T_cond,x=1)
sigma=surfacetension(F$,T=T_cond)
cp_liq=specheat(F$,T=T_cond,x=0)
cp_vap=specheat(F$,T=T_cond,x=1)
{one\muv_liq=1/(mu_liq*vol_liq_cond)
one\muv_vap=1/(mu_vap*vol_gas_cond)}
h_vap=enthalpy_vaporization(F$,T=T_cond)
```

SOLUTION

Unit Settings: SI K kPa kJ mass deg

(Table 1, Run 21)

A_{cap} = 1.963E-07 [m^2]
cp_{liq} = 2.141 [kj/kg-k]
D_{ss} = 0.000889 [m]
h_{vap} = 180.5 [Kj/kg]
L_{turn} = 0.44 [m]
m_{liq} = 0.001459 [kg]
N_{lines} = 5.254E-07 [kmol]
P_r = 109.3 [kPa] {15.85 [psi]}
σ = 0.006113 [j/m^2]
T_{sat} = 78 [K]
vol_{liq} = 0.03488 [m^3/kmol]
V_1 = 0.00001359 [m^3]
V_{fill} = 1
$V_{liq,2}$ = 0.000001959 [m^3]
$V_{vap,2}$ = -1.445E-07 [m^3]

A_{ss} = 6.207E-07 [m^2]
cp_{vap} = 1.266 [Kj/kg-k]
$D_{swage,1}$ = 0.004394 [m]
$L_{adiabat}$ = 0.08 [m]
μ_{liq} = 1.028E-04 [Pa-s]
m_{PHP} = 1.457123E-03 [kg]
N_{PHP} = 5.202E-05 [kmol]
P_{fill} = 151.7 [kPa] {22 [psi]}
T_{amb} = 300 [K]
vol_{gas} = 5.666 [m^3/kmol]
$vol_{liq,cond}$ = 0.001342 [m^3/kg]
V_2 = 0.003601 [m^3]
$V_{fill,2}$ = 1.08
V_{php} = 1.814E-06 [m^3]

$A_{swage,1}$ = 0.00001517 [m^2]
DP = 36.25 [kPa] {5.258 [psi]}
$D_{swage,2}$ = 0.002794 [m]
L_{cond} = 0.07 [m]
μ_{vap} = 6.482E-06 [Pa-s]
m_{vap} = -0.000002178 [kg]
N_{turn} = 21
qual = -0.001495
T_{cond} = 90 [K]
$vol_{gas,cond}$ = 0.06632 [m^3/kg]
$vol_{liq,kg}$ = 0.001245 [m^3/kg]
V_3 = 0.000006548 [m^3]
V_{gas} = -2.068E-25 [m^3]
$V_{php,2}$ = 1.814E-06 [m^3]

$A_{swage,2}$ = 0.000006131 [m^2]
d_{cap} = 0.0005 [m]
F$ = 'Nitrogen'
L_{evap} = 0.07 [m]
MW = 28.01 [kg/kmol]
$N_{Down,V3}$ = 0.00005254 [kmol]
P_{close} = 115.4 [kPa] {16.74 [psi]}
R = 8.314 [kJ/kmol-K]
T_{PHP} = 80 [K]
$vol_{gas,kg}$ = 0.2023 [m^3/kg]
vol_{PHP} = 0.001245 [m^3/kg]
V_4 = 0.000001009 [m^3]
V_{liq} = 0.000001814 [m^3]
V_{tank} = 0.0036 [m^3]

No unit problems were detected.

KEY VARIABLES

(Table 1, Run 21)

DP = 36.25 [kPa] {5.258 [psi]} *Pressure Drop in Tank*
V_{fill} = 1 *Fill Ratio*

Parametric Table: Table 1

	V_{fill}	DP [kPa]
Run 1	0	*0.5835*
Run 2	0.05	*2.367*
Run 3	0.1	*4.15*
Run 4	0.15	*5.934*
Run 5	0.2	*7.717*
Run 6	0.25	*9.501*
Run 7	0.3	*11.28*
Run 8	0.35	*13.07*
Run 9	0.4	*14.85*
Run 10	0.45	*16.63*
Run 11	0.5	*18.42*
Run 12	0.55	*20.2*
Run 13	0.6	*21.99*
Run 14	0.65	*23.77*
Run 15	0.7	*25.55*
Run 16	0.75	*27.34*
Run 17	0.8	*29.12*
Run 18	0.85	*30.9*
Run 19	0.9	*32.69*
Run 20	0.95	*34.47*
Run 21	1	*36.25*

8.3 Appendix C: Test Plan

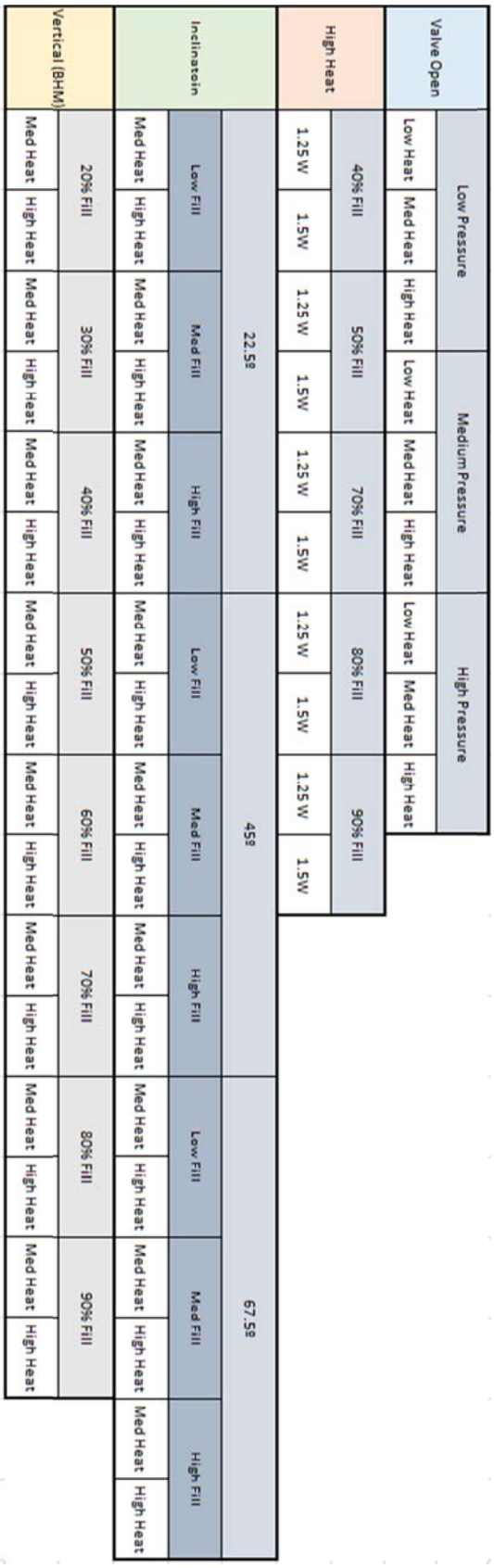

Valve Open												
Low Pressure				Medium Pressure				High Pressure				
Low Heat	Med Heat	High Heat		Low Heat	Med Heat	High Heat		Low Heat	Med Heat	High Heat		
High Heat												
1.25 W	1.5W	1.25 W	1.5W	1.25 W	1.5W	1.25 W	1.5W	1.25 W	1.5W	1.25 W	1.5W	
40% Fill		50% Fill		70% Fill		80% Fill		90% Fill				
Inclinatoin												
22.5º						45º					67.5º	
Low Fill		Med Fill		High Fill		Low Fill		Med Fill		High Fill		
Med Heat	High Heat	Med Heat	High Heat	Med Heat	High Heat	Med Heat	High Heat	Med Heat	High Heat	Med Heat	High Heat	Med Heat	High Heat
Vertical (BHM)												
20% Fill		30% Fill		40% Fill		50% Fill		60% Fill		70% Fill		80% Fill		90% Fill	
Med Heat	High Heat	Med Heat	High Heat	Med Heat	High Heat	Med Heat	High Heat	Med Heat	High Heat	Med Heat	High Heat	Med Heat	High Heat	Med Heat	High Heat

8.4 Appendix D: Evaporator Model

```
"Mason Mok
1/16th Symmetry
PHP Evaporator Thermal Analysis"

"Inputs"
k=500[W/m-K]                                        "conductivity of copper"
th=6*convert(mm,m)                                  "thickness of copper"
h=17.5*convert(mm,m)                                "overall height of quarter evap section"
h%=.05                                              "percentage of side dedicated to heat flux"
L=15.25*convert(mm,m)                               "overall length of quarter evap section"
M=20                                                "number of nodes in horizontal direction"
N=20                                                "number of nodes in vertical direction"
T_cond=75[K]                                        "temperature of condenser"
q_dot_total=.5[W]                                   "total q supplied by heater"
q_dot_h=q_dot_total/12                              "heat flux split between nodes"
q_dot_out_fcv=q_dot_total/(351.5)                   "q dot out for a full cv(internal node)"
q_dot_out_hcv=q_dot_out_fcv/2                       "q dot out for a half cv(edge)"
q_dot_out_qcv=q_dot_out_fcv/4                       "q dot out for a quater cv(corner)"
q_dot_check=(q_dot_out_fcv*(N-2)*(M-2))+(q_dot_out_hcv*54)+(q_dot_out_qcv*2) "sanity check"

"General Equations"
duplicate i=1,M                                     "creating x-locations"
    x[i]=(i-1)*L/(M-1)
    x_bar[i]=x[i]/L
end
DELTAx=L/(M-1)

duplicate j=1,N                                     "creating y-locations"
    y[j]=(j-1)*h/(N-1)
    y_bar[j]=y[j]/h
end
DELTAy=h/(n-1)

"cv energy balances"
"Internal Nodes"
duplicate i=2,(M-1)
    duplicate j=2,(N-1)
    (k*th)*((DELTAx/DELTAy)*(T[i,j+1]-T[i,j]) + (DELTAy/DELTAx)*(T[i-1,j]-T[i,j]) + (DELTAx/DELTAy)*(T[i,j-1]-T[i,j]) + (
DELTAy/DELTAx)*(T[i+1,j]-T[i,j])) - q_dot_out_fcv = 0
    end
end

"Bottom Nodes"
duplicate i=1,M
    T[i,1]=T_cond
end

"Top Nodes w/ q"
duplicate i=2,5
    q_dot_h + k*(((DELTAy*th)/(2*DELTAx))*(T[i-1,N]-T[i,N]) + ((DELTAx*th)/(DELTAy))*(T[i,N-1]-T[i,N]) + ((DELTAy*th)/(2*
DELTAx))*(T[i+1,N]-T[i,N])) - q_dot_out_hcv = 0
end

"Top Nodes w/ No q"
duplicate i=6,(M-1)
    k*(((DELTAy*th)/(2*DELTAx))*(T[i-1,N]-T[i,N]) + ((DELTAx*th)/(DELTAy))*(T[i,N-1]-T[i,N]) + ((DELTAy*th)/(2*DELTAx))*(
T[i+1,N]-T[i,N])) - q_dot_out_hcv = 0
end

"Left Nodes w/ q"
duplicate j=(N-4),(N-1)
    q_dot_h + k*(((DELTAx*th)/(2*DELTAy))*(T[1,j-1]-T[1,j]) + ((DELTAy*th)/(DELTAx))*(T[2,j]-T[1,j]) + ((DELTAx*th)/(2*
DELTAy))*(T[1,j+1]-T[1,j]))- q_dot_out_hcv = 0
end
```

```
"Left Nodes w/ No q"
duplicate j=2,(N-5)
    k*(((DELTAx*th)/(2*DELTAy))*(T[1,j-1]-T[1,j]) + ((DELTAy*th)/(DELTAx))*(T[2,j]-T[1,j]) + ((DELTAx*th)/(2*DELTAy))*(T[1,j+
1]-T[1,j])) - q_dot_out_hcv = 0
end

"Right Nodes"
duplicate j=2,(N-1)
    k*(((DELTAx*th)/(2*DELTAy))*(T[M,j+1]-T[M,j]) + ((DELTAy*th)/DELTAx)*(T[M-1,j]-T[M,j]) + ((DELTAx*th)/(2*DELTAy))*(
T[M,j-1]-T[M,j])) - q_dot_out_hcv = 0
end

"Top Left Corner"
2*q_dot_h + (k/2)*(((DELTAx*th)/DELTAy)*(T[1,N-1]-T[1,N]) + ((DELTAy*th)/DELTAx)*(T[2,N]-T[1,N])) - q_dot_out_qcv =0

"Top Right Corner"
(k/2)*(((DELTAx*th)/DELTAy)*(T[M,N-1]-T[M,N]) + ((DELTAy*th)/DELTAx)*(T[M-1,N]-T[M,N])) - q_dot_out_qcv =0

DELTAT=Max(T[1..M,1..N])-Min(T[1..M,1..N])
```